OCEANIC AND ATMOSPHERIC RESPONSE TO CLIMATE CHANGE OVER VARYING GEOLOGIC TIMESCALES

A Dissertation

by

STELLA C. WOODARD

Submitted to the Office of Graduate Studies of
Texas A&M University
in partial fulfillment of the requirements for the degree of

DOCTOR OF PHILOSOPHY

May 2011

Major Subject: Oceanography

Oceanic and Atmospheric Response to Climate Change Over Varying Geologic Timescales

OCEANIC AND ATMOSPHERIC RESPONSE TO CLIMATE CHANGE OVER VARYING GEOLOGIC TIMESCALES

A Dissertation

by

STELLA C. WOODARD

Submitted to the Office of Graduate Studies of
Texas A&M University
in partial fulfillment of the requirements for the degree of

DOCTOR OF PHILOSOPHY

Approved by:

Chair of Committee,	Deborah J. Thomas
Committee Members,	Ethan Grossman
	Mitchell Lyle
	Franco Marcantonio
	Niall Slowey
Head of Department,	Piers Chapman

May 2011

Major Subject: Oceanography

ABSTRACT

Oceanic and Atmospheric Response to Climate Change Over Varying Geologic Timescales.

(May 2011)

Stella C. Woodard, B.A., State University of New York-Oswego

Chair of Advisory Committee: Dr. Deborah J. Thomas

Global climate is controlled by two factors, the amount of heat energy received from the sun (solar insolation) and the way that heat is distributed Earth's surface. Solar insolation varies on timescales of 10s to 100s of thousands of years due to changes in the path of Earth's orbit about the sun (Milankovitch cycles). Earth's internal boundary conditions, such as paleogeography, the presence/absence of polar icecaps, atmospheric/oceanic chemistry and sea level, provide distribution and feedback mechanisms for the incoming heat. Variations in these internal boundary conditions may happen abruptly or, as in the case of plate tectonics, take millions of years. We use geochemical and sedimentological techniques to investigate the response of ocean chemistry, regional aridity and atmospheric and oceanic circulation patterns to climate change during both greenhouse and icehouse climates.

To explore the connection between orbitally-forced changes in solar insolation, continental aridity and wind, we generated a high-resolution dust record for ~58 Myr old deep-sea sediments from Shatsky Rise. Our data provide the first evidence of a

correlation between dust flux to the deep sea and orbital cycles during the Early Paleogene, indicating dust supply (regional aridity) responded to orbital forcing during the last major interval of greenhouse climate. The change in dust flux was comparable to that during icehouse climates implying subtle variations in solar insolation have a similar impact on climate during intervals of over-all warmth as they do during glacial-interglacial states.

The Carboniferous Period (359-299 Ma) marks a critical time in Earth's history when a series of tectonic and biological events caused a shift in the mean climate state from a global "greenhouse" to an "icehouse". Geochemical records extracted from sedimentary rocks deposited in shallow epicontinental seaways are increasingly being used to infer relationships between tectonism, carbon cycling and climate and therefore are assumed to reflect global ocean processes. We analyzed radiogenic isotopes in biogenic apatite along a North American transect to constrain the degree of geochemical coupling between the epicontinental seas and the open ocean. Our results argue strongly for decoupling of North American seaways from the open ocean by latest Mississippian time.

DEDICATION

To my family and friends who believed in me and helped me along the way.

ACKNOWLEDGEMENTS

I would like to thank my advisor and committee chair, Dr. Debbie Thomas, and my committee members, Dr. Marcantonio, Dr. Slowey, Dr. Grossman, and Dr. Lyle, for their guidance and support throughout the course of this research.

I extend my gratitude to the National Science Foundation, the Consortium for Ocean Leadership and the Texas Higher Education Coordinating Board for funding my research. This research used samples and data provided by the Integrated Ocean Drilling Program (IODP). I would like to acknowledge Drs. U. Röhl, T. Westerhold and S. Hovan for their help with Chapter II. I am indebted to Dr. B. Miller, Dr. A. Lyle, Dr. T. Olszewski, Dr. T. Yancey, Dr. A. Raymond, Dr. R. Popp, Dr. R. Guillemette Dr. D. Murphy, Dr. J. Strauss, Kelly Cole, Christopher F. Paul, Jonathan Sneed, Luz Romero and Matthew Hensley for providing laboratory, intellectual and technical support.

Appreciation also goes to my friends and colleagues at the Department of Oceanography faculty and staff for making my time at Texas A&M University a great experience. Finally, thanks to my family and Ricky Smith for their encouragement, patience and love.

TABLE OF CONTENTS

Page

ABSTRACT iii

DEDICATION v

ACKNOWLEDGEMENTS vi

TABLE OF CONTENTS vii

LIST OF FIGURES x

LIST OF TABLES xii

CHAPTER

I INTRODUCTION 1

II EVIDENCE FOR ORBITAL FORCING OF DUST ACCUMULATION DURING THE EARLY PALEOGENE GREENHOUSE 4

- Introduction 4
- Dust as a Paleoclimate Proxy 12
- Study Location and Sampling Strategy 14
- Analytical Methods 16
  - Carbonate Content 16
  - Dust Extraction 21
  - Eolian Grain Size 22
  - Mass Accumulation Rates 23
  - Statistics 25
- Results 27
- Discussion 30
  - Causes of Cyclic Sedimentation 30
  - Climatic Implications of Orbitally-paced Dust Accumulation 33
  - Implications of Grain Size Distribution of Dust at Site 1209 36
- Conclusions 39

CHAPTER Page

III TH DERIVED DUST FLUXES TO THE TROPICAL PACIFIC OCEAN, 58 MA 41

Introduction 41
Material and Methods 46
Site and Samples 46
Analytical Methods 50
Results 55
Discussion 56
Comparison of Different Dust Proxies 56
Evaluating Potential Non-eolian and Diagenetic Contributions to Extracted "Dust" 58
Paleoclimatic Implications of the ^{232}Th -based Dust Fluxes 62
Dust Sources Inferred From $^{4}He_{crustal}$ /^{232}Th Ratios 64
Mass Balance: Th Distribution in the Sediments 69
Conclusions 76

IV PROVENANCE OF CENTRAL PACIFIC DUST, 58 MA 77

Introduction 77
Site Selections and Methods 80
Results 84
Discussion 85
Seawater vs. Dust Signals 85
Dust Provenance 91
Conclusions 97

V RADIOGENIC ISOTOPIC COMPOSTION OF CARBONIFEROUS SEAWATER FROM N. AMERICAN EPICONTINENTAL SEAS 99

Introduction 99
Geologic Setting and Samples 102
Patlanoaya 102
Arrow Canyon, Bird Spring Shelf 103
US Midcontinent 104
Eastern Shelf of the Midland Basin 105
Methods 106
Results 111
Assessing the Preservation of the Biogenic Apatite Radiogenic Isotope Signals 113
Carboniferous Record of Nd Isotopes in North American

CHAPTER Page

Epicontinental Seas 117
$\varepsilon_{Nd}(t)$ as an Indicator of Glacio-eustasy, Bird Spring Shelf, Arrow Canyon, NV 119
Paleoclimatic Implications 127

VI CONCLUSIONS 129

REFERENCES 131

APPENDIX A 159

APPENDIX B 160

APPENDIX C 161

VITA 162

LIST OF FIGURES

Page

Figure 2-1 Globally Correlated Sedimentary Cycles 8

Figure 2-2 Paleocene Location of Shatsky Rise..... 11

Figure 2-3 Bulk Sedimentation Rates and Carbonate Content 17

Figure 2-4 Dust Fluxes and Grain Size 26

Figure 2-5 Spectral Analysis 29

Figure 2-6 Comparison of Dust Mass Accumulation Rates, Crustal ^{4}He Fluxes and Sedimentary Coarse Fraction 32

Figure 3-1 Pacific Ocean Site Map 47

Figure 3-2 Comparison of Bulk Sedimentation Rates and Sedimentary Dust Using Different Proxies 54

Figure 3-3 ^{232}Th-^{4}He$_{crustal}$ Source Plot 66

Figure 3-4 Distribution of Th Among Different Sediment Fractions 71

Figure 4-1 Compiled Radiogenic Isotope Data for Shatsky Rise Site 1209 85

Figure 4-2 Sr-Nd Isotope Source Plot for Dust..... 92

Figure 4-3 Potential Dust Sources and Transport Pathways to Site 1209, 58 Ma 94

Figure 4-4 Sr-Nd Isotope Source Plot for Shatsky Rise, North Africa and Asia..... 95

Figure 5-1 Paleogeographic Reconstructions of Carboniferous North America 100

Figure 5-2 Comparison of Nd Isotope Records from Different Types of Biogenic Apatite 111

Figure 5-3 Carboniferous $\varepsilon_{Nd}(t)$ of North American Epicontinental Seas 113

Figure 5-4 Carboniferous Global Marine Sr Isotopic Curve..... 114

Page

Figure 5-5 Crossplot of $\varepsilon_{Nd}(t)$ and $^{87}Sr/^{86}Sr$ 115

Figure 5-6 Mid-Carboniferous $\varepsilon_{Nd}(t)$ Record for Arrow Canyon 121

Figure 5-7 Detrital Sources to North American Epicontinental Seas 123

LIST OF TABLES

		Page
Table 2-1	Carbonate and Dust Data for Shatsky Rise, Site 1209	18
Table 2-2	Sedimentation Rates and Age Models for Site 1209	24
Table 3-1	Sedimentary [Th] for Site 1209	49
Table 3-2	[Th] of Biogenic and HH Leachable Sedimentary Fractions	52
Table 3-3	[Th] of Extracted “Dust”	52
Table 4-1	Radiogenic Isotope Data for Site 1209 Dust	83
Table 4-2	Radiogenic Isotope Data for 58 Ma Biogenics from Site 1209	86
Table 5-1	Sr and Nd Isotope Data for Carboniferous Biogenic Apatite	108
Table 5-2	Detrital Sources to North American Epicontinental Seas	124

CHAPTER I

INTRODUCTION

Global climate is controlled by two factors, the amount of heat energy received from the sun (solar insolation) and the way that heat is distributed Earth's surface. Solar insolation varies on timescales of 10s to 100s of thousands of years based on changes in the path of Earth's orbit about the sun (Milankovitch cycles). Earth's internal boundary conditions, such as paleogeography, the presence or absence of large ice sheets, evolution of organisms, atmospheric greenhouse gas concentrations, ocean chemistry and sea level, provide distribution and feedback mechanisms for the heat energy received. Variations in these internal boundary conditions may happen abruptly or, as in the case of plate tectonics, take millions of years. The sedimentary record provides a rich archive of these climatic and environmental variations over geologic time.

Over the Phanerozoic (past ~600 million years), Earth's climate has transitioned between relatively ice-free episodes (greenhouse), characterized by warm deep ocean temperatures and overall global warmth, and periods of extreme cold with extensive glaciation and permanent polar ice (icehouse). The wholesale shift between global "greenhouse" and "icehouse" climate modes happens gradually over millions of years, yet higher frequency changes are superimposed on the long term climate trend implying

---

This dissertation follows the style of *Paleoceanography*.

a certain level of climate variability regardless of the overall climate state. The temporal resolution of the geologic archive determines what questions we can answer about the evolution of Earth's climate.

Here, we examine the response of the ocean and atmosphere to climate change on two very different geologic timescales. We use deep-sea sediments to generate the first high resolution dust record capable of resolving changes in continental aridity and wind patterns on orbital timescales ~58 million years ago, during the early Cenozoic "greenhouse". This investigation provides a framework for understanding environmental responses to short-term climate variability driven by changes in solar insolation during an overall climate state very different from todays. We also generate a long term radiogenic isotope record to explore the transition from global "greenhouse" to "icehouse" during the Carboniferous Period (359-299 million years ago) using fossils from shallow marine rocks from North America. The resolution of the record we generated allows us to consider long-term variations in ocean circulation patterns as a result of tectonic uplift and closure of a circum-equatorial oceanic gateway as well as the degree of geochemical coupling between records from the shallow epicontinental seaways and the open ocean.

These studies contribute to our understanding of climate in different ways. Higher resolution studies provide a means of assessing the regional response of climate and the environment within the context of an overall "greenhouse" or "icehouse", while long-term studies provide insight into mechanisms driving changes in the global climate state. Our record of early Cenozoic dust fluxes indicates an environmental response to

orbital-forcing is comparable to that seen on glacial-interglacial timescales, implying processes operating during greenhouse intervals have a significant and similar impact on climate as during icehouse intervals.

CHAPTER II

EVIDENCE FOR ORBITAL FORCING OF DUST ACCUMULATION DURING THE EARLY PALEOGENE GREENHOUSE*

Introduction

The record of cyclic orbital variations in solar insolation (Milankovitch cycles) extends throughout most of Earth's history. The long-term persistence of all three Milankovitch cycles (precession, obliquity, and eccentricity) in the geologic record indicates that orbital insolation variations have had an impact on regional and global climate regardless of overall climate state. Yet, the expression of orbital cyclicity in the sedimentary archive has varied through geologic time [*Arthur et al.,* 1986; *Herbert and D'Hondt,* 1990; *Herbert et al.,* 1995; *MacLeod et al.,* 2001], likely as a consequence of changes in Earth's internal boundary conditions (e.g., the presence or absence of large ice sheets, variations in atmospheric greenhouse gas concentrations, ocean chemistry, sea level, and paleogeography).

Although strong interrelationships exist among the various Milankovitch parameters (e.g., precessional modulation by eccentricity), each orbital component influences a particular aspect of the climate system. Precessional variations in insolation are known to impact low latitude climate patterns by changing the seasonality of

---

*Reprinted with permission from "Evidence for orbital forcing of dust accumulation during the Early Paleogene greenhouse" by S.C. Woodard, D.J. Thomas, S. Hovan, U. Röhl and T. Westerhold, 2011. *Geochemistry, Geophysics, Geosystems*, 12, Q02007, copyright [2011] by American Geophysical Union.

insolation, and therefore seasonal contrasts, thereby exerting strong influence on the monsoons which ultimately determine precipitation [*Labeyrie et al.,* 2002]. Obliquity or the Earth's axial tilt, determines the sun's elevation above the horizon and therefore, the amount of summer insolation received at high latitudes [e.g. *Imbrie et al.,* 1993]. Changes in the distribution of insolation on Earth's surface, and consequently temperature gradients, may be a mechanism to connect low and high latitude climate by enhancing poleward material fluxes [*Raymo and Nisancioglu,* 2003]. Eccentricity variations directly influence the average solar insolation reaching Earth. Eccentricity cycles seem to dominate some climate records, yet researchers struggle to explain this climate response when the shorter orbital frequencies of precession and obliquity have more influence over the distribution of heat on Earth's surface. It may be that longer periodicities observed in the geologic record simply reflect an increasingly non-linear response of the climate system to precessional or obliquity forcing [e.g. *Maslin and Ridgwell,* 2005; *Liu et al.,* 2008].

During the Plio-Pleistocene icehouse, orbital cycles identified in stable isotope records are also found in the record of dust supply to the oceans and ice [*Rea,* 1994; *Tiedemann et al.,* 1994; *Rea et al.,* 1985; *Hovan et al.,* 1989; *Petit et al.,* 1999*; Svensson et al.,* 2000; *Winckler et al.,* 2008], deep-ocean circulation patterns [*Boyle and Keigwin*, 1987], deep-ocean carbonate ion concentrations [*Farrell and Prell,* 1989], and atmospheric greenhouse gas concentrations [*Petit et al*., 1999]. Variations in these climate parameters are all linked, directly or indirectly, to major fluctuations in

continental ice sheets and global temperatures [*Berger and Loutre*, 2004; *Short et al,* 1991].

Similar orbital cycles are recorded in deep-sea sediments of Early Paleogene age [e.g., *Norris and Röhl, 1999*; *Röhl et al.,* 2000, 2001, 2003, 2007; *Pälike et al.,* 2001; *Westerhold et al.,* 2007, 2008] – the last major greenhouse interval, ~65-45 million years ago. Numerous lines of evidence indicate that the Early Paleogene was a period of greenhouse global warmth, with little to no evidence of permanent ice at the poles [e.g., *Sluijs et al.,* 2009]. For example, evidence from recent drilling in the Arctic Ocean basin indicates a warm and brackish environment [*Moran et al.,* 2006; *Pagani et al.,* 2006] with warm-temperate, mixed conifer/deciduous forests colonizing the northern high-latitudes [*Sluijs et al.,* 2006; 2009]. The fossil record shows the range of subtropical flora extended at least to the mid-latitudes [*Hunt and Poole,* 2003; *Greenwood and Wing,* 1995], and mixed thermophilic/temperate insect assemblages are suggestive of a "highly equable climate" [*Greenwood et al.,* 2005]. Measurements of $\delta^{18}O$ in benthic foraminiferal tests estimate mid-late Paleocene deep-water temperatures of 7-10°C [e.g., *Zachos et al.,* 2001], implying high-latitude sea surface temperatures far above freezing. There is only very limited evidence of permanent polar ice during the early Cenozoic [*Schmitz,* 2003; *DeConto and Pollard,* 2003]. Thus the orbital frequency cycles found in Early Paleogene sediments cannot be attributed to the waxing and waning of large ice sheets, and must, therefore, reflect some other climatic response to changes in solar insolation.

Early Paleogene deep-sea sediments recovered from the western North Atlantic (Blake Nose), the southern Atlantic (Walvis Ridge) and the northwest Pacific (Shatsky Rise) contain lithologic cycles with established and accepted periodicities of 100 kyr and 400 kyr (Figure 2-1) [*Röhl et al.,* 2001, 2003; *Westerhold et al.,* 2008]. The cyclic lithology is precisely correlated among all locations and is sufficiently long and continuous to imply a global-scale controlling mechanism – orbitally forced changes in insolation. Furthermore, the cyclostratigraphy established by the global correlation of the lithologic cycles [*Westerhold et al.,* 2008] is now accepted as the basis for the Paleogene timescale, enabling the most precise inter-site correlation possible and cited as evidence for the relative completeness of various stratigraphic sections [e.g., *Schulte et al.,* 2010]. However, the connection between orbital scale lithologic cycles and the presumed associated insolation forcing is more spatially variable for Cretaceous and early Paleogene sediments than during the Pleistocene, suggesting a more complex climatic response. For example, lithologic cycles in Early Paleogene and Late Cretaceous Blake Nose sediments are dominated by the precessional cycle with a minor component of eccentricity [e.g., *MacLeod et al.,* 2001]. These cycles are interpreted to reflect productivity variations driven by cyclic changes in upwelling intensity and/or delivery of nutrients via continental weathering [*Kroon et al.,* 2001; *Norris and Röhl*, 1999; *Pälike et al.*, 2001; *Röhl et al.,* 2000; 2001; 2003; 2007]. Precessional and eccentricity cycles in the South Atlantic (Rio Grande Rise and Walvis Ridge) may reflect changes in carbonate dissolution rates, terrigenous sediment supply, or sea surface productivity [*Herbert and D'Hondt,* 1990; *Herbert et al.,* 1995]. Unraveling the nature of the lithologic cycles

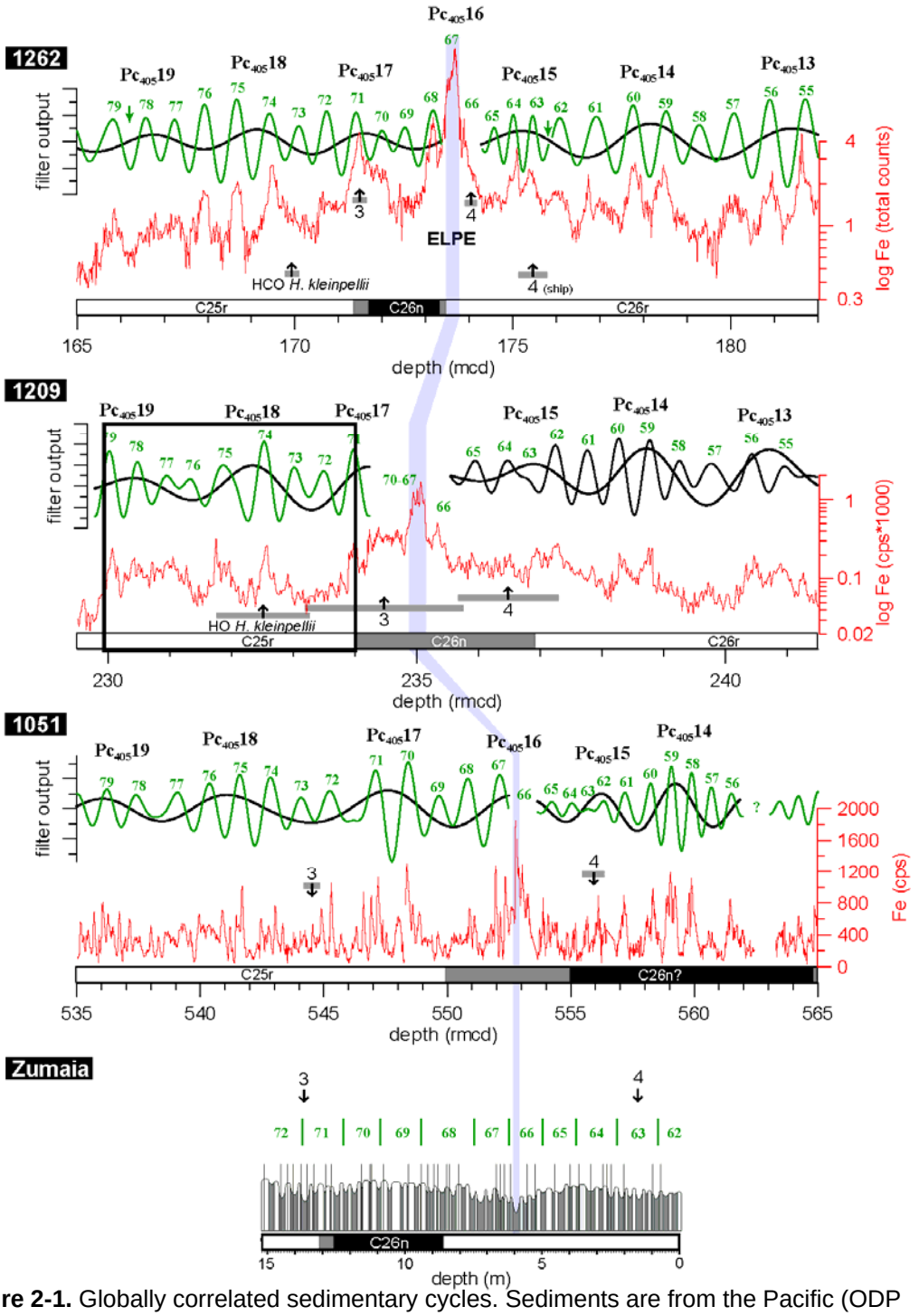

Figure 2-1. Globally correlated sedimentary cycles. Sediments are from the Pacific (ODP Site 1209) and the Atlantic (ODP Sites 1262, 1051) Oceans as well as land section Zumaia used for orbital calibration of Paleocene time [*Westerhold et al.,* 2008]. Black box highlights section used in this study, 800 kyr interval spanning ~4.2 m of sediments from Site 1209, Shatsky Rise. Reprinted from Palaeogeography Palaeoclimatology Palaeoecology, 257, *Westerhold et al.*, Astronomical calibration of the Paleocene time, p. 387, Copyright (2008), with permission from Elsevier.

(e.g., what are the relative changes in dissolution, terrigenous inputs, productivity, etc.) is crucial toward understanding which aspects of the climate system are impacted by orbital variations in insolation.

The first step toward understanding how orbitally driven changes in insolation impact climate during greenhouse intervals is to reconstruct how the input signal is translated to the sedimentary record. The biogenic carbonate component of marine sediments has been a sensitive recorder of orbital cyclicity throughout geologic time [e.g., *Arthur et al.,* 1986; *Bottjer et al.,* 1986; *Herbert and D'Hondt,* 1990], because several aspects of the climate system ultimately dictate carbonate content in deep-sea sediments. The calcium carbonate content of pelagic sediments is controlled by surface-water production of carbonate microfossils (supply), the preservation of carbonate during sedimentation and burial (dissolution), and the flux of other sedimentary constituents (dilution). Thus a decrease in sedimentary carbonate content may result from diminished production, increased dissolution, a relative increase in terrigenous sediment supply, or a combination of these factors. Each of these factors is a function of prevailing climate parameters. Sea-surface productivity is strongly dependent on wind stress and upwelling of nutrient-rich waters, or nutrient inputs from weathering and runoff. The corrosiveness of deep and bottom waters is controlled by atmospheric pCO_2 and deep-ocean circulation. Delivery of terrigenous sediments to the deep sea, by wind or hemipelagic plumes, depends upon on continental weathering and runoff, both of which are tied to regional climate

It is likely that several of the above climatic parameters varied in concert during the Early Paleogene as they did during the Pleistocene. Thus, identifying which factors controlled the accumulation of calcium carbonate and caused the lithologic cycles with orbital frequencies is complicated. However, we can eliminate several variables through careful selection of the study location. In remote regions of the ocean, far from any paleo-shoreline, the only likely source of continentally derived materials is the wind [*Rea,* 1994; *Rea et al.,* 1985]. By selecting a site located in the center of an ocean basin during the targeted study interval, we can eliminate cyclic changes in hemipelagic inputs as a mechanism for diluting the calcium carbonate content. Furthermore, if the paleo-location of the site was within a subtropical gyre, sea surface productivity would have been consistently low and relatively stable, effectively eliminating cyclic changes in carbonate production as a variable.

Shatsky Rise presents such a location. During the Early Paleogene, paleo-geographic reconstructions place Shatsky Rise in the center of the subtropical Pacific gyre, far from the continents (Figure 2-2) [*Hay et al.,* 1999]. A section of ~58 Myr old sediments recovered from the rise during Ocean Drilling Program (ODP) Leg 198 consists predominantly of nannofossil ooze with varying amounts of clay. The lithologic cycles manifest as slight variations in sedimentary carbonate identified by changes in magnetic susceptibility and sedimentary Fe content. In deep-sea sediments, variations in magnetic susceptibility and Fe content are often inversely proportional to carbonate content and likely represent changes in terrigenous clay minerals. It is important to note that the Fe content is not itself a direct proxy of terrigenous silicate minerals, but a useful

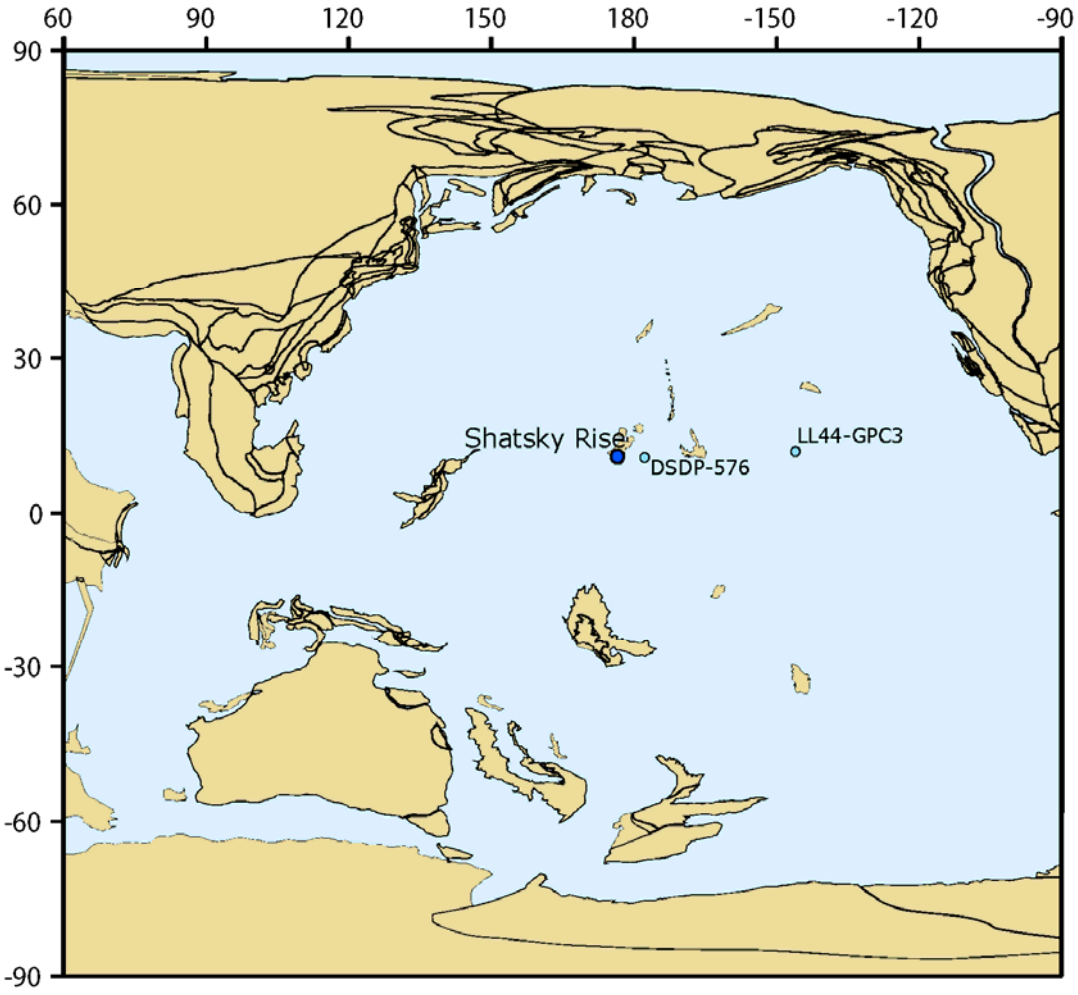

Figure 2-2. Paleocene location of Shatsky Rise. ODP Site 1209 (blue), LC44-GPC3 and DSDP Site 576 (light blue), in the Pacific Ocean. Black lines denote plate boundaries and do not imply elevation above sea level. 58 Ma plate reconstruction was created based on magnetic frame of reference (www.odsn.de; *Hay et al.* [1999]).

first order gauge of clay content. The concentration of terrigenous material must be determined independently. By selecting Shatsky Rise as the study location, we can effectively eliminate two of the four potential causes of the recorded lithologic cycles: hemipelagic inputs and significant variations in sea surface productivity. Thus, we focus on the relative contributions of dust accumulation (as a potential mechanism for

carbonate dilution) and carbonate dissolution to the generation of the recorded lithologic cycles.

Dust as a Paleoclimate Proxy

The mineralogy of alumino-silicate material deposited on the seafloor is similar to that of atmospheric dust transported by the overlying winds [*Windom,* 1975; *Prospero et al.,* 1981; *Janecek and Rea,* 1983; *Chuey et al.,* 1987]. This suggests ocean currents do not transport eolian material significant distances after it settles to the sea surface. Researchers have exploited this observation by using eolian material isolated from deep-sea sediments as a proxy for atmospheric circulation patterns and vigor [*Clemens*, 1998; *Janecek and Rea,* 1983; 1985; *Hovan and Rea,* 1992], dust source regions and changes in the aridity and/or vegetation cover of those regions [*Rea,* 1994; *Kohfield and Harrison,* 2001; *Vandenberg and Jarrard,* 2004; *Stancin et al.,* 2008].

Eolian grain size and mass accumulation rates (MARs) fluctuate independently, implying each records the response of a different combination of environmental parameters [e.g., *Rea,* 1994]. The average grain size of dust deposited in the open ocean indicates wind intensity [*Hovan and Rea,* 1992; *Rea,* 1994] or shifts in the location of prevailing winds (e.g., features such as the ITCZ or westerlies) [*Janecek and Rea,* 1985; *Prospero,* 2002; *Hyeong et al.,* 2006]. In order for dust to be transported long distances the velocity of the transporting wind must be sufficiently strong to keep it suspended in the atmosphere [*Pye,* 1987]. Therefore, changes in the average grain size of

accumulating dust are interpreted to reflect variations in wind strength over the region throughout time.

The rate of dust accumulation in a given location depends upon the load carried by the wind. This is controlled by several factors, notably the aridity of the dust source region and its proximity to the depositional site [e.g., *Rea,* 1994 and references therein], hydrologic cycling, wind intensity, vegetation cover, and glacial erosion [e.g., *Harrison et al.,* 2001 and references therein]. Arid regions tend to produce the most dust [e.g., *Clemens and Prell,* 1990; *Harrison et al.,* 2001]. Yet a region needs some level of rainfall to facilitate weathering of rock minerals and soil development, which ultimately supply material of suitable size to be entrained by the winds. If a region becomes hyper-arid (< 100 mm of precipitation annually), dust generation declines and thus, dust flux declines [*Pye,* 1989]. While the development of hyper-arid conditions is of some concern, decreased dust MARs in the sedimentary record are typically interpreted to represent more a humid climate at the dust source [*Rea,* 1994; *Hovan et al.,* 1989; *Vandenberg and Jarrard,* 2004; *Holmes et al,* 2004].

Dust is produced by erosion of soils and exposed unconsolidated sediments scoured by the wind [*Gillette, 1977*; *Alfaro and Gomes,* 2001]. In order for dust to be transported out over the oceans far from its source, it must be injected sufficiently high into the atmosphere [*Pye,* 1987; *Rea,* 1994]. Large windstorms are an obvious mechanism for entraining dust and moving it to the upper troposphere where it can travel great distances. Therefore, the injection of dust into the atmosphere is likely to occur in pulses brought about by seasonal variations in wind intensity and storms [*Windom,* 1975;

Pye, 1987]. New work by *McGee et al.* [2010] supports this notion, suggesting the "gustiness" related to steep meridional temperature gradients was the fundamental driver of glacial increases in dust accumulation. *Clemens* [1998] observed a seasonal dust deposition in the Arabian Sea related to the onset of summer monsoonal circulation. This indicates dust accumulation records may reflect variations in storm frequency rather than changes in environmental parameters such as source region aridity or relative wind intensity. However, in regions of the ocean where sedimentation rates are low, benthic organisms mix the uppermost sediments, removing any seasonal signals. Therefore, in slowly accumulating marine sediments bioturbation smears temporally fluctuating signals such that only robust climatic shifts occurring on timescales >1000 years are preserved in the lithologic record [*Rea et al.,* 1985].

Study Location and Sampling Strategy

Shatsky Rise, presently in the northwest Pacific Ocean (32°N, 158°E), is the only location with a known orbital lithologic record of Paleocene age appropriate for investigating changes in atmospheric dust. Plate reconstructions place Shatsky Rise in the center of the northern tropical Pacific (~15-20° N) near the center of the subtropical gyre, during the early Paleogene [*Hay et al.,* 1999] (Figure 2-2). The paleo-location, remote from ocean ridges and active volcanoes, makes significant contribution of ash to the sediments, and subsequent alteration of the eolian signal, unlikely. The southern end of the rise presents a simplified depositional environment where the oligotrophic waters of the ancient gyre resulted in low, relatively stable production rates [*Bralower et al.,*

2006]. Most importantly, the distance of this site far from any ancient coastline makes wind the most likely mechanism for terrigenous sediment delivery.

We analyzed sediments from ODP Site 1209, situated on the southern high of Shatsky Rise, at ~2300 m paleo-water depth. At this site the recovered sedimentary section appears exclusively pelagic and uninfluenced by bottom water currents [*Bralower et al.,* 2002]. The early Paleogene age sediment is dominantly very fine-grained material (nannofossils and clay) with occasional horizontal laminations [*pers.observation, SCW 2007*], further indicating it did not experience post-depositional winnowing. We sampled approximately 4.2 m of the sedimentary section spanning eight consecutive 100 kyr eccentricity cycles that are ~58 million years old [*Westerhold and Röhl,* 2006; *Westerhold et al.,* 2008] (Figure 2-1, peaks 79-71). Eight to ten samples, spaced ~2-4 cm apart (representing ~6-10 kyr of time), were taken to adequately characterize each eccentricity cycle.

We chose an interval of "normal" sedimentation (excluding the late Paleocene – early Eocene hyperthermals) to examine the effect of orbital forcing on deep-sea lithology without the need to account for possible influences of anomalous climatic events. In particular, the extreme climate events in the geologic record (such as the Early Paleogene hyperthermals) have received great attention in the past decade as potential analogs for the rate and magnitude of future warming. However, it is equally important to understand the characteristic "background" variability of the "greenhouse" climate system. Our data provide a context for understanding the general relationships between

changes in orbital parameters, boundary conditions and climate during periods of overall global warmth.

Analytical Methods

All samples were freeze-dried to remove water. Approximately 0.5 g of sediment was separated and homogenized with an agate mortar and pestle for carbonate content analysis. The remaining 3-4 g of sediment subjected to chemical treatments to extract dust.

Carbonate Content

Percent total carbon was determined on bulk sediment samples using a UIC CM 5012 CO_2 Coulometer at Texas A&M University. Five to 10 mg samples were weighed into ceramic boats and combusted at 1000°C in a high temperature furnace. Coulometer measurements were taken using a 3-4 minute count time and one minute purge time between samples. Analyses of two lab standards, reagent grade sucrose (%C = 41.6% ± 0.6, 2s.d., N=21) and Midway sediment (%C = 2.64% ± 0.04, 2s.d., N=525) were used to monitor instrument performance. Replicates were analyzed for one quarter of the samples and are included in Table 2-1; averages corrected for organic carbon content are plotted as percent carbonate in Figure 2-3.

Four samples (~50 mg each) were acidified using 1N HCl to remove carbonate, then analyzed for organic carbon content. Percentages of organic carbon were low and uniform between samples. The average organic carbon content (0.04 ±0.009%, 2 s.d.)

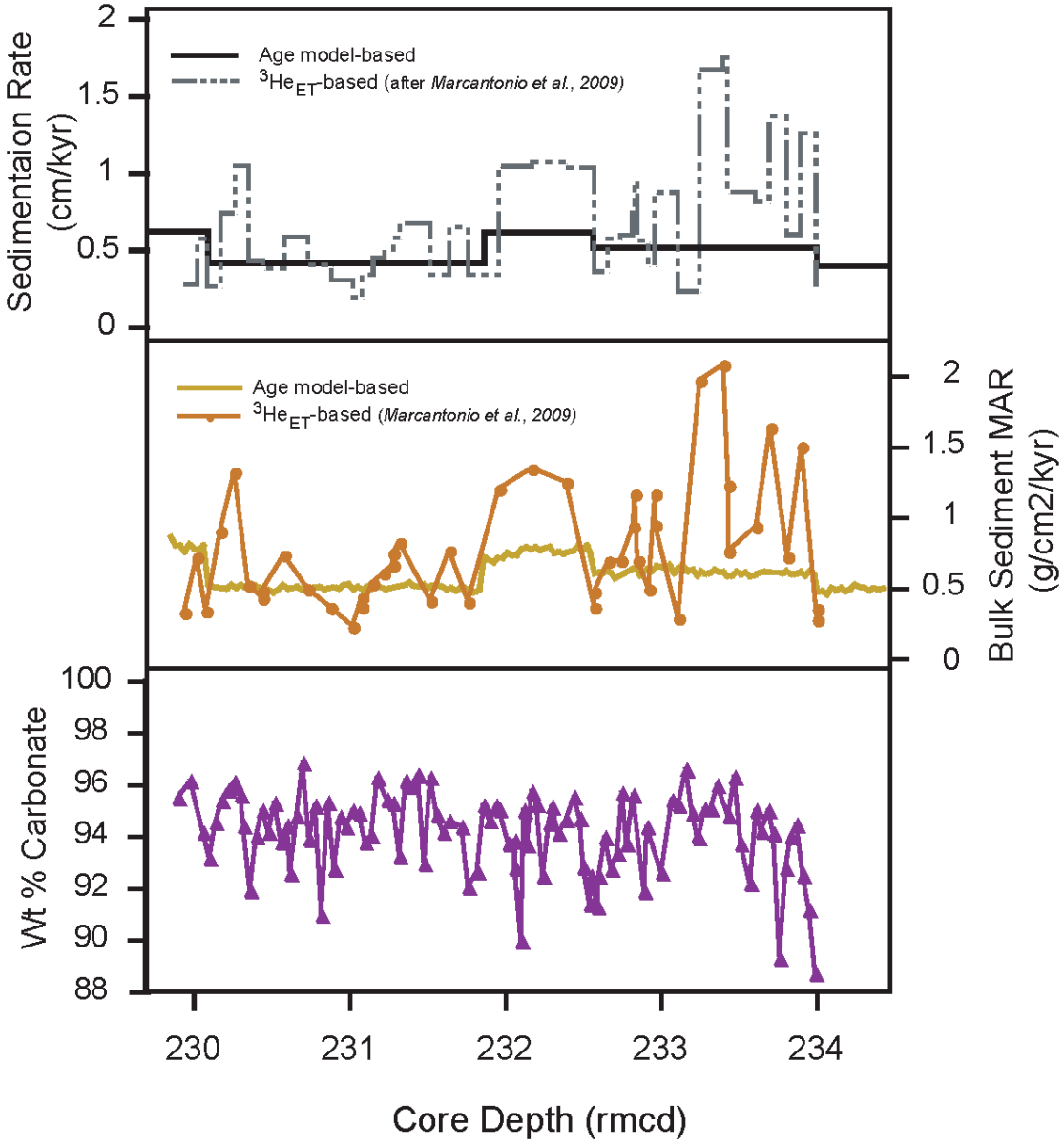

Figure 2-3. Bulk sedimentation rates and carbonate content. Comparison of linear sedimentation rates (LSR) calculated from tie points used in orbital calibration of *Westerhold et al.,* [2008] option 1 and sediment fluxes derived using $^{3}He_{ET}$ constant flux as well as bulk sediment mass accumulation rates (MARs) determined using both LSR-based and $^{3}He_{ET}$-based sedimentation models. Sedimentary carbonate content (wt %) is shown in purple.

was subtracted from the measured total carbon to determine percent carbonate for each sample (Figure 2-3).

Table 2-1. Carbonate and Dust Data for Shatsky Rise, Site 1209

Sedimentary Carbonate Content					Eolian Mass Accumulation Rates and Grain Size								
Sample ID			Core Depth	% CaCO3	Sample ID			Core Depth	Dust Fraction	Dry Bulk Density	Dust MAR	Median Particle Diameter	
**	Hole	Core-Section, Interval (cm)	rmcd		**	Hole	Core-Section, Interval (cm)	rmcd	mg/g sed	g/cm^3	mg/cm^2/kyr	µm	ϕ_{50}
	1209C	12-4 10-11	229.89	95.51		1209C	12-4 28-29	230.07	10.541	1.293	8.51	2.72	8.52
	1209C	12-4 18-19	229.97	96.14		1209C	12-4 32-33	230.11	8.802	1.231	4.54	2.93	8.42
R	1209C	12-4 18-19	229.97	96.21		1209C	12-4 37-38	230.16	6.241	1.223	3.20	2.76	8.50
	1209C	12-4 26-27	230.05	94.11		1209C	12-4 42-43	230.21	3.932	1.208	1.99	2.50	8.64
R	1209C	12-4 26-27	230.05	94.23		1209C	12-4 44-45	230.23	4.113	1.267	2.18	2.59	8.59
	1209C	12-4 30-31	230.09	92.12		1209C	12-4 46-47	230.25	3.989	1.213	2.03	-----	-----
R	1209C	12-4 30-31	230.09	93.85		1209C	12-4 52-53	230.31	6.177	1.267	3.28	3.03	8.37
R	1209C	12-4 30-31	230.09	93.61		1209C	12-4 56-57	230.35	6.383	1.205	3.22	2.58	8.60
	1209C	12-4 34-35	230.13	93.95		1209C	12-4 60-61	230.39	8.030	1.250	4.20	2.63	8.57
R	1209C	12-4 34-35	230.13	95.19		1209C	12-4 64-65	230.43	6.733	1.213	3.42	2.54	8.62
	1209C	12-4 38-39	230.17	94.87	R	1209C	12-4 64-65	230.43	10.835	1.192	5.41	-----	-----
R	1209C	12-4 38-39	230.17	95.97		1209C	12-4 68-69	230.47	7.590	1.176	3.74	2.62	8.58
	1209C	12-4 42-43	230.21	95.81		1209C	12-4 72-73	230.51	6.099	1.136	2.90	2.61	8.58
	1209C	12-4 44-45	230.23	96.15		1209C	12-4 75-76	230.54	5.211	1.189	2.60	2.71	8.53
R	1209C	12-4 44-45	230.23	95.74		1209C	12-4 78-79	230.57	5.979	1.259	3.15	2.40	8.70
	1209C	12-4 46-47	230.25	96.12		1209C	12-4 81-82	230.6	4.004	1.208	2.03	2.80	8.48
	1209C	12-4 50-51	230.29	95.64		1209C	12-4 84-85	230.63	9.551	1.210	4.84	2.65	8.56
	1209C	12-4 52-53	230.31	94.44		1209C	12-4 88-89	230.67	7.056	1.227	3.63	2.34	8.74
	1209C	12-4 56-57	230.35	91.95		1209C	12-4 93-94	230.72	6.662	1.226	3.42	2.44	8.68
	1209C	12-4 60-61	230.39	94.03		1209C	12-4 96-97	230.75	4.601	1.216	2.34	2.69	8.54
	1209C	12-4 64-65	230.43	95.24		1209C	12-4 100-101	230.79	6.812	1.224	3.49	2.32	8.75
R	1209C	12-4 64-65	230.43	94.83		1209C	12-4 104-105	230.83	5.846	1.186	2.90	2.85	8.45
	1209C	12-4 68-69	230.47	94.18		1209C	12-4 108-109	230.87	5.043	1.211	2.56	2.57	8.61
	1209C	12-4 72-73	230.51	95.32		1209C	12-4 112-113	230.91	6.580	1.215	3.35	2.87	8.44
	1209C	12-4 76-77	230.55	94.21		1209C	12-4 118-119	230.97	9.486	1.267	5.04	2.59	8.59
R	1209C	12-4 76-77	230.55	92.47		1209C	12-4 122-123	231.01	9.251	1.196	4.63	2.41	8.70
R	1209C	12-4 76-77	230.55	94.68		1209C	12-4 126-127	231.05	7.739	1.229	3.98	2.77	8.50
	1209C	12-4 80-81	230.59	94.44		1209C	12-4 128-129	231.07	8.069	1.191	4.02	2.60	8.59
	1209C	12-4 82-83	230.61	92.11		1209C	12-4 132-133	231.11	7.411	1.232	3.82	2.83	8.46
R	1209C	12-4 82-83	230.61	93.05		1209C	12-4 134-135	231.13	5.959	1.197	2.99	2.58	8.60
	1209C	12-4 86-87	230.65	94.82		1209C	12-4 138-139	231.17	6.195	1.250	3.24	2.66	8.55
	1209C	12-4 90-91	230.69	96.87		1209C	12-4 144-145	231.23	4.765	1.192	2.38	2.52	8.63
	1209C	12-4 94-95	230.73	93.92		1209C	12-4 148-149	231.27	5.342	1.188	2.66	2.63	8.57
	1209C	12-4 98-99	230.77	95.22		1209C	12-5 2-3	231.31	3.836	1.188	1.91	2.57	8.61
	1209C	12-4 102-103	230.81	92.19		1209C	12-5 6-7	231.35	3.532	1.263	1.87	2.55	8.61
R	1209C	12-4 102-103	230.81	89.66		1209C	12-5 10-11	231.39	1.563	1.306	0.85	2.81	8.48
R	1209C	12-4 102-103	230.81	91.13		1209C	12-5 14-15	231.43	2.342	1.242	1.22	2.94	8.41
	1209C	12-4 106-107	230.85	95.33		1209C	12-5 18-19	231.47	2.434	1.271	1.30	2.74	8.51
R	1209C	12-4 106-107	230.85	95.34		1209C	12-5 22-23	231.51	2.638	1.224	1.35	2.67	8.55
	1209C	12-4 110-111	230.89	92.78		1209C	12-5 26-27	231.55	-----	-----	-----	2.65	8.56
	1209C	12-4 114-115	230.93	94.79		1209C	12-5 42-43	231.71	6.198	1.210	3.14	2.74	8.51
	1209C	12-4 118-119	230.97	94.39		1209C	12-5 46-47	231.75	10.438	1.203	5.26	2.69	8.54
	1209C	12-4 122-123	231.01	94.76		1209C	12-5 50-51	231.79	10.309	1.141	4.93	2.54	8.62

Table 2-1. continued

Sedimentary Carbonate Content					Eolian Mass Accumulation Rates and Grain Size								
	Sample ID		Core Depth	% CaCO3		Sample ID		Core Depth	Dust Fraction	Dry Bulk Density	Dust MAR	Median Particle Diameter	
**	Hole	Core-Section, Interval (cm)	rmcd		**	Hole	Core-Section, Interval (cm)	rmcd	mg/g sed	g/cm^3	mg/cm^2/kyr	μm	ϕ_{50}
R	1209C	12-4 122-123	231.01	95.30		1209C	12-5 54-55	231.83	6.693	1.181	3.31	2.64	8.57
	1209C	12-4 126-127	231.05	94.93		1209C	12-5 58-59	231.87	8.471	1.173	6.16	2.93	8.42
	1209C	12-4 130-131	231.09	93.80		1209C	12-5 62-63	231.91	12.644	1.114	8.73	2.78	8.49
	1209C	12-4 134-135	231.13	94.06		1209C	12-5 66-67	231.95	5.909	1.157	4.24	2.54	8.62
	1209C	12-4 138-139	231.17	96.30		1209C	12-5 70-71	231.99	6.334	1.157	4.54	2.94	8.41
	1209C	12-4 144-145	231.23	95.44		1209C	12-5 74-75	232.03	7.212	1.197	5.35	2.77	8.49
	1209C	12-4 148-149	231.27	95.32		1209C	12-5 78-79	232.07	3.766	1.197	2.79	2.60	8.59
	1209C	12-5 2-3	231.31	94.97		1209C	12-5 81-82	232.1	3.759	1.264	2.94	2.61	8.58
R	1209C	12-5 2-3	231.31	91.56		1209C	12-5 87-88	232.16	3.751	1.261	2.93	2.70	8.54
	1209C	12-5 6-7	231.35	96.17		1209C	12-5 90-91	232.19	2.683	1.280	2.13	2.78	8.49
	1209C	12-5 10-11	231.39	95.97		1209C	12-5 93-94	232.22	2.472	1.256	1.92	2.85	8.46
	1209C	12-5 14-15	231.43	96.39		1209C	12-5 97-98	232.26	3.724	1.275	2.94	2.66	8.55
	1209C	12-5 18-19	231.47	92.98		1209C	12-5 102-103	232.31	3.656	1.218	2.76	2.64	8.56
	1209C	12-5 22-23	231.51	96.31		1209C	12-5 106-107	232.35	4.714	1.232	3.60	2.77	8.50
	1209C	12-5 26-27	231.55	94.84		1209C	12-5 109-110	232.37	3.247	1.211	2.44	2.72	8.52
	1209C	12-5 30-31	231.59	94.18		1209C	12-5 113-114	232.42	6.944	1.245	5.36	2.66	8.56
	1209C	12-5 34-35	231.63	94.54		1209C	12-5 117-118	232.46	6.576	1.296	5.28	2.58	8.60
R	1209C	12-5 34-35	231.63	94.71		1209C	12-5 122-123	232.51	11.366	1.306	9.19	2.72	8.52
	1209C	12-5 42-43	231.71	94.40		1209C	12-5 128-129	232.56	13.009	1.178	7.94	2.49	8.65
	1209C	12-5 46-47	231.75	92.08		1209C	12-5 134-135	232.61	8.426	1.194	5.21	2.77	8.50
	1209C	12-5 52-53	231.81	92.67		1209C	12-5 138-139	232.65	4.951	1.211	3.11	2.69	8.54
	1209C	12-5 56-57	231.85	94.22		1209C	12-5 142-143	232.68	5.675	1.176	3.46	2.83	8.47
R	1209C	12-5 56-57	231.85	96.22		1209C	12-5 147-148	232.73	4.312	1.232	2.75	2.82	8.47
	1209C	12-5 60-61	231.89	94.63		1209C	12-6 2-3	232.77	4.437	1.232	2.83	2.76	8.50
	1209C	12-5 64-65	231.93	95.20		1209C	12-6 7-8	232.82	3.716	1.239	2.38	2.84	8.46
	1209C	12-5 66-67	231.95	95.07		1209C	12-6 10-11	232.84	3.938	1.255	2.56	2.88	8.44
	1209C	12-5 72-73	232.01	93.76		1209C	12-6 14-15	232.86	6.426	1.152	3.84	2.69	8.54
	1209C	12-5 76-77	232.05	94.90		1209C	12-6 16-17	232.91	4.658	1.240	2.99	2.85	8.46
	1209C	12-5 76-77	232.05	92.80		1209C	12-6 23-24	232.96	4.016	1.279	2.66	2.98	8.39
	1209C	12-5 80-81	232.09	90.00		1209C	12-6 27-28	232.99	32.880	1.266	17.43	2.85	8.45
	1209C	12-5 82-83	232.11	95.04		1209C	12-6 30-31	233.03	3.893	1.250	2.52	2.81	8.48
	1209C	12-5 84-85	232.13	93.70		1209C	12-6 34-35	233.06	4.162	1.294	2.79	2.71	8.53
	1209C	12-5 87-88	232.16	95.76		1209C	12-6 38-39	233.08	3.345	1.188	2.06	2.74	8.51
	1209C	12-5 90-91	232.19	95.26		1209C	12-6 42-43	233.14	4.328	1.274	2.86	2.71	8.53
	1209C	12-5 94-95	232.23	92.49		1209C	12-6 46-47	233.18	2.222	1.213	1.40	2.41	8.70
	1209C	12-5 98-99	232.27	94.55		1209C	12-6 50-51	233.22	5.906	1.148	3.51	2.57	8.61
	1209C	12-5 100-101	232.29	95.04		1209C	12-6 52-53	233.23	5.415	1.148	3.22	2.81	8.48
R	1209C	12-5 100-101	232.29	95.33		1209C	12-6 53-54	233.25	3.557	1.211	2.23	2.40	8.70
	1209C	12-5 104-105	232.33	93.73		1209C	12-6 56-57	233.27	4.129	1.176	2.52	2.70	8.53
R	1209C	12-5 104-105	232.33	94.57		1209C	12-6 60-61	233.31	3.960	1.184	2.43	2.74	8.51
	1209C	12-5 109-110	232.38	94.66	R	1209C	12-6 60-61	233.31	4.257	1.184	2.61	3.08	8.34
	1209C	12-5 114-115	232.43	95.55		1209C	12-6 64-65	233.35	4.512	1.226	2.86	2.72	8.52
	1209C	12-5 118-119	232.47	94.72		1209C	12-6 67-68	233.38	5.335	1.200	3.32	2.76	8.50

Table 2-1. continued

Sedimentary Carbonate Content					Eolian Mass Accumulation Rates and Grain Size								
Sample ID			Core Depth	% CaCO3	Sample ID			Core Depth	Dust Fraction	Dry Bulk Density	Dust MAR	Median Particle Diameter	
**	Hole	Core-Section, Interval (cm)	rmcd		**	Hole	Core-Section, Interval (cm)	rmcd	mg/g sed	g/cm^3	$mg/cm^2/kyr$	µm	ϕ_{50}
	1209C	12-5 120-121	232.49	92.84		1209C	12-6 71-72	233.43	3.073	1.143	1.82	2.61	8.58
	1209C	12-5 124-125	232.53	91.41		1209C	12-6 75-76	233.45	5.560	1.148	3.31	2.89	8.44
	1209C	12-5 126-127	232.54	92.50		1209C	12-6 79-81	233.49	4.983	1.197	3.09	2.65	8.56
	1209C	12-5 130-131	232.58	92.28		1209C	12-6 82-83	233.52	5.546	1.170	3.36	2.59	8.59
R	1209C	12-5 130-131	232.58	90.33	R	1209C	12-6 82-83	233.52	-----	-----	-----	2.76	8.50
	1209C	12-5 131-132	232.59	92.49		1209C	12-6 86-87	233.56	6.906	1.143	4.09	2.66	8.55
	1209C	12-5 136-137	232.63	93.98		1209C	12-6 90-91	233.6	5.978	1.157	3.58	2.79	8.49
	1209C	12-5 140-141	232.67	92.78		1209C	12-6 94-95	233.63	5.361	1.180	3.28	2.62	8.58
	1209C	12-5 145-146	232.71	93.40		1209C	12-6 100-101	233.69	7.088	1.266	4.65	2.57	8.60
	1209C	12-5 148-149	232.74	95.70		1209C	12-7 4-5	233.73	6.626	1.192	4.09	2.84	8.46
	1209C	12-6 2-3	232.77	93.74		1209C	12-7 8-9	233.77	6.244	1.183	3.83	2.48	8.66
	1209C	12-6 6-7	232.81	95.63		1209C	12-7 12-13	233.8	3.216	1.211	2.02	2.90	8.43
	1209C	12-6 14-15	232.88	91.91		1209C	12-7 16-17	233.84	6.559	1.173	3.99	2.60	8.59
	1209C	12-6 16-17	232.9	94.39		1209C	12-7 22-23	233.9	10.092	1.197	6.26	3.13	8.32
	1209C	12-6 26-27	232.99	92.62		1209C	12-7 24-25	233.92	13.636	1.148	8.11	2.87	8.44
	1209C	12-6 34-35	233.06	95.37		1209C	12-7 28-29	233.96	23.455	1.210	14.70	2.97	8.40
R	1209C	12-6 34-35	233.06	95.41		1209C	12-7 32-33	233.99	27.163	1.177	16.56	3.39	8.20
R	1209C	12-6 34-35	233.06	95.51									
	1209C	12-6 38-39	233.1	95.24									
	1209C	12-6 43-44	233.15	96.61									
	1209C	12-6 47-48	233.19	94.91									
	1209C	12-6 50-51	233.22	93.56									
R	1209C	12-6 50-51	233.22	94.57									
	1209C	12-6 52-53	233.23	93.98									
	1209C	12-6 56-57	233.27	95.08									
	1209C	12-6 60-61	233.31	95.11									
	1209C	12-6 64-65	233.35	96.00									
	1209C	12-6 72-73	233.42	94.65									
R	1209C	12-6 72-73	233.42	94.98									
	1209C	12-6 76-77	233.46	96.34									
	1209C	12-6 80-81	233.5	93.74									
	1209C	12-6 86-87	233.56	92.20									
	1209C	12-6 90-91	233.6	95.03									
	1209C	12-6 94-95	233.63	94.51									
R	1209C	12-6 94-95	233.63	93.95									
	1209C	12-6 99-100	233.68	95.03									
	1209C	12-7 2-3	233.71	94.14									
	1209C	12-7 6-7	233.75	89.34									
	1209C	12-7 10-11	233.79	94.50									
R	1209C	12-7 10-11	233.79	92.46									
R	1209C	12-7 10-11	233.79	91.40									
	1209C	12-7 14-15	233.82	94.01									
	1209C	12-7 18-19	233.86	94.49									

Table 2-1. continued

Sedimentary Carbonate Content					Eolian Mass Accumulation Rates and Grain Size								
Sample ID			Core Depth	% CaCO3	Sample ID			Core Depth	Dust Fraction	Dry Bulk Density	Dust MAR	Median Particle Diameter	
**	Hole	Core-Section, Interval (cm)	rmcd		**	Hole	Core-Section, Interval (cm)	rmcd	mg/g sed	g/cm^3	mg/cm^2/kyr	µm	ϕ_{50}
	1209C	12-7 22-23	233.9	92.37									
R	1209C	12-7 22-23	233.9	92.68									
	1209C	12-7 26-27	233.94	91.19									
	1209C	12-7 30-31	233.98	88.73									
	1209C	12-7 34-35	234.01	90.13									
	1209C	12-7 38-39	234.05	91.86									

** R denotes a replicate sample

Dust Extraction

Refractory alumino-silicates were isolated from ~3-4 g of bulk sediment through a well-established series of chemical extractions [*Rea and Janecek*, 1981; *Clemens and Prell,* 1990; *Hovan,* 1995]. To remove carbonate, sediments were placed on a shaker table in 25% acetic acid for 2 hours. Sediments were then leached in a warm (80°C) sodium dithionate-sodium citrate solution buffered with sodium bicarbonate to remove oxy-hydroxides and zeolites. Opal removal by sodium carbonate was not necessary as previous analyses indicated the sediment used in this study contained no biogenic silica [*Bralower et al.*, 2006]. The isolated material, operationally defined as "eolian dust", was rinsed several times to remove any traces of chemical residue, freeze-dried and massed to determine the sediment's eolian weight percent (Table 2-1). Estimates of sedimentary dust content from biogenic sediments using this method are generally reproducible within 10-15% [*Rea and Janecek,* 1981; *Hovan et al.,* 1991].

We emphasize the fact that the extracted "dust" residue is operationally defined and therefore may contain materials of volcanic or authigenic origin. However, XRD

and Nd isotope analyses indicate the majority of the isolated material is comprised of quartz, feldspars, mica and clay minerals, which implies a continental source. The $\varepsilon_{Nd}(t)$ values of the extracted dust also support a typical shale composition derived from continental sources and rule out authigenic contributions to the fine fraction [*Woodard et al.*, 2009; *Woodard and Thomas*, 2009].

Eolian Grain Size

Grain size distributions of the eolian component were determined using a 256 channel Beckman Multisizer 4 Coulter Counter (Indiana University of Pennsylvania) with a 50μm aperture and 150,000-particle count. Samples were suspended in a 5 g/L calgon solution and sonicated for 5 minutes prior to analysis to evenly disperse the material. Each sample was analyzed twice and the resulting distributions averaged. Grain sizes for each sample represent the median volume percent and are expressed as median diameters, ϕ_{50} (Table 2-1, Appendix B), where

$$\phi_{50} = -\log_2(\text{diameter in mm})$$

Variation in median grain size between replicate samples was <15%.

Relative wind intensity changes were estimated by comparing the squares of the median grain size diameters ($D_{H,L}$) of two samples, which we assumed represent the ratio of high to low wind intensities (R_W) [after *Janecek and Rea*, 1985].

$$R_W = (D_H)^2 / (D_L)^2$$

Mass Accumulation Rates

Sediment mass accumulation rates (MAR_{bulk}) were determined using the equation:

$$MAR_{bulk} = LSR \bullet \rho_{bulk} (\bullet f_x)$$

where LSR is the linear sedimentation rate (cm/kyr), ρ_{bulk} is the dry bulk density (g/cm^3) and f_x is the weight percent fraction of the component of interest. The age model we employ to determine the linear sedimentation rates (Figure 2-3, Table 2-2) is based on the orbital cyclostratigraphy established by *Westerhold et al.* [2008] and widely accepted as the new basis for the Paleogene time scale. The age tie-points (Table 2-1) are determined in relation to the orbital solution provided by *Laskar et al.* [2004], which uses the more stable long eccentricity period of 405 kyr. Linear interpolation between datums (biostratigraphic, magnetostratigraphic, orbital) has been the convention for calculating sedimentation rates in pre-Pleistocene sections, and the availability of the astronomical age model represents a significant improvement in the temporal resolution of datums (which are often several hundred thousand to millions of years apart in the Paleocene).

An alternate sedimentation model has been presented by *Marcantonio et al.* [2009] using extraterrestrial (ET) ^3He constant flux as a proxy for sediment accumulation. The bulk sediment MAR is determined by dividing the known flux of $^3He_{ET}$ by the amount measured in a sediment sample. This method determines the MAR without the need for an independent age model or interpolation between tie points and gives an "instantaneous" flux of material to the seafloor. However, linear sedimentation

Table 2-2. Sedimentation Rates and Age Models for Site 1209

Depth (rmcd)	$^3He_{ET}$-based LSR*	Age (kyr)**	Depth (rmcd)	Age (kyr)***	Tie-point Derived LSR
229.93	0.28	57924.1	227.57	57326	0.62
230.01	0.58	57952.6	230.08	57728	0.42
230.07	0.27	57962.9	231.86	58153	0.62
230.07	0.27	----	232.56	58266	0.52
230.16	0.75	57995.9	324.00	58544	
230.25	1.05	58007.9			
230.34	0.44	58016.4			
230.43	0.37	58036.9			
230.43	0.417	----			
230.57	0.60	58075.0			
230.72	0.41	58100.2			
230.87	0.31	58136.3			
231.01	0.20	58181.3			
231.07	0.38	58210.8			
231.07	0.32	----			
231.14	0.46	58232.6			
231.21	0.51	58247.8			
231.27	0.551	58259.6			
231.27	0.621	----			
231.31	0.681	58266.8			
231.51	0.35	58296.1			
231.63	0.66	58330.4			
231.75	0.35	58348.6			
231.95	1.05	58406.2			
232.16	1.08	58426.2			
232.38	1.04	58446.6			
232.56	0.32	58463.8			
232.56	0.42	----			
232.65	0.58	58491.7			
232.73	0.61	58505.4			
232.81	0.77	58518.6			
232.82	0.95	58519.9			
232.84	0.57	58522.0			
232.91	0.41	58534.3			
232.95	0.97	58544.0			
232.95	0.79	----			
233.1	0.24	58563.0			
233.24	1.68	58621.3			
233.39	1.76	58630.2			
233.42	1.09	58631.9			
233.42	0.68	----			
233.6	0.82	58658.4			
233.69	1.38	58669.3			
233.8	0.61	58677.3			
233.89	1.27	58692.1			
233.99	0.25	58700.0			
233.99	0.31	----			

*Calculated by dividing $^3He_{ET}$ sediment fluxes from Marcantonio et al. (2009) by dry bulk densities
**Age model determined using $^3He_{ET}$-based LSR when base of C25r = 58.7 Ma (Dinares-Turrell, 2007)
***Tie-point ages used in astronomical calibration of Paleocene time (Westerhold et al., 2008; Laskar et al., 2004)

rates may be derived by dividing the $^3He_{ET}$ based bulk sediment MARs by the dry bulk density (see equation above). In order to assess how sensitive our dust record is to the choice of a sedimentation model, we calculated linear sedimentation rates from the $^3He_{ET}$ MARs and compare both age model-based and $^3He_{ET}$-based bulk sediment and dust mass accumulation rates.

Gamma Ray Attenuation (GRA)-wet bulk density measurements were used to estimate dry bulk density by exploiting the linear relationship between shipboard physical properties measurements of wet and dry bulk density (after Lyle, 2003). An additional correction of 0.32 g/cm^3 was subtracted from GRA-bulk density prior to calculation of ρ_{bulk} values to account for the offset between measured bulk density and those given by GRA [*Bralower et al.,* 2002]. Dust MARs were determined by multiplying the MAR_{bulk} by the weight percent fraction (f_x) of the non-dissolvable mineral component of the sediment (Figure 2-4, Table 2-1).

Statistics

Statistical correlations were performed using KaleidaGraph (Version 4.03). Confidence intervals were established using unpaired t-tests. Spectral analysis of dust MARs and grain size was conducted using the SSA-MTM Toolkit (Version 4.4) available online at: www.atmos.ucla.edu/tcd/ssa/. Power spectra were estimated using the multi-taper method with a resolution of two, three tapers and a frequency ranging from 0 to 1/2 Nyquist frequency [*Ghil et al.,* 2002]. Power spectrum confidence intervals are based on red noise null hypothesis [*Mann and Lees,* 1996]. We tested two different

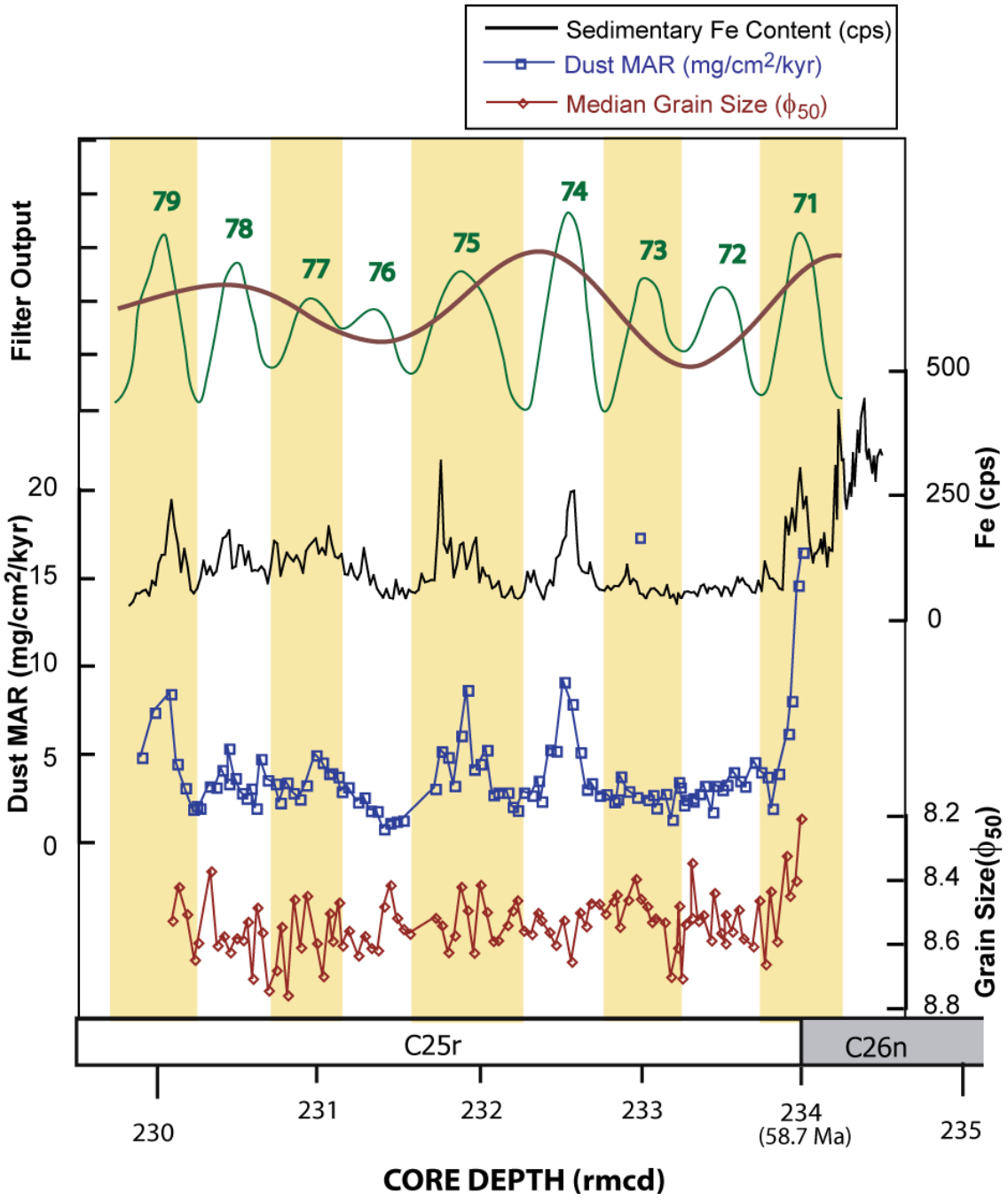

Figure 2-4. Dust fluxes and grain size. Mass accumulation rates (blue) and median grain sizes (dark red) generated for Shatsky Rise sediments span nine consecutive short eccentricity cycles. Measured iron intensities (black) and interpreted eccentricity cycles, 400 kyr (pink), 100 kyr (green) from *Westerhold et al.* [2008]. Core depth in revised meters composite depth (rmcd) from [*Westerhold and Röhl,* 2006]. Estimated age of boundary between magnetochrons C26n and C25r is 58.7 Ma [*Dinares-Turrell,* 2007; ICS website, Subcomission for Stratigraphic Information: http://stratigraphy.science.purdue.edu/ gssp/].

age models for the dust flux records, one based on linear sedimentation rates using the widely accepted orbital age model developed by *Westerhold et al.* [2008], and the other based on sedimentation rates calculated from $^{3}He_{ET}$ derived sediment fluxes. All data was interpolated to even 10-kyr spacing prior to spectral analysis. To account for asymmetry, datasets were detrended and the mean removed.

Results

Sedimentary carbonate content is high over the entire interval, ranging from 88.7 to 96.9 weight percent (Table 2-1, Figure 2-3). Weight percent carbonate negatively correlates with Fe content ($R = -0.441$, $p < .001$, Figure 2-3). Bulk sediment MARs calculated using the orbital age model-based LSR averaged 0.60 ± 0.21 (2 s.d.) g/cm^2/kyr. Average bulk MARs calculated using $^{3}He_{ET}$ accumulation are slightly higher, 0.78 ± 0.88 (2s.d.) g/cm^2/kyr [*Marcantonio et al.,* 2009]. However, $^{3}He_{ET}$-based MARs exhibit a much larger range, 0.24 – 2.1 g/cm^2/kyr than orbital age model-based MARs (range = 0.46 – 0.87 g/cm^2/kyr, Figure 2-3). Linear sedimentation rates determined using both methods are plotted in Figure 2-3. LSRs based on $^{3}He_{ET}$-based MARs are much more variable than those derived using the age model perhaps due to the higher resolution of the $^{3}He_{ET}$-based record (31 sample depths vs. four age model tie points, Table 2-2).

Sedimentary dust content ranged from ~0.2 to 2.7% (Table 2-1), and the variations in dust accumulation (Figure 2-4) correlate positively with sedimentary Fe content ($R = 0.58$, $p < .0001$). Eolian dust MARs over the eight consecutive cycles are

low, averaging only 3.9 ± 5.4 (2 s.d.) mg/cm^2/kyr. Despite low accumulation rates the Site 1209 record displays up to four-fold fluctuations about the mean with dust MARs ranging from a minimum of 0.9 mg/cm^2/kyr to a maximum of 16.6 mg/cm^2/kyr (Figure 2-4). An alternate set of Dust MARs calculated using sedimentation rates derived from $^3He_{ET}$ constant flux proxy [*Marcantonio et al.,* 2009] average 5.1 ± 6.1 (2s.d.) mg/cm^2/kyr and show a range of 1.1 to 16.1 mg/cm^2/kyr). These variations are similar to those based on the orbital age model MAR_{bulk} (Appendix A). The most pronounced increases in dust flux occur over eccentricity peaks 71, 74, 75 and 79 (Figure 2-4), intervals characterized by the coincidence of 100 kyr and 400 kyr eccentricity maxima. There are minor or absent increases in dust MAR over eccentricity peaks 72, 76 and 77 (Figure 2-4), where 400 kyr eccentricity minima overlap with 100 kyr maxima (the high dust content coinciding with peak 73 (Figure 2-4) is marked by a single, anomalous data point. The dust MAR calculated from this data point, 17.43 mg/cm^2/kyr, was the highest of any generated in this study and likely reflects some error in the preparation or discuss this data point further and exclude it from the dataset used for spectral analysis).

Spectral analysis of the dust MAR record returned significant MTM power spectra at frequencies corresponding to orbital parameters. Power spectrum maxima are observed at 23, 42, 67 and 119 thousand-year periodicities when the dust record is tied to the LSR-based age model (Figure 2-5a) implying eccentricity, obliquity and precessional forcing. Spectral analysis of dust MARs using the $^3He_{ET}$-based age model returns significant frequencies corresponding to 77, 41 and 30 thousand-year periodicities

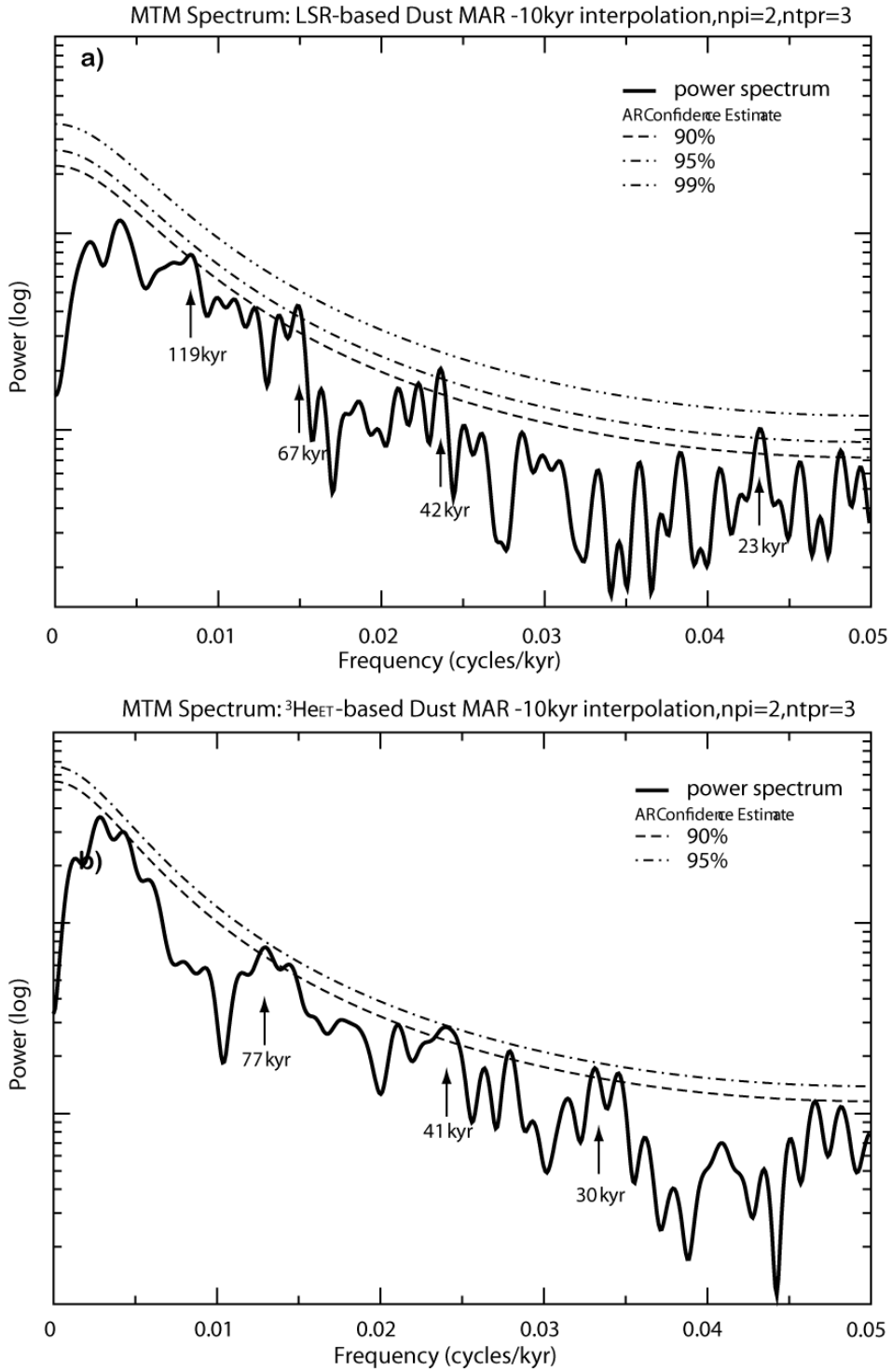

Figure 2-5. Spectral analysis. **a)** MTM power spectrum of dust mass accumulation rate data using orbital LSR-based age modle. Significant power is found at frequencies of 0.043, 0.024, 0.015, 0.008 cycles/kyr. **b)** MTM power spectrum for dust fluxes when $^{3}He_{ET}$ -based age model is used. Significant frequencies found at 0.033, 0.024 and 0.013 cycles/kyr. All data was detrended, mean removed and interpolated to even 10 kyr spacing prior to spectral analysis.

(Figure 2-5b). In this case obliquity appears as the only orbital parameter pacing the dust MAR record.

Eolian grain size distributions range from median values of 8.75ϕ to 8.2ϕ. The record exhibits a slight fining upwards through stratigraphic section (Figure 2-4). High and low amplitude variations in median grain size occur on timescales shorter than the eccentricity cycles (Figure 2-4). The MTM power spectrum generated for dust grain size reveals significant periodicities of 63, 38, 25 and 17 kyr. However, these periodicities do not correspond to known orbital parameters.

Discussion

Causes of Cyclic Sedimentation

The variations in dust accumulation at Site 1209 correlate closely with changes in sedimentary Fe content. This tight coherence suggests that variations in eolian dust accumulation were paced by orbital frequencies, and spectral analysis of the dust record supports this finding (Figure 2-5). Thus cyclic changes in "dilution" by terrigenous sediments, in this case eolian dust, indeed contributed to the observed lithologic cycles.

However, the amount of "dilution" by dust was only sufficient to have changed sedimentary carbonate contents by ~1.5 % (assuming constant carbonate production rates). As indicated in Figure 2-3, sedimentary carbonate content varied by up to ~8%, therefore we must consider the potential contribution of carbonate dissolution to the variations in lithology. This is particularly important given the

relatively shallow CCD during the Early Paleogene [e.g., *van Andel et al.,* 1975; *Rea and Lyle,* 2005].

Carbonate dissolution might lead to apparent changes in the concentration of other sedimentary phases, however the variations in bulk sediment and carbonate accumulation recorded at Shatsky Rise are simply too small to explain the observed lithologic cycles (Figure 2-4). For example, assuming carbonate export to the deep ocean is 1 g/cm^2/kyr and dust flux is constant at .005 mg/cm^2/kyr, dissolution of ~80% of the carbonate at depth could explain the maximum range in sedimentary carbonate content (~89-97 %). Such high calculated dissolution rates could drive the large changes observed in the $^3He_{ET}$-based bulk sediment MAR record and explain nearly the entire range in sedimentary dust content (0.5-2.2%). However, this would require the bulk sediment MARs to decrease by 5 to 10 – fold during periods of dust maxima. Such large bulk accumulation rate changes are not observed in the data (Figures 2-3 and 2-4) indicating the variations in dust flux occurred independently of carbonate dissolution.

The observation that dust accumulation rates varied independently of carbonate accumulation is also supported by the fact that the dust and carbonate records do not mirror each other (Figures 2-3 and 2-4). Furthermore, *Marcantonio et al.* [2009] noted that the $^3He_{ET}$-based bulk sediment MAR appears to mimic the sedimentary cycles picked out in the Fe record. Thus dust flux estimates based on two completely different sedimentation models, the $^3He_{ET}$ constant flux proxy [*Marcantonio et al.,* 2009] and the orbital age tie-point based LSR, display similar patterns in dust accumulation (Appendix

A). Therefore, independent changes in the accumulation of both sedimentary components are required to explain the full range of variability observed in the data.

The record of coarse fraction content, an established proxy for carbonate dissolution [e.g., *Broecker and Clark,* 1999] (Figure 2-6), which in this depositional setting consists entirely of foraminiferal tests, further corroborates this finding [*Westerhold et al.,* personal comm]. Comparison of the coarse fraction data [*Westerhold et al.,* submitted to Paleoceanography] with dust accumulation indicates that carbonate

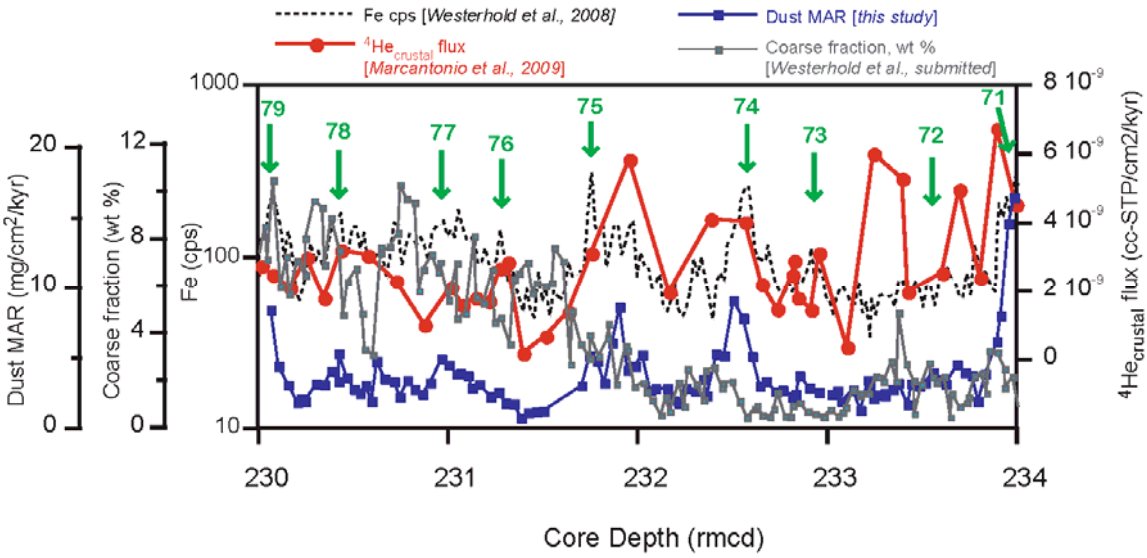

Figure 2-6. Comparison of dust mass accumulation rates (blue) (*this study*), crustal ^{4}He fluxes (red) [*Marcantonio et al.* 2009] and sedimentary coarse fraction (grey) [*Westerhold et al., submitted*]. Crustal ^{4}He fluxes are based on sedimentation rates derived from extraterrestrial ^{3}He constant flux and assumed to represent terrigenous inputs [*Marcantonio et al.* 2009]. Sedimentary Fe content is plotted (broken line) with eccentricity peaks labeled for reference (green) [*Westerhold et al.*, 2008; *Marcantonio et al.*, 2009].

preservation (higher weight percentage coarse fraction) does not control the rate of dust accumulation.

Comparison of the dust accumulation rates with $^4He_{crustal}$ fluxes (an independent proxy for dust in marine sediments) indicates that both records demonstrate

a similar pattern of dust maxima and minima that correlate to the Fe cyclostratigraphy (Figure 2-6). It is not possible to directly compare accumulation rates derived from the two methods (it is not possible to convert the $^4He_{crustal}$ flux estimates to mg/cm^2/kyr because the end-member composition of crustal ^{4}He is not known [e.g., *Patterson et al.,* 1999]. Regardless, the coherence of the two independently generated dust accumulation records strengthens our conclusion that dust accumulation to the central tropical North Pacific was orbitally paced during the Early Paleocene greenhouse. In fact, *Marcantonio et al*. [2009] concluded that the $^4He_{crustal}$ fluxes correlate to the record of Fe counts, and suggested the possibility that dust fluxes were controlled by eccentricity variations, but this could not be proven due to the relatively low resolution of their data set. Furthermore, many of the differences between the two records can be reconciled by the overall lower resolution of the ^{4}He-based record.

Climatic Implications of Orbitally-paced Dust Accumulation

The dust accumulation data from Site 1209 demonstrates the relationship between orbital forcing and dust supply during a greenhouse climate. Dust fluxes to Shatsky Rise are similar to dust MARs determined in contemporaneous Paleocene sediments at nearby site LL44-GPC3, ~12 mg/cm^2/kyr [*Janecek and Rea,* 1983]. All of these Paleocene dust MARs are approximately an order of magnitude less than modern dust accumulation rates for the central tropical North Pacific [*Rea,* 1994; *Uematsu et al.,* 1985]. The lower rates of accumulation are consistent with a more humid greenhouse atmosphere and fewer or smaller dust source deposits.

The distribution of the insolation signal across Earth's surface is primarily modified by orbital cycles with shorter periodicities [*Berger and Loutre*, 2004*; Holmes et al.*, 2004]. The presence of the 41 & 42 kyr periodicities identified by spectral analysis of our record, regardless of age model used, links dust accumulation during a greenhouse climate to obliquity variations. As discussed earlier, obliquity controls meridional insolation gradients. Steepened insolation gradients would cause steepened temperature and atmospheric pressure gradients likely promoting conditions favorable for the development of large low-pressure systems - the meteorological mechanism suggested to explain the majority of dust deposited in the oceans far from continental sources [*Pye,* 1987]. Recent work by *McGee et al.* [2010] points out that only ~0.3% of wind is strong enough to entrain the majority of dust and increases in Quaternary dust accumulation occurs during times of enhanced meridional gradients and the prevalence of strong winds. If dust MARs are determined by the strength of wind storm activity, obliquity-driven increases in meridional insolation gradients could explain increased dust fluxes in our "greenhouse" record.

The pattern of dust accumulation clearly coincides with the 100- and 400-kyr changes in lithology (Fe counts) indicating a strong component of eccentricity forcing of dust accumulation. Yet spectral analysis of the record using the LSR-based age model indicates that all three orbital parameters (eccentricity, obliquity and precession) contributed to variations in dust accumulation (Figure 2-4). It is significant that the amplitude of eccentricity-paced variations in our early Paleogene dust accumulation record was comparable to that recorded in Pacific Ocean Pleistocene glacial-interglacial

sedimentary sequences (~two- to four-fold) [*Kohfield and Harrison,* 2001; *Winckler et al.,* 2008]. This suggests that the relative impact of orbitally-induced changes in dust accumulation may have been similar during the Pleistocene and Paleocene.

The causal relationship between eccentricity forcing and the factors that influence dust supply is relatively straightforward. Eccentricity is the only orbital parameter that controls the total amount of solar radiation received by Earth annually [e.g., *Pälike,* 2005]. At maximum eccentricity, the global variation in annual solar insolation can be as much as 24% causing the greatest seasonal contrasts to occur in both hemispheres [*Williams et al.,* 2007; *Pälike,* 2005]. Such seasonal contrasts during a greenhouse climate would likely have manifested themselves as wet-dry variations [*Barron,* 1995; *Williams, et al.,* 2007]. During maximum eccentricity (maximum seasonality) dust source regions would have experienced drier dry seasons leading to increased dust generation and wetter wet seasons allowing chemical weathering and runoff to recharge dust source regions with fine-grained materials. Variations in hydrologic cycling would have also impacted vegetation cover, in turn affecting dust supply. The coincidence of 100 kyr and 400 kyr eccentricity maxima would have amplified that seasonal contrast even further, explaining the largest peaks in dust accumulation (Figures 2-3 and 2-4).

The signal from climatic precession is always present in insolation time series and is modulated in amplitude by eccentricity [*Pälike,* 2005]. This leads to variability in the timing of periods of maximum insolation with respect to Earth's seasons and ultimately effects the latitudinal distribution of the seasons. The 23 and 119 kyr

periodicities identified by spectral analysis suggest a connection with 100 kyr eccentricity forcing modulating precession [*Maslin and Ridgwell,* 2005].

The coincidence of high dust MARs with eccentricity maxima as well as presence of obliquity and precessional components in the dust flux record implies that enhanced dust production/transport was tied to strong seasonality. Intensification of seasonal contrasts during eccentricity maxima in the form of amplified wet-dry cycles, specifically the enhanced aridity of the dry season, provides a plausible mechanism for increased dust delivery. In addition, enhanced seasonality may increase dust storm generation causing higher dust fluxes to the pelagic ocean [*Pye,* 1987; *McGee et al.,* 2010]. This explanation is also consistent with the monsoonal type climate suggested to have dominated global atmospheric circulation patterns during the Paleogene [*Lawrence et al.,* 2003; *Holmes et al.,* 2004].

Implications of the Grain Size Distribution of Dust at Site 1209

While the flux of dust to the open ocean provides a relative constraint on the supply of dust available, the grain size distribution is dictated by variations in sandblasting efficiency, the size of soil aggregates at the source region, and wind speed [*Muhs and Bettis,* 2003; *Alfaro and Gomes,* 2001]. As the wind transports dust away from its source the majority of the particles settle out. However, *Gillette et al.* [1974] showed that particles with a diameter of <14 μm are essentially "non-settling" and can remain suspended in the atmosphere indefinitely. Particles in this size range are capable of long distance travel in the upper troposphere where they form part of the background

atmospheric aerosol and are largely removed by precipitation. This is supported by studies modeling atmospheric dust [*Schütz et al,* 1981], and sea-floor sediment data [*Janecek,* 1985] that indicate by >2000 km distance from shore atmospheric dust is in equilibrium with transporting winds [*Janecek and Rea,* 1985; *Pye,* 1987]. When the atmospheric dust load reaches equilibrium state, the grain size distribution of the dust remains constant proportional to the transporting wind velocity at the time.

Dust accumulating in the region of Shatsky Rise was likely transported thousands of kilometers from its source. The grain size distributions of our samples are typical of those classified as "dominantly to entirely eolian" [*Rea and Hovan*, 1995] (Appendix B). If we assume the region supplying dust to the central Pacific Ocean 58Ma did not change appreciably over our ~800 kyr interval, then physical conditions (i.e. saltation-sandblasting or soil aggregate size) dictating grain size at the source likely remained constant over the interval. Therefore, our dust grain size record can be interpreted to reflect changes in the carrying capacity of the wind whether controlled by absolute changes in wind speed or changes in the dominant delivery pathway of particles to the remote ocean.

Median grain size diameters of dust deposited on Shatsky Rise at ~58 Ma exhibits significant high frequency variability ranging from 2.3 - 3.4μm (8.75ϕ to 8.2ϕ) (Figure 2-4, Table 2-1), well within the "non-settling" size fraction range. The range of median grain sizes in the ~800-kyr Site 1209 record is consistent with coeval values reported from nearby DSDP Site 576 and LL44-GPC3 to the east (Figure 2-2) (~8.7ϕ and ~8.4ϕ, respectively) [*Rea et al*, 1985; *Janecek and Rea*, 1983]. However, the

variations in Site 1209 median grain size do not reflect known orbital frequencies (Figure 2-4).

Regardless of the lack of orbital periodicity, the eolian grain size distributions shed important light on the intensity of atmospheric circulation during the Early Paleogene greenhouse. The grain size record from Shatsky Rise is similar to that of eolian dust deposited in the Pacific Ocean over the past 750 kyr. Median grain sizes of dust deposited beneath the westerlies (Core KK75-02) and in the eastern equatorial Pacific (DSDP Site 503) ranged from 8.81ϕ to 8.37ϕ and from 8.79ϕ to 8.25ϕ, respectively [*Janecek and Rea,* 1985; *Janecek,* 1985]. Based on paleo-location, it is likely that Shatsky Rise lay within the tropical trade wind belts at ~58 Ma. Variations in wind intensity spanning several Pleistocene glacial-interglacial cycles (past 750 kyr) average 22% beneath the westerlies (KK75-02) and 36% under the trade winds (Site 503) [*Janecek and Rea,* 1985]. Assuming dust deposited on Shatsky Rise was in equilibrium with transporting winds, we estimate relative wind intensity fluctuated by as much as 30-50% from the change in median grain size (see Methods). These values suggest relative trade wind strength and patterns were at least as variable in the early to late Paleocene as during the Pleistocene icehouse and the vigor of atmospheric circulation may have been comparable to the modern regime. Alternatively, similarities observed between our record and Quaternary grain sizes might simply reflect the natural variability in grain size distribution of background aerosol particles transported far out over the pelagic ocean, although they do imply that winds in the upper troposphere had similar carry-capacities.

Conclusions

The new records of eolian dust grain size and accumulation on Shatsky Rise for the time period ~58 Ma provide insight into the response of the paleoenvironment to orbitally paced changes in solar insolation. The range of eolian grain sizes analyzed is similar to that of dust presently accumulating in the central Pacific Ocean. This implies atmospheric circulation may have been as vigorous during the greenhouse at ~58 Ma as it has been throughout the late Cenozoic icehouse, corroborating other recent evidence that equator-to-pole thermal gradients may have been steeper than previously believed. The overall dust fluxes, however, were substantially less than modern due to an overall more humid atmosphere or fewer/smaller dust source regions during the early Paleogene (or a combination of both).

The accumulation of dust at Shatsky Rise ~58 Ma is strongly correlated to the orbitally paced lithologic cycles defined by sedimentary Fe content. Thus we conclude that dust accumulation was likely controlled by the same forcing function – orbital eccentricity – establishing for the first time that eccentricity variations in solar insolation influence climate during greenhouse intervals as has been determined for glacial-interglacial climate intervals. The data suggest that source regions supplying dust to the tropical North Pacific may have experienced amplified wet-dry cycles corresponding with orbital eccentricity maxima, and the relative response of dust supply to eccentricity forcing during the last major interval of greenhouse climate was comparable to that during the Pleistocene.

Intervals of increased dust accumulation may “dilute” the total calcium carbonate accumulation, yet the recorded dust changes only account for a fraction of the total carbonate change. Therefore, some other mechanism controlling carbonate preservation at the seafloor must also have responded to orbital forcing, driving the total lithologic change (defined by the Fe or magnetic susceptibility variations) and accounting for the remaining difference in carbonate content.

CHAPTER III

TH DERIVED DUST FLUXES TO THE TROPICAL PACIFIC OCEAN, 58 MA

Introduction

Geologic records of atmospheric (eolian) dust are increasingly used in paleoclimatic reconstructions because modern studies suggest mineral dust plays an important role, both directly and indirectly, as a climate feedback mechanism. Dust absorbs and scatters incoming solar radiation directly influencing the global heat budget. Additionally, dust grains of sufficiently small size can provide seeding material for clouds thereby impacting the planet's hydrologic cycle. The presence of large amounts of dust in the atmosphere may also modify cloud properties. Since clouds serve as barriers for incoming UV in the atmosphere and outgoing IR radiation from Earth's surface, their modification by dust indirectly impacts Earth's radiative heat balance [*Ramanathan et al.,* 2001; *Kaufman et al.,* 2002]. Increased dust fluxes may play an important role in modulating climate through the development of ice clouds, especially in the tropics [*Hoose et al.,* 2010]. Furthermore, eolian dust deposited in the ocean may spur primary production. Partial dissolution of detrital minerals at the sea surface releases iron [*Jickells et al.,* 2005; *Duce and Tindale,* 1991; *Mahowald et al.,* 2005], an important micro-nutrient that limits phytoplankton productivity in approximately one third of the Earth's surface oceans [*Boyd et al,* 2005]. Therefore, increased dust flux to the open ocean may generate a positive climate feedback by stimulating the biologic

pump causing enhanced carbon export to the deep ocean thus drawing down atmospheric CO_2.

Most high-resolution geologic reconstructions of eolian dust focus on the late Neogene (last few million years) because of the abundance of well-dated sedimentary records and availability of ice cores. In general, studies of late Neogene dust records preserved in marine sediments indicate dust flux varied in concert with global ice growth and decay recorded by marine $\delta^{18}O$ [*Clemens and Prell,* 1990; *Rea,* 1994; *Hovan et al.,* 1989; 1991; *Winckler et al.,* 2008; *Muhs and Bettis,* 2003; *Patterson et al.,* 1999; *Petit et al.,* 1999; *EPICA,* 2004]. Dust records from ice cores show 10 to 20 fold increases in dust deposited in Greenland [e.g *Biscaye et al.,* 1997] and Antarctic [*Petit et al.,* 1999] ice sheets during the last glacial maxima. Tropical dust fluxes varied in concert with those at higher latitudes but the magnitude of variation was less, only ~2-fold [*Winckler et al.,* 2008]. These records indicate a global-scale control of atmospheric dust. Changes in dust flux have been connected to source region aridity and meteorological conditions that promote the development of large storm fronts [*Pye,* 1989; *McGee et al.,* 2010; *Prospero,* 1996; *Rea,* 1994 and references therein]. The increased dust flux during glacial periods are interpreted to reflect the reduction of atmospheric humidity [*Hovan et al.,* 1989; *Rea et al,* 1994], desert region expansion [*Pokras and Mix,* 1985; *Maher et al.,* 2010] and decreased vegetation cover [*Rea,* 1994; *Pye,* 1987; *Bergengren et al.,* 2001], as well as increased equator-to-pole temperature/pressure gradients responsible for wind storm development [*McGee et al.,* 2010].

The response of atmospheric dust fluxes to changing environmental conditions during the greenhouse climate of the early Paleogene is not as well constrained as during the Neogene due, in part, to the lack of high-resolution sedimentary records. New astronomically tuned age models of Paleocene and Eocene time [*Westerhold et al.,* 2008; *Pälike et al.,* 2001] provide the opportunity to resolve dust fluxes in recently drilled deep sea sediments at a resolution high enough for comparison with Neogene "icehouse"records (e.g. *Holmes et al*., 2004; *Marcantonio et al.,* 2009; *Woodard et al.,* 2011].

Early Paleogene dust reconstructions are also hampered by our inability to quantitatively measure the dust content of these sediments. "Traditional" chemical extraction techniques isolate refractory aluminosilicates from the sediments by dissolving biogenic carbonate, silica and apatite as well as authigenic oxy-hydroxides and zeolites [*Rea and Janecek,* 1981; *Hovan,* 1995]. The refractory non-dissovable minerals are thus operationally defined as "eolian dust", but this fraction may contain volcanic ash and authigenic clays [e.g. *Olivarez et al.,* 1991; *Krissek and Janecek,* 1993; *Weber et al.,* 1996]. Studies of older sediments may be complicated by high abundances of authigenic material due to their relatively longer diagenetic history [*Ziegler et al.,* 2007a]. The potential for minerals derived from volcanic or authigenic sources to inflate estimates of the eolian dust flux in deep sea sediments has led to the use of independent geochemical proxies for dust such as sedimentary crustal ^{4}He and ^{232}Th concentrations. These proxies have proven successful in Neogene sedimentary sections where the volcanic contribution to the refractory sedimentary component was as much as 50% [e.g.

Patterson et al., 1999; *Marcantonio et al.,* 2001; *McGee et al.,* 2007; *Winckler et al.,* 2008].

Helium in deep-sea sediments is derived from two primary sources, U-Th bearing minerals and interplanetary dust particles (IDPs) [e.g. *Farley,*1995; *Marcantonio et al.,* 1995]. The He isotopic composition indicates the source of the He to the sediments. In typical deep-sea settings >99% of the ^{3}He contained in the sediments is derived from extraterrestial sources [*Hiyagon,* 1994; *Farley and Eltgroth,* 2003; *Marcantonio et al.,* 1995, 1996, 2009]. The ^{3}He/^{4}He ratio of the extraterrestrial end-member has remained essentially constant at ~2.4 x10^{-4} throughout the Cenozoic [*Neir and Schlutter,* 1992; *Marcantonio et al.,* 2009] allowing for the calculation of helium contributed to the sediment by terrestrial inputs. The vast majority of ^{4}He is derived from terrestrial sources through alpha decay of U and Th, elements abundant in upper continental crust and virtually absent in volcanic materials [*Taylor and McLennan,* 1995; *Patterson et al.,* 1999; *Marcantonio et al.,* 1998].

^{232}Th is delivered to the ocean in association with continentally derived materials [*Koczy,* 1966]. Upper continental crust typically contains more than an order of magnitude more ^{232}Th relative to basaltic volcanic material (10.7 ppm vs. 0.22 ppm, *Taylor and McLennan,* [1985]). Therefore the majority of ^{232}Th in seawater is sourced from the continents. Thorium is highly particle reactive with an oceanic residence time of 10-40 yrs [*Chen et al.,* 1986; *Clegg and Whitfield,* 1991], but particle scavenging of Th is likely a reversible process [*Bacon and Anderson,* 1982; *Nozaki et al.,* 1981, 1987]. Recent studies suggest that ^{232}Th in deep-sea sediments is associated with detrital

minerals and thus its presence correlates with terrigenous inputs into the ocean [*Roy-Barman et al.,* 1996; *Marcantonio et al.,* 1995, 2001; *Anderson et al.,* 2006]. A global compilation of ^{232}Th content measured in modern loess and dust samples indicates a concentration range of ~7-14 ppm [*McGee et al.,* 2007]. The 7 ppm variation indicates heterogeneity in the ^{232}Th concentrations of weathered materials in the source regions. A growing body of work suggests that normalizing analyzed sedimentary ^{232}Th concentrations to the average upper continental crust value of 10.7 [*Taylor and McLennan,* 1995] permits accurate estimation of overall dust accumulation [e.g. *McGee et al.,* 2007; *Winckler et al.,* 2008]. ^{232}Th -based dust fluxes to the Arabian Sea were used to link variations in low latitude southwest monsoon to climate records from the North Atlantic providing evidence for a global teleconnection between atmospheric processes over the past 110 kyr [*Pourmand et al.,* 2004]. ^{232}Th has also been used to develop late Neogene glacial-interglacial eolian records in equatorial Pacific where previous dust studies were hindered by the large volcanic sedimentary component [*McGee et al.,* 2007; *Winckler et al.,* 2008].

In this study, we use the ^{232}Th content of ~58 Ma, carbonate-rich sediments from Shatsky Rise to quantify eolian dust and compare these data with estimates of dust accumulation from the same sedimentary section based on "traditionally" extracted dust [*Woodard et al.,* 2011] and $^{4}He_{crustal}$ concentrations [*Marcantonio et al.,* 2009]. All three records show similar patterns of variation in dust flux, and these variations correspond to cyclic changes in orbital eccentricity [*Westerhold et al.,* 2008; *Woodard et al.,* 2011]. A comparison of the $^{4}He_{crustal}$ and ^{232}Th concentrations suggests that there were at least

two sources of dust to the central subtropical North Pacific during the late Paleocene, but variations in dust provenance do not appear related to orbital forcing. In addition, we find that the majority of the sedimentary ^{232}Th is associated with leachable oxyhydroxide coatings and the refractory extracted "dust". This suggests that sedimentary Th concentrations may be useful in estimating the total dust flux to the ocean surface - the dust that dissolves in the water column as well as that preserved at the seafloor.

Materials and Methods

Site and Samples

The study location is Ocean Drilling Program (ODP) Site 1209 cored at the southern end of Shatsky Rise (Figure 3-1), presently located in the northwestern Pacific Ocean (32°39'N, 158°30'E). Shatsky Rise presents an ideal location for investigating atmospheric dust fluxes during the early Paleogene. Paleogeographic reconstructions place Site 1209 in the central subtropical North Pacific, ~15-20°N during the Paleocene (Figure 3-1). This location would have been remote from continental coastlines effectively eliminating the potential for contamination of the eolian signal by hemipelagic sedimentation [*Rea et al.,* 1985; *Rea,* 1994]. Furthermore, the section has orbital age control established using globally correlative eccentricity-scale variations in the sedimentary iron content [*Westerhold et al.,* 2008].

We measured the thorium concentration of 60 bulk sediment samples over a 4.5 m sedimentary interval spanning ~800,000 kyr of time some 58 million years ago (Table 3-1). We previously generated sedimentary helium abundances and isotopic composition

analyses [*Marcantonio et al.,* 2009] and analyses of eolian content determined using the "traditional" chemical extraction technique [*Woodard et al.,* 2011], on the same sedimentary section.

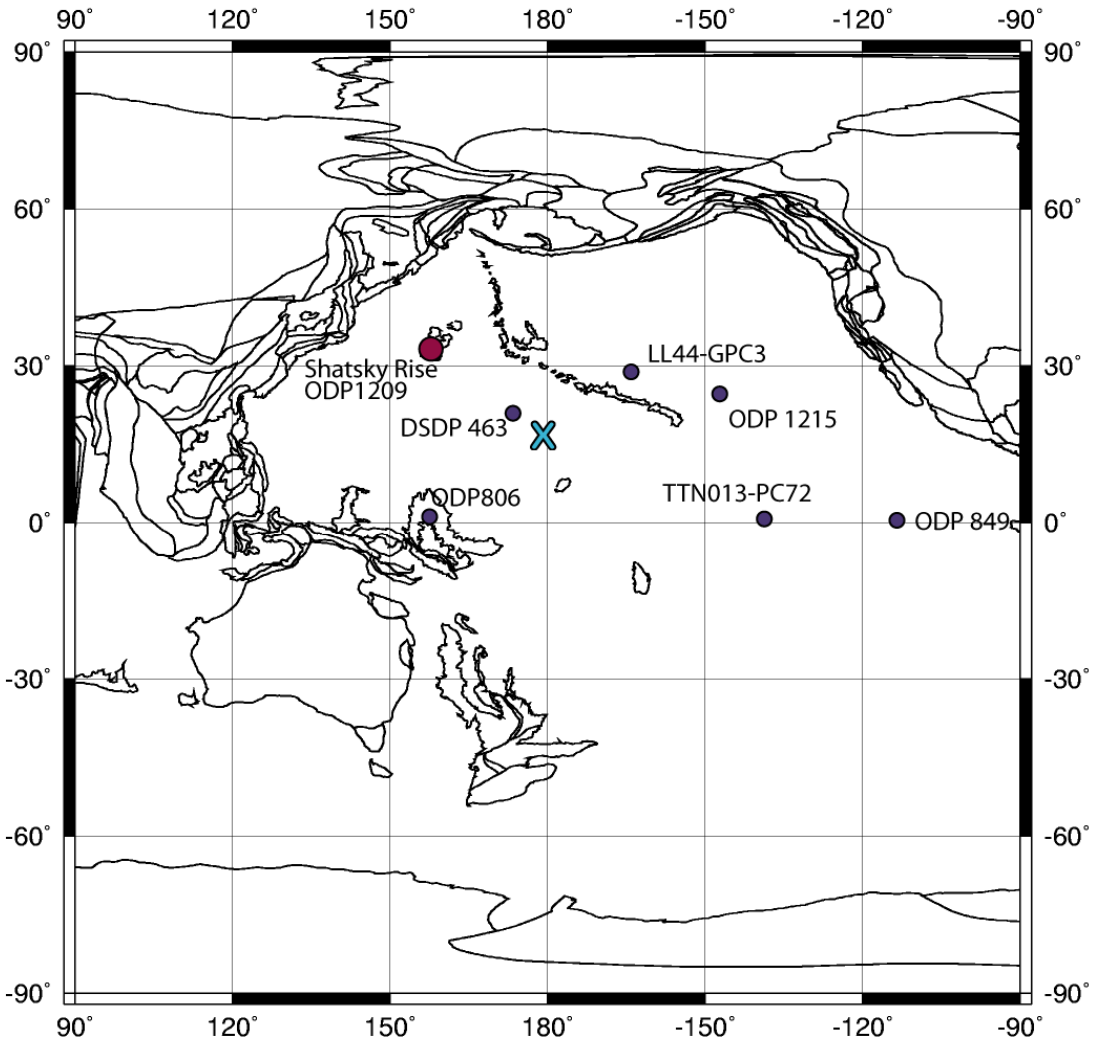

Figure 3-1. Pacific Ocean site map. Location of ODP Site 1209 (red) in the northwest Pacific Ocean as well as other deep sea sediment sites (purple) discussed in the text. Location of Shatsky Rise ~58 Ma based on paleo-reconstructions of *Hay et al.* [1999] is indicated by light blue "x".

To further investigate how the thorium signal is distributed in the sediments, we measured the Th content contained within the biogenic fraction (weak acid dissolvable)

and oxyhydroxide sedimentary coatings (hydroxylamine hydrochloride (HH) leachable) of an additional five bulk sediment samples. Earlier studies indicate carbonate content varies from 88-96 weight percent over the study interval [*Woodard et al.*, 2011] and consists primarily of nannofossil ooze with only a minor foraminiferal component and no biogenic silica [*Bralower et al.,* 2002]. We assume biogenic component consists of both biogenic carbonate (i.e., nanoplankton and foraminiferal remains) and apatite (i.e., fish debris), which dissolve completely after exposure to weak acetic acid. The HH leachable sedimentary fraction consists primarily of Fe-Mn based oxy-hydroxide coatings which form as authigenic precipitates on the exterior of marine particulates [*Haley et al.,* 2004; *Gutjahr et al.,* 2007]. In oxic waters, these coatings incorporate trace metals directly from porewaters within a few centimeters of the sediment-water interface and record the geochemical composition of the water mass bathing the seafloor [*Haley et al.,* 2004]. We also analyzed the Th content of the refractory non-dissolvable mineral component of seven "dust" samples extracted using the traditional technique. Due to the high carbonate content, our samples were subject to large weighing errors (50-75%) of the decarbonated residue and extracted sediment residue. As a result we were only able to determine the HH leachable weight percent of two samples (see Table 3-2) and unable to determine the [Th] content of the residual sediment. The Th content of in remaining HH leachate samples is estimated assuming HH leachable component is 0.15% of the total sediment by mass.

Table 3-1. Sedimentary [Th] for Site 1209

ODP Site	Core Section/ Interval (cm)	Depth (rmcd)	^{232}Th [ppb]	Sedimentary Dust Content* (mg/g sediment)	^{232}Th-based Dust Flux** (mg/cm^2/kyr)
1209C	12-4 10-11	229.89	111	10.4	
1209C	12-4 18-19	229.97	153	14.3	7.7
1209C	12-4 30-31	230.09	282	26.3	12.6
1209C	12-4 38-39	230.17	139	13.0	12.5
1209C	12-4 46-47	230.25	153	14.3	19.1
1209C	12-4 56-57	230.35	190	17.8	9.4
1209C	12-4 64-65	230.43	212	19.8	9.3
1209C	12-4 80-81	230.61	174	16.3	11.2
1209C	12-4 80-81	230.61	158	14.8	10.1
1209C	12-4 94-95	230.73	238	22.2	11.1
1209C	12-4 106-107	230.87	143	13.3	5.0
1209C	12-4 122-123	231.01	238	22.2	5.4
1209C	12-4 134-135	231.13	144	13.4	7.1
1209C	12-4 148-149	231.27	193	18.1	13.1
1209C	12-5 2-3	231.31	142	13.3	11.2
1209C	12-5 6-7	231.35	67	6.3	4.7
1209C	12-5 18-19	231.47	62	5.8	2.9
1209C	12-5 22-23	231.51	59	5.5	2.3
1209C	12-5 34-35	231.63	114	10.7	8.3
1209C	12-5 42-43	231.71	215	20.1	10.8
1209C	12-5 46-47	231.75	221	20.7	8.6
1209C	12-5 50-51	231.79	184	17.2	9.9
1209C	12-5 60-61	231.89	192	18.0	17.5
1209C	12-5 68-69	231.97	129	12.0	14.8
1209C	12-5 76-77	232.05	137	12.8	16.4
1209C	12-5 80-81	232.09	132	12.4	16.2
1209C	12-5 86-87	232.15	86	8.0	10.8
1209C	12-5 98-99	232.27	93	8.7	11.4
1209C	12-5 104-105	232.33	91	8.5	10.9
1209C	12-5 110-111	232.39	89	8.3	10.1
1209C	12-5 118-119	232.47	127	11.9	10.1
1209C	12-5 126-127	232.54	219	20.5	10.8
1209C	12-5 131-132	232.59	277	25.8	13.6
1209C	12-5 140-141	232.67	114	10.7	7.5
1209C	12-5 142-143	232.68	109	10.2	7.2
1209C	12-5 148-149	232.74	109	10.1	7.5
1209C	12- 6 2-3	232.77	100	9.4	7.8
1209C	12-6 7-8	232.82	108	10.1	11.9
1209C	12-6 14-15	232.88	113	10.6	6.3
1209C	12-6 18-19	232.91	107	10.1	5.2
1209C	12-6 26-27	232.99	82	7.7	6.7
1209C	12-6 34-35	233.06	65	6.1	3.1
1209C	12-6 38-39	233.1	83	7.8	2.4
1209C	12-6 43-44	233.15	97	9.1	8.2
1209C	12-6 47-48	233.19	82	7.7	10.6

Table 3-1. continued

ODP Site	Core Section/ Interval (cm)	Depth (rmcd)	^{232}Th [ppb]	Sedimentary Dust Content* (mg/g sediment)	^{232}Th-based Dust Flux** (mg/cm^2/kyr)
1209C	12-6 53-54	233.24	87	8.1	16.1
1209C	12-6 60-61	233.31	109	10.2	20.8
1209C	12-6 64-65	233.35	105	9.8	20.2
1209C	12-6 72-73	233.42	72	6.7	6.8
1209C	12-6 80-81	233.5	105	9.8	9.6
1209C	12-6 90-91	233.6	113	10.5	10.0
1209C	12-6 94-95	233.63	133	12.4	14.7
1209C	12-7 6-7	233.75	114	10.7	12.3
1209C	12-7 10-11	233.79	140	13.1	10.8
1209C	12-7 10-11	233.79	155	14.5	11.9
1209C	12-7 22-23	233.9	303	28.3	39.6
1209C	12-7 26-27	233.94	225	21.1	19.5
1209C	12-7 30-31	233.98	420	39.3	17.6
1209C	12-7 38-39	234.05	242	22.6	
1209A	23-3 96-97	234.64	407	38.0	

*Determined by normalizing to average upper continental crust, [^{232}Th] = 10.7 ppm (Taylor and McLennan, 1995)
**Calculated using $^3He_{ET}$-based sediment fluxes from Marcantonio et al. (2009)

Analytical Methods

Freeze-dried bulk sediment samples were thoroughly homogenized in an agate mortal and pestle. Bulk sediment and refractory extracted "dust" samples, 0.1 g and 5-10 mg respectively, were spiked with 50 ng ^{229}Th and completely digested using HF, HNO_3 and $HClO_4$ at 200°C. Th concentrations were determined via isotope dilution on the Thermo Element XR inductively coupled plasma mass spectrometer (ICP-MS) in the R. Ken Williams '45 Radiogenic Isotope Geoscience Laboratory at Texas A&M University. Samples were analyzed using a 30 second uptake followed by a 60 second count time with a 10 minute wash between samples. A 2 ppb U-500 enriched uranium standard (^{235}U/^{238}U = 1) was measured every fifth sample and used to correct for machine fractionation during the analysis and monitor drift. Fractionation corrections were generally low, <0.2%/amu. Tailing from ^{232}Th on ^{229}Th was also corrected. Replicate analyses were performed for two samples, and differences in [^{232}Th] between replicates

were <12%.

To separate biogenic and oxy-hydroxide sedimentary fractions for ^{232}Th determination we modified methods used by *Gutjahr et al.* [2007] and *Haley et al.* [2004]. The biogenic fraction (carbonate and apatite) was removed from ~0.3 g of bulk sediment by shaking in a 48:52 mixture of 1M acetic acid and 1M Na acetate buffer for 2 hrs. The solution was then centrifuged and the decanted supernatant plus 3 milli-Q water rinses were combined and saved for analysis. The residual solids were dried, weighed and leached with a solution of 0.02M hydroxylamine HCl suspended in 20% acetic acid to extract the oxy-hydroxides. Samples were centrifuged, the supernatant decanted and the remaining sediment freeze-dried and weighed. The decanted solutions, termed "biogenic" and "HH leachable", were spiked with ^{229}Th, allowed to equilibrate for 48 hrs, then dried down, re-suspended in 2% HNO_3 and analyzed on the ICP-MS. Procedural blanks were run with each method. In all cases, blanks contained ^{232}Th concentrations equaling <2% of that measured in the samples. Therefore, no blank corrections were necessary.

Sedimentary dust content was estimated by normalizing bulk sediment ^{232}Th concentrations to that of average upper continental crust, 10.7 ppm [*Taylor and McLennan,* 1995]. ^{232}Th-based dust fluxes are then calculated by multiplying the estimated sedimentary dust content by bulk sediment accumulation rates (MAR_{bulk}):

$$^{232}\text{Th-based dust flux} = \frac{[^{232}\text{Th}]_{\text{sample}}}{10.7\ \text{ppm}} * \text{MAR}_{\text{bulk}}$$

^{230}Th-normalized MARs are often used in conjunction with ^{232}Th to determine eolian fluxes [e.g. *Marcantonio et al.,* 2001; *Pourmand et al.,* 2004] because both ^{230}Th and ^{232}Th can be measured during the same analysis. However this technique is not useful for early Paleogene sedimentary sequences due to the relatively short half-life of ^{230}Th (75.38 kyrs).

Table 3-2. [Th] of Biogenic and HH Leachable Sedimentary Fractions

Sample ID	Depth (rmcd)	Biogenic ^{232}Th [ppb]	HH Leachable ^{232}Th [ppm]
12-4 148-149	231.27		47.1*
12-5 42-43	231.71		28.8
12-5 46-47	231.75	8.9	48.7
12-5 80-81	232.09		79.1*
12-5 110-111	232.39	6.3	25.5*
12-5 148-149	232.74		36.4*
12-6 64-65	233.35	8.1	27.5*
12-7 10-11	233.79		45.9*

*Estimated value if wt% = 0.15

Table 3-3. [Th] of Extracted "Dust"

Sample ID	Depth (rmcd)	Refractory Aluminosilcates♥ ^{232}Th [ppm]
12-4 30-31	230.09	5.0
12-4 94-95	230.73	4.7
12-5 2-3	231.31	4.4
12-5 18-19	231.47	3.7
12-5 34-35	231.63	3.6
12-5 60-61	231.89	3.6
12-5 142-143	232.68	4.4

♥Material isolated using "traditional" chemical extraction method

In order to estimate sedimentary MARs we calculated two bulk sedimentation models for this interval. One is tied to an astronomical calibration of Paleocene time based on globally correlated variations in sedimentary Fe content [*Westerhold et al.*, 2008] and the orbital solution provided by *Laskar et al.* [2004]. This model relies on linear sedimentation rates (LSR) interpolated between four age-tie points over the interval studied. Bulk sediment fluxes are calculated by multiplying the LSR by dry bulk density derived from shipboard physical properties [*Woodard et al.*, 2011]. The other sedimentation model is presented by *Marcantonio et al.* [2009] and uses the extraterrestrial (ET) ^{3}He constant flux proxy. It is assumed that over geologically short time periods (< 1 Myr) the flux of ^{3}He bearing IDPs to the deep sea occurs at a constant rate. Thus sediment MARs can be determined for any sedimentary interval by dividing the flux of $^3He_{ET}$ by the concentration of $^3He_{ET}$ measured in a sample. Bulk sedimentation rates calculated from both age models indicate low accumulation rates at Shatsky Rise during the study interval (<2.1 g/cm^2/kyr), consistent with an oligotrophic pelagic setting. However, the sediment accumulation rates determined by *Marcantonio et al.* [2009] display a larger range and are temporally more variable than those calculated using linear sedimentation rates (Figure 3-2a). The difference is likely due to the fact that the $^3He_{ET}$ proxy estimates the "instantaneous" vertical rain rate of sediment for each sample analyzed while sedimentation rates based on the other method are smoothed due to interpolation between widely spaced age tie-points [*Marcantonio et al.*, 2009]. The range of variability in the $^3He_{ET}$ derived sediment accumulation rates encompasses that found using the orbital tie-point LSR model, therefore we used the

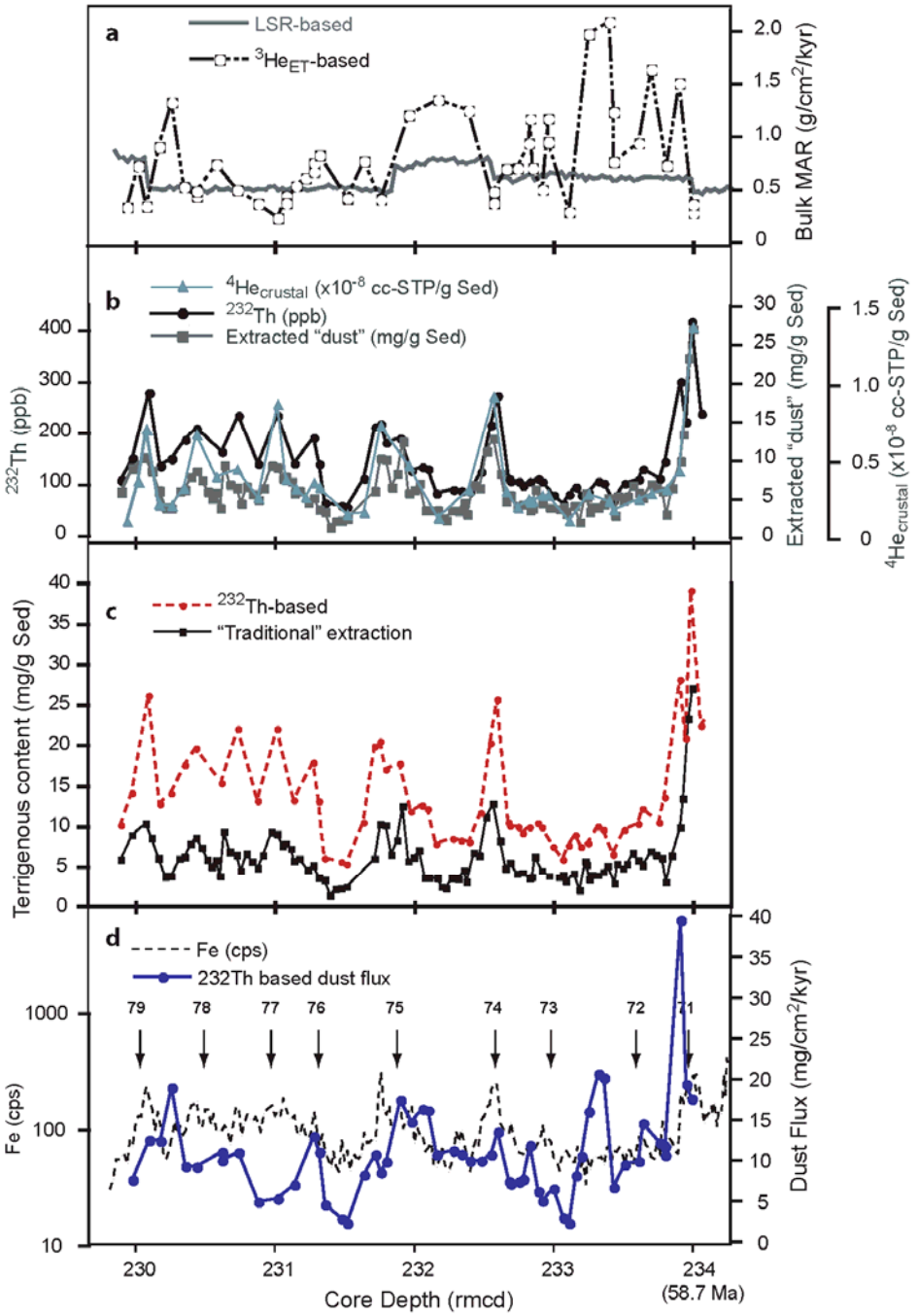

Figure 3-2. Comparison of bulk sedimentation rates and sedimentary dust using different proxies. **a**) Bulk sediment MARs calculated using $^{3}He_{ET}$ constant flux proxy [*Marcantonio et al.,* 2009] and interpolated LSRs [*Woodard et al.,* 2011]. **b**) ~800 kyr record of bulk sedimentary concentrations of [^{232}Th] (this study), calculated [$^{4}He_{crustal}$] [*Marcantonio et al.,* 2009] and the extracted non-dissolvable mineral component [*Woodard et al.,* 2011]. **c)** Comparison of terrigenous sedimentary content determined from measured [^{232}Th] and the extracted "dust" record [*Woodard et al.,* 2011]. **d)** ^{232}Th -based dust flux determined using $^{3}He_{ET}$ constant flux MARs [*Marcantonio et al.,* 2009]. XRF Fe content is plotted for reference [*Westerhold et al.,* 2008]; peaks 71-79 correspond to 100 kyr eccentricity cycles.

$^{3}He_{ET}$ derived bulk sediment MARs (Appendix C) for determination of Th-based dust accumulation and to compare dust fluxes in to the central subtropical Pacific during the early Paleogene with other records. When $^{3}He_{ET}$ based MARs were unavailable for a specific sample, we estimated bulk sedimentation rates by linear interpolation between $^{3}He_{ET}$ tie points.

Results

Bulk sediment Th concentrations range from 59 to 420 ppb (Table 3-1) and average 151 (±71, s.d.) ppb. The variations in sedimentary Th content are similar to changes in extracted dust (Woodard et al., 2011) and crustal ^{4}He concentrations [*Marcantonio et al.,* 2009] (Figure 3-2b). The Th-based sedimentary dust content ranges from 0.6 to 3.9 wt percent after normalization to average upper continental crust (assuming that all sedimentary Th is wind-blown terrigenous material). These percentages are slightly higher than those determined using "traditional" chemical extraction (0.2 – 2.7%; *Woodard et al.* [2011]) although the pattern of variation is similar (Figure 3-2c). The Th-based dust flux averages 11.0 ±5.9 (s.d.) mg/cm^{2}/kyr over the entire interval and ranges from 2.4 – 39.6 mg/cm^{2}/kyr. In general dust fluxes exhibit 2 to 3-fold fluctuations about the mean. The maximum dust flux occurs as an isolated point early in the record (~234 rmcd) and is nearly double other dust flux maxima observed in the record.

^{232}Th concentrations of the refractory extracted "dust" samples average 4.20 ppm (±0.57, s.d.; Table 3-2). The biogenic sedimentary component (weak acid dissolvable)

comprises the majority of the sediments by weight, but contains low Th concentrations (< 10 ppb, N=3). We find that ~98-99% of the total sediment is "biogenic" in the three samples analyzed. Th concentrations in the HH leachate were high (average 38.7 ppm, N=2). The HH leachable material comprised less than 0.25% of the bulk sediment.

Discussion

Comparison of Different Dust Proxies

The Site 1209 bulk sediment Th concentration record provides an opportunity to evaluate the use of Th concentrations as a proxy for eolian dust accumulation during the early Paleogene. For the first time we can compare records of all three dust proxies generated from the same sedimentary section in order to assess the fidelity of these tools.

The three records demonstrate similar trends, particularly in the lower portion of the sedimentary sequence in which the sampling resolution is comparably high (Figure 3-2b). While the similarity between the ^{232}Th and $^{4}He_{crustal}$ patterns is not surprising given the genetic relationship between the two nuclides, the coincidence of all three is significant and supports the use of these techniques in early Paleogene sedimentary sequences.

Although the dust proxy records show similar patterns of variation, the ^{232}Th-based estimate of sedimentary dust content (normalized to average upper continental crust) is roughly 40-60% higher than that determined using the "traditional" chemical extraction (Figure 3-2c). There are two potential reasons for the difference in reconstructed dust content. The first is that the "traditional" dust record is biased toward

low values because of sediment loss during the chemical extraction. Small losses can significantly impact the calculated flux, especially in carbonate-rich sediments where the lithologic component is < 5% [*Hovan,* 1995; *Zeigler et al.,* 2007a]. The repeated washing and decanting involved in the traditional method of "dust" extraction can lead to errors of ±10-15% in the sedimentary dust content [*Rea and Janecek,* 1981; *Hovan et al,* 1991]. However, if this were the case, we would expect that samples containing lower percentages of dust to be most affected by systematic losses of sediment during extraction, resulting in a greater discrepancy between the ^{232}Th -based and "traditional" records for low content values. But there is no consistent pattern of discrepancies between the two techniques in the data (Figure 3-2c).

Alternatively, the ^{232}Th concentration of bulk sediment may overestimate the fraction of terrigenous sediment that accumulates on the seafloor. While the majority of the ^{232}Th measured in the sediment is derived from the continents, it is not necessarily bound in detrital minerals. Elevated concentrations of dissolved ^{232}Th have been observed in the upper ocean and in remote regions (such as the central Pacific) are attributed to dissolution of eolian dust [*Hiroseand sugimura,* 1987; *Tsunogai et al.,* 1994; *Guo et al.,* 1995; *Clegg and Whitfield,* 1991]. Dissolved thorium is rapidly scavenged by particulates in the water column and transported to the seafloor where it is incorporated into the sediments. Therefore the bulk sediment ^{232}Th content may represent the *total eolian dust flux to the sea surface*, not only what is preserved at the seafloor but also that fraction that dissolves in the water column. The traditionally extracted "dust" represents only the non-dissolvable mineral fraction stored in the

sedimentary record. This assertion is supported by our data regarding how Th is partitioned within the sediments and explored further in the following sections.

Evaluating Potential Non-eolian and Diagenetic Contributions to Extracted "Dust"

One reason for exploring independent proxies for dust accumulation, particularly for older geologic intervals, is that limited evidence exists which suggests the traditionally extracted dust fraction may be influenced by volcanic or authigenic contributions. Chemical isolation of the non-dissolvable mineral fraction (dust) does not remove volcanics or clay minerals formed authigenically. The coherence of the ^{232}Th and traditionally extracted dust records from ODP Site 1209 suggest that both proxies reflect the same process – accumulation of eolian dust.

On the basis of the combined ^{232}Th and traditionally extracted dust records, we can rule out significant volcanic contributions at Shatsky Rise. Basaltic material contains over an order of magnitude less ^{232}Th than upper continental crust [*Taylor and McLennan,* 1985], thus the presence of typical volcanic ash would increase apparent "dust" content while diluting the ^{232}Th signal which is not observed in the records (Figure 3-2c). Furthermore, the remote location of Shatsky Rise during the early Paleogene renders contamination by volcanic ash unlikely. Geochemical studies of recent sediments deposited in the central North Pacific confirm >85% of extracted "dust" is of continental origin indicating that volcanic material is not effectively transported large distances across the ocean [*Olivarez et al.,* 1991; *Weber et al.,* 1996]. Shatsky Rise also was far from active ocean spreading centers during our study interval

[*Rea and Dixon,* 1983].

The new ^{232}Th data combined with the $^{4}He_{crustal}$ data also rule out a significant authigenic component to the Shatsky Rise dust fraction. Recent geochemical analyses by *Zeigler et al.* [2007a,b] identified a significant contribution of authigenic mineral phases in "dust" extracted using the traditional technique from carbonate-rich North Pacific sediments (ODP Site 1215), calling into question the use of traditional methods to reconstruct dust fluxes in material older than 50 Myr. REE profiles of the extracted dust exhibited a negative Ce anomaly similar to that observed in seawater, and they posited that this signal reflected the predominance of authigenic minerals in the dust fraction (although the authigenic mineral phase carrying the seawater signature was not identified). If the extracted dust fraction were dominated by authigenic minerals, such mineralogy would have had significantly lower ^{232}Th concentrations, hence lower ^{232}Th-based flux estimates. Furthermore, widespread alteration of the reconstructed dust flux at other pelagic locations is unlikely for the following reasons. 1) The formation of large quantities of authigenic alumino-silicates requires a source of mobile silica [*Mackin and Aller,* 1984; *Michalopoulos and Aller,* 2004; *MacKenzie and Kump,* 1995]. Sources include biogenic amorphous silica or volcanic glass, both of which are readily leached and can react with available Al, Mg and Fe to form clay minerals. The early Paleogene sediments deposited at Shatsky Rise and other locations used in contemporaneous dust reconstructions [e.g., *Rea,* 1994] contained no significant traces of siliceous microfossils [*Bralower et al.,* 2002] and insignificant amounts of volcanic glass. 2) XRD analysis of the extracted dust from Shatsky Rise indicates a mineral assemblage associated with

weathered continental crust: quartz, feldspar and kaolinite [*Woodard et al.,* 2011]. 3) ^{4}He cannot be incorporated into minerals by adsorption on surfaces, particle scavenging or biogenic uptake; rather it "grows" into minerals by alpha decay of U and Th [*Patterson et al.,* 1999; *Farley,* 1995]. Additionally, the typical path length for a ^{4}He particle during alpha recoil is 10-30 μm [*Farley et al.,* 1996], much greater than the average grain size of the "dust" extracted from the sediments [*Woodard et al.,* 2011]. Therefore, precipitation of authigenic minerals would contribute mass to the extracted "dust" component of the sediment without adding any ^{4}He.

The evidence cited above for minimal authigenic contributions to the dust fraction in pelagic sediments can be reconciled with the findings of *Ziegler et al.* [2007a]. We argue that the geochemical evidence cited by *Ziegler et al.* [2007a] was influenced by selection of a sedimentary section that was subject to a more complex diagenetic history. The carbonate-rich sedimentary sequence at Site 1215 is much more condensed than at Site 1209 due to carbonate dissolution as the region thermally subsided over time and passed through the lysocline and eventually below the CCD. In addition, the carbonate-rich sequence at Site 1215 is directly overlain by pelagic red clays containing metaliferous deposits related to hydrothermal plume accumulation [*Ruhlin and Owen,* 1986; *Zeigler et al.,* 2007b]. Mobile silica and metal elements from these plume deposits may have provided material for mineral formation and contributed to the geochemical signatures of the unidentified authigenic phases observed in the older sediments at Site 1215.

The coherent relationship between sedimentary ^{232}Th and crustal ^{4}He

concentrations indicates that the terrigenous sedimentary fraction was not impacted by diagenetic alteration. While both elements are introduced to the ocean in association with terrigenous materials, they are present in different phases and therefore are subject to different oceanic processes. ^{4}He exists as a gas and is implanted into a mineral's crystalline lattice. The minerals are subsequently weathered to a grain size small enough to be capable of long-distance eolian transport [*Farley,* 1995; *Patterson et al.,* 1999]. In deep sea sediments the majority of ^{4}He is stored by trace minerals (e.g. zircon, sphene, igneous apatite) which comprise a very small proportion of the eolian dust load [*Martel et al.,* 1990; *Patterson et al,* 1999]. A long term record of $^{4}He_{crustal}$ in marine sediments indicates that these minerals retain their original ^{4}He signature over a period of at least 70 Myr [*Farley,* 1995]. Th-rich detrital mineral phases certainly contribute to the sedimentary Th content, yet seawater also contains a Th load which is delivered to the deep ocean via scavenging, primarily by colloidal particles which are incorporated into larger aggregates and rapidly transported to the deep sea [*Honeyman and Santschi,* 1989; *Roy-Barman,* 2009]. More than 50% of the ^{232}Th present in modern pelagic ocean sediments may exist in this sorbed phase and rather than locked in mineral lattices [*Robinson et al.,* 2008; *Roy-Barman et al.,* 1996]. Early diagenetic reactions at the sediment water interface often remobilize trace metals and could drive variations in ^{232}Th content by releasing adsorbed Th to the overlying water column. Low pore water concentrations [*Somayaju and Church,* 1973] combined with relatively high particle reactivity provide convincing evidence that ^{232}Th has limited mobility in the sedimentary column [*Antal,* 1966; *Bernat and Goldberg,* 1969]. The coherence of our ^{232}Th data with

$^{4}He_{crustal}$ records, in addition to the coherence with the traditionally extracted dust, argues against significant remobilization of Th due to sedimentary diagenesis.

Paleoclimatic Implications of the ^{232}Th -based Dust Fluxes

The average dust flux calculated using bulk sediment ^{232}Th concentrations is more than double that determined using the traditional "dust" extraction method, 11.1 mg/cm^2/kyr vs 5.1 mg/cm^2/kyr [*Woodard et al.,* 2011]. Even so, our record indicates dust flux to the central Pacific was at least 4 times lower during the study interval 58 Ma than during the late Quaternary. The dust flux calculated for core-top sediments from nearby DSDP Site 463 (21°21N, 174°40E) is ~41 mg/cm^2/kyr [*Rea and Janecek,* 1981]. This value is comparable to modern dust fluxes to the central subtropical N. Pacific average 50-100mg/cm^2/kyr [e.g. *Jickells et al.,* 2005], 5 to 10x greater than during the study interval. The overall lower average dust fluxes reconstructed for the early Paleogene are likely related to a relatively more humid atmosphere characteristic of global greenhouse climate [*Rea et al.,* 1985; *Rea,* 1994]. However, if by analogy the atmospheric dust flux during the early Paleogene was a function of source region aridity and the prevalence of strong winds as indicated by high-resolution Quaternary records [e.g. *Rea,*1994 and references therein; *McGee et al.,* 2010], then variations in dust mass accumulation in deep sea sediments deposited during greenhouse climate intervals must reflect environmental changes large enough to impact the supply of dust available for entrainment and transport.

The Th-based dust fluxes vary significantly over the ~800 kyr record. The

highest amplitude variations are observed in the lower half of the record where dust flux maxima are as much as 8 times minima values (Figure 3-2d). Peaks in dust accumulation tend to coincide with increased sedimentary Fe content. Exceptions to this pattern are most evident at ~231 rmcd, where an inverse relationship is observed, and at ~233.35 rmcd where a large increase in dust flux is not mimicked in the Fe record. The general agreement between our Th-based dust flux record and eccentricity cycles, identified using the sedimentary Fe [*Westerhold et al.,* 2008], implies a connection between orbital changes in solar insolation and some aspect of dust production and/or entrainment.

Environmental changes driven by orbitally paced insolation variations are well documented for the late Neogene glacial-interglacial cycles [e.g. *Zachos et al.,* 2001 and references therein]. Our early Paleogene record implies a similar response to orbital forcing ~58 Ma, assuming the variations in dust accumulation are driven by changes in the hydrologic cycle and/or frequency of large wind storms. The connection between variations in dust accumulation and orbital parameters lies in the amount and distribution of solar energy received by the Earth directly impacting annual seasonality and meridional temperatures gradients [*Palike,* 2005].

Increases in dust accumulation generally coincide with eccentricity maxima [*Marcantonio et al.,* 2009; *Woodard et al.,* 2011; this study]. Peak eccentricity would cause greater seasonal contrasts and steepened meridional temperature gradients [*Palike,* 2005; *Berger and Loutre,* 2002], both of which promote dust generation. Seasonality in tropical to sub-tropical regions typically is based on moisture, thus enhanced seasonality would lead to a more pronounced dry season, potentially increasing dust production.

Steepened meridional temperature gradients drive differences in atmospheric pressure resulting in stronger winds and the development of more large low-pressure systems, the meteorological mechanism responsible for long range dust transport [*Pye,* 1987; *McGee et al.,* 2010]. Changes in surface temperature and pressure gradients would likely influence rainfall patterns as well. Regardless of the precise mechanism responsible for enhanced dust generation/accumulation during eccentricity maxima, the new ^{232}Th data confirm previous assertions that orbitally forced changes in solar insolation caused variations in dust accumulation during the early Paleogene greenhouse.

Dust Sources Inferred From $^{4}He_{crustal}$ /^{232}Th Ratios

Linear relationships between sedimentary $^{4}He_{crustal}$ and ^{232}Th concentrations have been used to validate ^{232}Th fluxes as a proxy for eolian dust accumulation [*Anderson et al.,* 2006; *McGee et al.,* 2007] and as indicators of dust provenance [e.g. *Winckler et al.,* 2008]. Such work is based on the assumption is that the $^{4}He_{crustal}$ /^{232}Th ratio will increase with the age of the source rock due to the production of ^{4}He by the radioactive decay of U and Th. Thus, dust weathered from areas comprised of old cratonic bedrock will have high $^{4}He_{crustal}$ /^{232}Th ratios relative to that supplied from younger or more volcanic-bearing source regions. A recent study of late Neogene sediments spanning an equatorial transect in Pacific Ocean produced three linear $^{4}He_{crustal}$ /^{232}Th relationships and indicated a west to east decrease in $^{4}He_{crustal}$ /^{232}Th ratios [*Winckler et al.,* 2008]. This gradient was interpreted to reflect a change in the source of terrigenous sediment supply. Dust deposited from 160°E to 140°W reflected an older crustal source,

presumably Asian loess, while at 110°W, the source was significantly younger crust, probably from South America [*Winckler et al.,* 2008].

The relationship between the Site 1209 $^{4}He_{crustal}$ and ^{232}Th abundances indicates two distinct linear correlations ($R^2 > 0.9$) suggesting at least two source regions that supplied dust to Shatsky Rise ~58 Ma (Figure 3-3a). While $^{4}He_{crustal}$ /^{232}Th ratios do not absolutely or uniquely identify dust provenance, the data suggest relatively old continental sources of dust. Source rocks accumulate ^{4}He over time as the result of radiogenic production, The relatively high $^{4}He_{crustal}$ /^{232}Th ratios suggest source rocks with a long enough history to accumulate ^{4}He. Variations in the provenance indicated by the $^{4}He_{crustal}$ /^{232}Th ratios likely reflect the competing influence of the differerent dust sources.

One possible scenario to explain the changes in dust provenance invokes a main continental dust source represented by the high $^{4}He_{crustal}$ /^{232}Th endmember which is periodically diluted by particles with low $^{4}He_{crustal}$ /^{232}Th ratios. Dust reaching Shatsky Rise ~58 Ma would most likely be carried by the northeast trade winds, assuming a wind regime similar to the modern. Source regions to the east include North and Central America and northern Africa. We consider northern Africa a potential dust source because it is comprised of relatively old cratonic rock and vegetation models indicate it was likely sparse savannah and shrubland at the time [*Sewall et al.,* 2000], rendering it a prime region for dust production. In addition, the Panamanian gateway was open during the Paleogene and the Atlantic Ocean was narrower [*Cande and Kent,* 1995], making long distance transport of dust to the central Pacific more likely. Thus, dust from

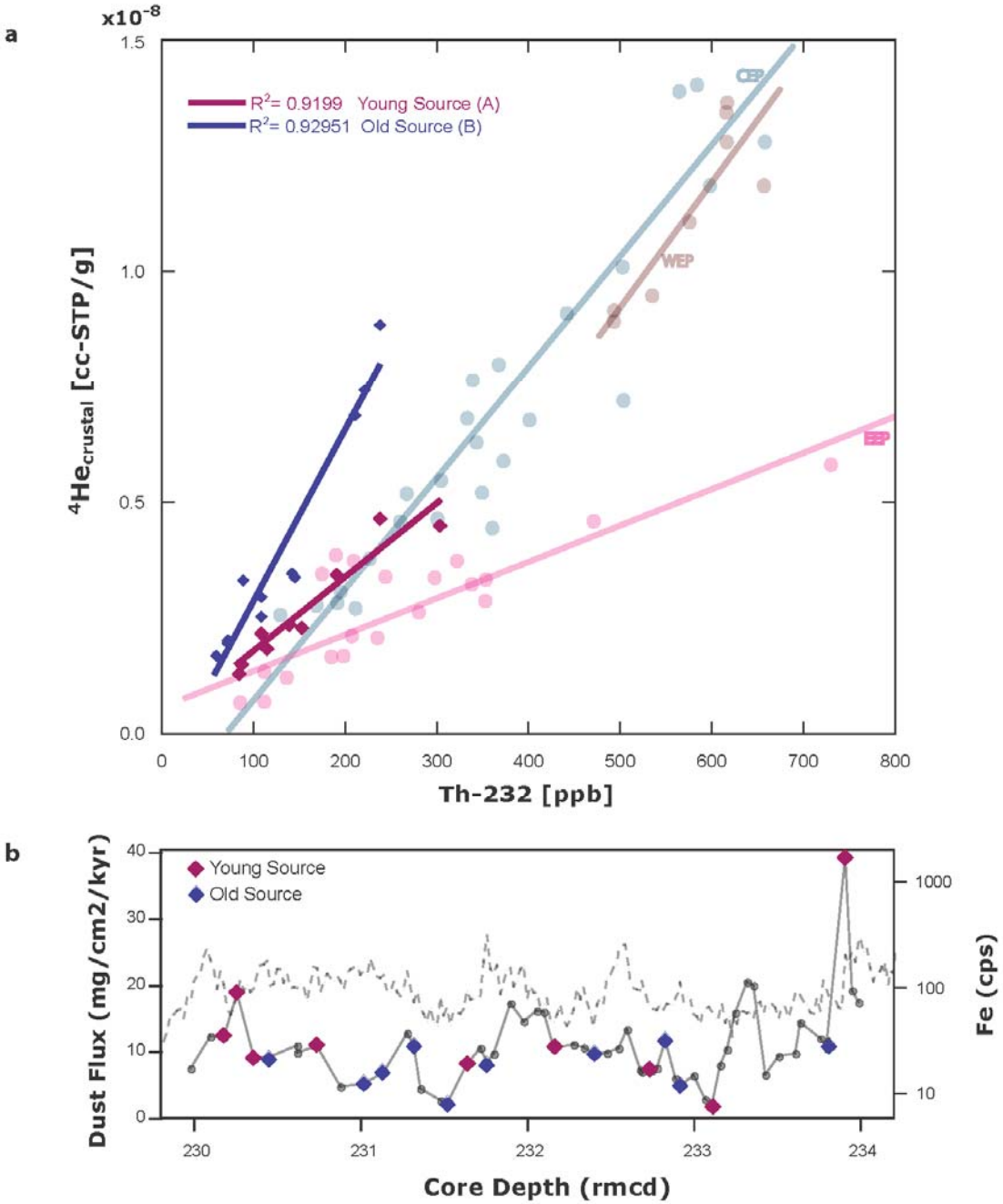

Figure 3-3. ^{232}Th-^{4}He$_{crustal}$ source plot. **a**) Sedimentary ^{4}He$_{crustal}$ [*Marcantonio et al,* 2009] plotted against ^{232}Th concentrations. Two distinct linear trends suggest dust was supplied to by "older" (blue) and "younger" (pink) continental sources. Faded lines [modified from *Winckler et al,* 2008] represent Quaternary dust from the eastern equatorial Pacific (EEP, ODP Site 849), central equatorial Pacific (CEP, TTN013-PC72) and western equatorial Pacific (WEP, ODP Site 806). **b)** ^{232}Th-based dust flux record with source variations indicated by color. Changes in dust source do not appear related to eccentricity changes identified by sedimentary Fe content [*Westerhold et al.,* 2008].

northern Africa may have been the main source of the ”old” dust component in our record. This is because material sourced from the Caribbean and North/Central America likely would have been derived from arc volcanism which was active throughout the early Cenozoic [*Meschede and Frisch,* 1998; *Mitchell and Blissett,* 1999]. Magmas with andesitic compositions are common for Paleogene age ignimbrites and contain on average 4.8 ppm ^{232}Th [*Taylor and McLennan,* 1995] but virtually no ^{4}He [*Marcantonio et al.,* 1995]. Sporadic additions of andesitic material generated by arc volcanism could dilute the African dust, thus lowering the sedimentary $^{4}He_{crustal}$ /^{232}Th ratios.

The above scenario is supported by the observation that changes in $^{4}He_{crustal}$/^{232}Th ratios (ie. switch from ”older” to ”younger” source) are not cyclic and do not correspond to orbitally-paced changes in dust accumulation (Figure 3-3b). This indicates variations in orbital forcing were probably not responsible for the changes observed in dust source. It is therefore reasonable to assume that generally random additions of andesitic material generated by arc volcanism and unrelated to climate could account for the lowered $^{4}He_{crustal}$ /^{232}Th ratios.

It is also important to consider a potential dust source to the west of Shatsky Rise during the early Paleogene. Today expansive loess deposits in Asia yield such vast quantities of dust that material entrained in westerly winds is transported over the entire North Pacific Ocean, where it comprises the majority of the eolian component of deep sea sediments as far south as the equator [*Nakai et al.,* 1993; *Rea,* 1994]. If an analogous large dust-producing regions existed in Asia during the Paleogene, then it could have impacted the study site. Comparison of our record with equatorial Pacific sediments

deposited over the last 500 kyrs, indicates the "younger" of our dust sources is similar to the "older" (Asian) source identified by *Winckler et al,* [2008] (Figure 3-3a). If we assume that the lower $^{4}He_{crustal}$ /^{232}Th ratio represents an Asian dust source, then the higher ratios must reflect a source region dominated by older rocks. The paleolocation of Site 1209 at ~15-20°N was near what is the modern boundary between the westerlies and the northeastern trade winds. Migration of this boundary could have caused variations in the relative amounts of Asian dust reaching the central subtropical North Pacific, allowing proportionally more "old" dust supplied from Africa by the trade winds to accumulate at Site 1209. However, this interpretation is at odds with long-term records of dust provenance based on REE and radiogenic isotope geochemistry [*Kyte et al.,* 1993; *Pettke et al.,* 2002; *Hyeong et al.,* 2005].

The εNd composition of eolian dust from Site LL44-GPC3 (just east of Site 1209) indicates two sources of dust to the central Pacific during the early Cenozoic - older terrigenous material from Asia (εNd = -10) and younger volcanic material form the Americas (εNd >-5) [*Kyte et al.,* 1993; *Pettke et al.,* 2002]. The variations in dust provenance are interpreted to reflect the paleo-location of the inter-tropical convergence zone (ITCZ) [*Pettke et al.,* 2002; *Hyeong et al.,* 2005]. Enhanced precipitation along the ITCZ forms an effective barrier to dust transport between hemispheres [*Rea,* 1994]. If the ITCZ was pushed north to 20-30ºN latitude during the early Paleogene then subtle fluctuations in its position would determine whether dust reaching the subtropical Pacific was supplied from the Asia, the Americas [e.g. *Pettke et al.,* 2002; *Hyeong et al.,* 2005] or Africa. Our ^{4}He crustal/^{232}Th record indicates little influence of young volcanic

material, thus it is unlikely that the dust source variations relate to changes in the ITCZ as suggested by *Pettke et al.* [2002] and *Hyeong et al.* [2005]. However, we cannot rule out the possibility that the ITCZ was located north of Shatsky Rise, 58 Ma. In this case, the "older" component of dust would have to have been supplied from the Southern Hemisphere or from Africa with varying additions of relatively younger material from South/Central America. Australia may have been such an "older" dust source. Today Australia is hyper-arid and deflated of fine-grained material capable of long range eolian transport, but during the early Paleogene greenhouse the continent experienced a warm temperate climate with seasonally arid conditions in the north [*Martin,* 2006], making it a potentially important dust source region.

Mass Balance: Th Distribution in the Sediments

Although we have limited data, it is possible to construct a general mass balance to explain how Th is distributed in the sediments. The total Th content of the sediment is represented by:

$$[^{232}\mathrm{Th}]_{\mathrm{total}} = f_{\mathrm{B}}[^{232}\mathrm{Th}]_{\mathrm{B}} + f_{\mathrm{HH}}[^{232}\mathrm{Th}]_{\mathrm{HH}} + f_{\mathrm{R}}[^{232}\mathrm{Th}]_{\mathrm{R}}$$

$$\text{when} \quad f_{\mathrm{B}} + f_{\mathrm{HH}} + f_{\mathrm{R}} = 1$$

B, HH and R represent the biogenic, HH leachable oxy-hydroxide and refractory non-dissolvable mineral components of the sediments, f is the estimated fractional percentage and $[^{232}\mathrm{Th}]$ is the average Th concentration of component (x). By assuming the average Th content of each of the sedimentary fractions (biogenic, HH leachable and

refractory) given in Table 3-2 is representative of the entire sedimentary column and generally estimating average sedimentary percentages of each component to be 98.8% (weak acid dissolvable biogenics), 0.2% (HH leachable) and 1.0% (refractory minerals), we calculate the total sedimentary ^{232}Th concentration to be 128 ppb. This agrees well with the average measured bulk sediment ^{232}Th of 151 ppb and confirms that our estimated averages adequately reflect the relative inputs of each of the different sedimentary components.

Figure 3-4 illustrates how the total measured ^{232}Th is distributed among the three sedimentary fractions. The majority of the ^{232}Th is contained in the HH leachable (61%) and refractory mineral (33%) sediment fractions even though on average they account for less than 1.5% of the total sediment mass. Only 6% of the ^{232}Th resides in the biogenic fraction. This agrees with other studies that find very low ^{232}Th concentrations in biogenic carbonates [*Delaney and Boyle,* 1983; *Robinson et al.,* 2004, 2008; *Adkins et al.,* 1998] Furthermore, *Robinson et al* [2008] found 30-50% of the total ^{232}Th in modern deep sea sediments is present as adsorbed species rather than lattice bound in detrital mineral grains. They suggest that measurement of adsorbed and total ^{232}Th may be used quantify dissolved and total detrital fluxes to the ocean. This has significant potential as a paleoceanographic tool to estimate eolian inputs of micro-nutrients, which limit primary production in some oceanic regions. However, to make use of this tool, we must confirm that the ^{232}Th we measured was derived from dissolution of dust at the sea surface directly above and has not been added by lateral transport or boundary scavenging.

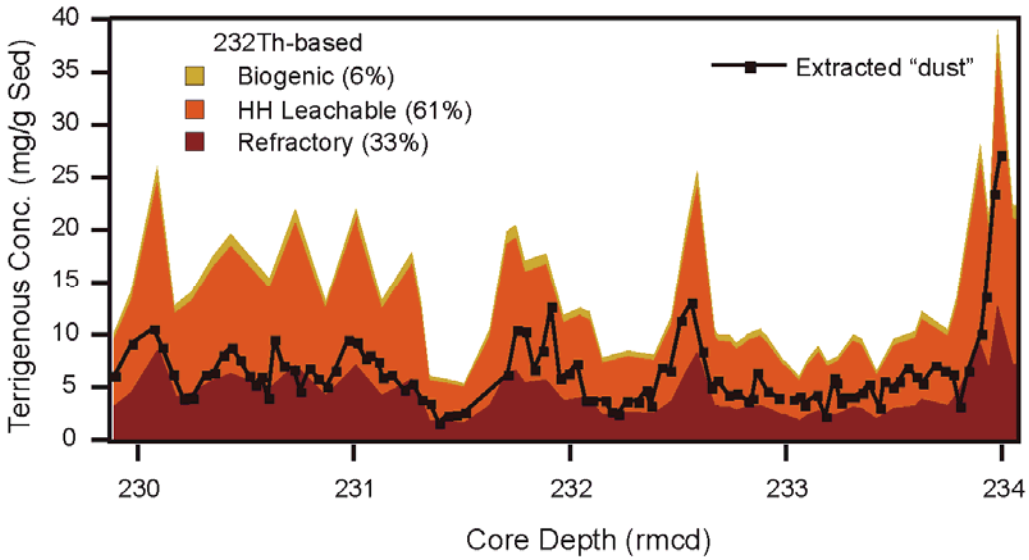

Figure 3-4. Distribution of Th among different sediment fractions. Biogenic (yellow), HH leachable oxy-hydroxides (orange) and refractory non-dissolvable mineral phases (red). The traditional extracted "dust" record, plotted in black [*Woodard et al.*, 2011], compares in magnitude to the dust content estimated using the average [^{232}Th] contributed by the refractory extracted "dust".

Our conversion of bulk sediment Th concentrations to dust fluxes relies on normalization of the measured sedimentary ^{232}Th content to 10.7 ppm (average upper continental crustal value given by *Taylor and McLennan* [1985]), but the refractory non-dissolvable minerals extracted from the sediments contains only an average Th concentration of 4.2 ppm. This would imply that the refractory material is comprised of <50% terrigenous material or that there is significantly less ^{232}Th in the extracted "dust" than previously assumed. We already have discounted the possibility of substantial volcanic or authigenic contributions to the extracted "dust" based on ^{232}Th considerations, however these arguments are based on the assumed upper crustal ^{232}Th concentration and therefore are circular for the problem at hand. But analysis of the Nd isotopic composition of the extracted dust provides an independent check on the origin

of the dust minerals. The average Nd isotopic composition of the extracted "dust", expressed in epsilon notation, is -11.2, which indicates a continental source as opposed to typical reconstructed ~58 Ma seawater values for Site 1209 which average ~-3.2 [*Thomas,* 2004] (See Chapter 4 for a thorough discussion). Any significant authigenic component would have increased the Nd isotopic composition of the dust fraction due to the large difference between contemporaneous detrital and seawater compositions. Therefore, we must consider mechanisms that might impart lower than expected ^{232}Th concentrations in the terrigenous material comprising the extracted "dust".

One possibility is that the more humid climate of the "greenhouse" world enhanced chemical weathering on land during the early Cenozoic, causing the detrital minerals formed to reflect a more altered geochemical signature. *Cole et al.* (2009) observed ^{232}Th concentrations of only 6-7 ppm in dust extracted from sediments deposited at ODP Site 658 during the African Humid Period, 12 ka. They determined the dust was in fact derived from the Saharan region and enhanced chemical weathering at the source altered the geochemical signature [Cole et al., 2009]. Climate models [*Huber et al.,* 2000; *Shellito et al.,* 2003; *Sewall et al.,* 2000], the presence of vast Paleocene age coal deposits [*Ross and Ross,* 1984; *Shah et al.,* 1993; *Retallak et al.,* 1996] and overall lower dust fluxes [*Rea.,* 1994; *Woodard et al.,* 2011] indicate the Early Paleogene was substantially more humid than any time during the recent geologic past. Thus, intense chemical weathering of soil and sediments in dust source regions may result in removal of Th from the mineral lattice causing the low ^{232}Th concentrations observed in the refractory component of our record.

Alternatively, the extracted dust may contain significantly less ^{232}Th than "typical" upper continental crust because the detrital mineral assemblage preserved in the sediments is biased toward Th-poor minerals. For example, quartz is abundant in continental rocks, contains virtually no Th, survives chemical weathering and is stable in seawater [*Sevier,* 1962; *Leinen et al.,* 1986; *Patterson et al.,* 1999]. Other minerals such as feldspars are subject to intense chemical weathering and convert to clays, which are more susceptible to dissolution/leaching in seawater due to their larger surface area and cation exchange capacity [*Carroll,* 1958]. The XRD data indicate the presence of both clay minerals and feldspar in our extracted "dust", but the results are not quantitative. While much semi-quantitative work has been done to show that the seafloor mineral assemblages reflect that of mineral aerosols being transported above [e.g. *Johnson,* 1979; *Merrill et al.,* 1994; *Leinen and Heath,* 1981], the absolute quantification of each mineral type and proportional relationship to the minerals comprising aerosols' source remains largely undetermined [e.g. *Johnson,* 1979]. Therefore, the selective preservation of Th-poor minerals in excess of the proportion found in typical continental source material might explain the discrepancy between the ^{232}Th of the extracted refractory "dust" component and the accepted value for upper continental crust. This mechanism could release ^{232}Th from the crystalline lattice and make it available to adsorb to the outside of particles where it may be incorporated into oxy-hydroxide coatings.

An extension of our mass balance equation can be used to consider validity of the theory presented above. If we assume that the Th contained in both the refractory and

HH leachable fraction is related to terrigenous dust in the sediments, then the total Th in the dust can be expressed as:

$$[^{232}\mathrm{Th}]_{\mathrm{dust}} = \frac{f_{\mathrm{HH}}[^{232}\mathrm{Th}]_{\mathrm{HH}} + f_{\mathrm{R}}[^{232}\mathrm{Th}]_{\mathrm{R}}}{f_{\mathrm{dust}}}$$

where, $f_{\mathrm{dust}} = f_{\mathrm{HH}} + f_{\mathrm{R}}$

Solving this equation using the average measured Th concentrations and the assumed sedimentary percentages of the HH leachable and refractory non-dissolvable mineral fractions yields a dust ^{232}Th concentration of 10 ppm, remarkably similar to the average ^{232}Th content of upper continental crust (10.7 ppm). The agreement between our calculated dust Th concentration and the expected value based on average upper continental crust argues for syndeposition of ^{232}Th contained detrital particles and that which has been released by dissolution and subsequently stored in HH leachable oxy-hydroxide coatings. The linear relationship between the sedimentary [$^{4}\mathrm{He}_{\mathrm{crustal}}$] and [^{232}Th] corroborates this finding. Although stored in separate sedimentary fractions, the ^{232}Th signal preserved in the sediments is indicative of the total ^{232}Th input by eolian deposition to the ocean above. Furthermore, if we consider only the lattice bound ^{232}Th (i.e. 33% of the bulk sediment ^{232}Th) as representative of "dust" preserved in the sediment, our ^{232}Th-based record of sedimentary dust content becomes remarkably similar in magnitude to the dust record determined by traditional chemical extraction, especially for the latter part of the record (Figure 3-4 , [*Woodard et al.*, 2011]).

Our finding that nearly the entire ^{232}Th signal attributable to detrital inputs is associated with refractory minerals and their oxy-hydroxide coatings agrees with modern studies of the marine Th cycle. *Roy-Barman et al.* [1996] found distinct differences between profiles of dissolved ^{232}Th and other Th isotopes. The differences were attributed to the fact that the source of ^{232}Th to the ocean is solely in conjunction with continental material while other Th isotopes are produced in situ by the radioactive decay of their parent isotopes (e.g. U or Pa). Modeling suggests that much of the ^{232}Th which appears dissolved (passes through a 0.2 μm filter) is not "truly in solution" rather it is present on very fine particles [*Roy-Barman et al.,* 1996; *Roy-Barman,* 2009]. If ^{232}Th released from detrital particles is stored on colloids, then a kinetic relationship between particles and colloids might generate an "apparent equilibrium" between dissolved and particulate ^{232}Th [*Honeyman and Santschi*, 1989]. Coagulation of colloids into larger aggregates would then be a viable mechanism for transport of ^{232}Th to the deep sea. Our findings support the idea that, regardless of its phase, the majority of ^{232}Th in the ocean is never really "free" to behave as a dissolved species, but remains intimately associated with the particles from which it was derived.

We recognize that further study is needed to more clearly address how ^{232}Th is stored in the sediments. In order to use ^{232}Th content of different sedimentary fractions as indicators of total and dissolved oceanic dust fluxes, it is important to confirm significant migration of lattice bound Th to the oxy-hydroxide coatings does not occur in the sedimentary column post-depositionally.

Conclusions

Our records indicate that dust fluxes to Shatsky Rise, 58 Ma, varied on orbital timescales. Sedimentary ^{232}Th concentrations provide an independent estimate of dust fluxes to deep sea sediments of early Cenozoic age. The ^{232}Th-based dust fluxes show a similar pattern of variation as those determined using the traditional chemical extraction method, but are higher overall. It appears the majority of the sedimentary Th load is present as a sorbed species in the oxy-hydroxide leachable sedimentary fraction. However, coherence between sedimentary ^{232}Th and crustal ^{4}He contents suggests syndeposition of both the lattice-bound and dissolved Th. Therefore, ^{232}Th-based estimates may represent the total dust flux to the sea surface, that which dissolves, plus that which settles to the seafloor and accumulates in the sedimentary record.

CHAPTER IV

PROVENANCE OF CENTRAL PACIFIC DUST, 58 MA

Introduction

Eolian dust extracted from deep-sea sediments provides a proxy record of continental climate and atmospheric circulation. Temporal changes in the marine dust record reflect the response of dust source areas to vegetation and humidity changes as well as the pattern of prevailing winds delivering the dust to the ocean's surface. Increased dust accumulation rates are typically interpreted to reflect a change in aridity of the dust source region [e.g. *Rea,* 1994] and/or the prevalence of strong winds [*McGee et al.*, 2010]. These variables are climatically linked - changes in the distribution of heat across Earth's surface may alter the positioning of major wind belts and precipitation patterns, thus influencing both the production and transport of mineral aerosols. In addition, these variations are paced by orbital climate cycles, implying a connection between solar insolation and dust production [e.g. *Hovan et al.,* 1989; *Rea et al.,* 1994; *Kutzbach,* 1989; *Winckler et al.,* 2008; *Woodard et al.,* 2011]. However, a change in the source of dust may also cause variations in eolian accumulation rates, making knowledge of dust provenance important to accurately reconstruct the impact of climate change on the environment.

Radiogenic isotopes have been used extensively to "fingerprint" the eolian component of deep-sea sediments and determine provenance. Rocks and their constituent minerals often acquire unique isotopic compositions of Sr and Nd due to

fractionation of the parent nuclide from the radiogenic daughter due to differences in elemental compatibility. As crust is formed, ^{86}Sr and ^{144}Nd, as well as ^{87}Rb and ^{147}Sm (the parent isotopes of ^{87}Sr and ^{143}Nd), are partitioned differently between the solid and melt [*Faure and Mensing,* 2005]. Early differentiation of the Earth caused Nd and Rb to concentrate in the crust (more incompatible) while Sm and Sr were enriched in the residual mantle (less incompatible). Subsequent decay of ^{87}Rb and ^{147}Sm to ^{87}Sr and ^{143}Nd generated two isotopically distinct reservoirs: the mantle, characterized by low $^{87}Sr/^{86}Sr$ and high $^{143}Nd/^{144}Nd$, and continental crust with high $^{87}Sr/^{86}Sr$ and low $^{143}Nd/^{144}Nd$. Oceanic crust is generated along mid-ocean ridges through volcanism driven by mantle convection and therefore has a mantle-like Sr-Nd isotopic composition. Isotopic variations in continental crust arise due to the age, degree of melting, and lithology, giving rise to different regions with unique isotopic signatures. By measuring the isotopic signature of eolian dust extracted from seafloor sediments it may be possible to identify the continental terrane from which that material was derived.

This technique has been used successfully to identify the major regions supplying dust to the world's oceans. Today northern Africa, Asia, the Middle East and Patagonia are the dominant dust sources to the North Atlantic, North Pacific, Indian and Southern Oceans, respectively [*Grousett and Biscaye,* 2005]. Seasonal variability in dust source has been identified in the Arabian Sea, and is related to the Southwest monsoon [*Pease et al.,* 1998], but bioturbation and compaction processes average out these short-term variations in longer geologic records.

Radiogenic isotope analyses of glacial-interglacial dust suggest variations in dust source on orbital timescales [e.g. *Pokras and Mix,* 1985; *Sun et al.,* 2008; *Revel-Rolland,* 2006]. Dust deposited in East Antarctica was supplied primarily from Patagonia during glacial periods and Australia was a potentially dominant source during interglacials based on changes in dust $\varepsilon_{Nd}(0)$ from >-5, characteristic of S. America, to -5 to -15, values similar to eastern Australia and New Zealand [*Revel-Rolland et al.,* 2006]. These variations are attributed to the influence of changing continental conditions on dust production rather than changes in dust transport.

Long-term records of dust provenance derived from the pelagic clay sequence of North Pacific core GPC-3 suggest Asia has been a source of dust to the northern Pacific Ocean for most of the Cenozoic [*Kyte et al.,* 1993; *Nakai et al.,* 1993; *Jones et al.,* 1994; *Pettke et al.,* 2000; 2002]. However, *Pettke et al.* (2002) document variations in the radiogenic isotopic composition of early Cenozoic dust from GPC-3 and interpret these as shifts in the dust source from an older continental source (radiogenic Pb and Sr with unradiogenic Nd) to a younger volcanic source (unradiogenic Sr and Pb with radiogenic Nd). The younger source is interpreted as a mixture of Central American continental dust and arc volcanics delivered via the southern hemisphere trade winds. Such a scenario could only have been possible if the Intertropical Convergence Zone (ITCZ) was located further north than its modern position because the ITCZ make is an effective barrier to inter-hemispheric dust transport. Unfortunately stratigraphic age control in this very low accumulation red clay sequence is insufficient to resolve the timing of these dust source variations in relation to orbitally-forced climate change.

To investigate the potential connection between climate, dust source region and paleowinds during the early Cenozoic, we generated a high resolution record of Nd and Sr isotopes using eolian material extracted from 58 Ma, carbonate rich sediments deposited on Shatsky Rise, northwest Pacific Ocean (ODP Site 1209). In addition, we analyzed the Nd isotopic composition of fossil fish debris and the Sr isotopic composition of planktonic foraminifera to reconstruct contemporaneous seawater values. Our data indicate that the extracted dust fraction was not influenced by any authigenic (seawater-derived) contribution, confirming the use of extracted dust to investigate ancient eolian sedimentation and provenance. The combined Sr-Nd isotopic composition of the dust is best explained by a primary supply of dust from North Africa with periodic inputs of Central American arc volcanic material.

Site Selection and Methods

Shatsky Rise presents an ideal location for this study. Due to its remote paleogeographic location in the central sub-tropical Pacific gyre (~15-20ºN latitude), wind is the most likely transport mechanism for terrigenous material to the site. Early Paleogene age sediments recovered from ODP Site 1209 contain globally correlative lithologic cycles (variations in carbonate content) with orbital periodicities [*Röhl et al.,* 2004]. These cycles, identified using sedimentary Fe content, provide a basis for the astronomically tuned timescale for the Paleocene [*Westerhold et al.,* 2008], making it possible to investigate the impact of orbitally forced insolation changes on deep-sea sediment lithology and chemistry during a greenhouse climate interval.

We determined the Nd and Sr isotopic composition of 44 "dust" samples as well as 19 fish debris (Nd) and eight foraminiferal (Sr) samples, spanning eight consecutive eccentricity cycles, representing ~800 kyr of time some 58 Ma. These samples represent a subset of those studied as part of a larger project investigating orbital variations in dust flux and grain size [*Woodard et al.,* 2011; Chapters 2 & 3] and sediment accumulation rates using the extra-terrestrial (ET) ^{3}He constant flux proxy [*Marcantonio et al.,* 2009]. We have previously reported sedimentary dust accumulation rates, carbonate content, ^{232}Th concentrations, helium isotopic composition and abundances as well as two possible sedimentation models, one derived from age tie-point linear sedimentation rates [*Westerhold et al.,* 2008; *Laskar et al.,* 2004], and the other based on sedimentary $^{3}He_{ET}$ [*Marcantonio et al.,* 2009] (See Chapters 2 & 3). The results of the aforementioned studies indicate both bulk sediment and dust mass accumulation rates varied on orbital timescales.

The "dust" component was separated from the bulk sediment using the traditional chemical extraction technique [*Janecek and Rea,* 1981; *Clemens and Prell,* 1991; *Hovan,* 1995] and subsequently dissolved using concentrated HF + HNO_3+HCl. It should be noted that extracted "dust" is operationally defined as the non-dissolvable aluminosilicate sedimentary fraction and as such may contain materials from volcanogenic or authigenic sources [e.g. *Weber et al.,* 1996; *Olivarez et al.,* 1991]. Fish debris and foraminiferal tests were hand picked from the >63 μm and >250 μm sedimentary fractions, respectively. Fish debris was cleaned using an established oxidative/reductive cleaning protocol [e.g. *Boyle and Keigwin,* 1985] and dissolved in

2N HNO_3. Foraminiferal tests were sonicated in ethanol and purified water, then dissolved using buffered acetic acid [*DePaolo et al.,* 1983]. Radiogenic isotopes were separated using two-stage column chemistry. RE Spec cation exchange resin was used to obtain bulk REE and Sr splits. The Sr was further purified using Sr Spec cation exchange resin in 100 μL Teflon columns. Nd was separated from the REE split by chromatographic separation using methyllactic acid in quartz glass columns. Isotopes were analyzed via thermal ionization mass spectrometry (TIMS) in the R. Ken Williams Radiogenic Isotope Geosciences Laboratory at Texas A&M. Sr was loaded in ~2 μL 0.0035M H_3PO_4 on single rhenium filaments between 0.5 μL aliquots of TaF. Nd was loaded in ~1 μL 2N HCL on double rhenium filaments and analyzed as a metal. Within run normalization factors were 0.1194 for $^{86}Sr/^{88}Sr$ and 0.7219 for $^{146}Nd/^{142}Nd$. Machine performance was monitored by running Sr standard NBS 987 ($^{87}Sr/^{86}Sr = 0.710245$) and Nd standard JNdi-1 ($^{143}Nd/^{144}Nd = 0.512103459$). External machine reproducibility based on the above standards was 29 ppm (2 standard deviations) for Sr and 13 ppm (2 s.d.) for Nd. All reported errors are 2 standard errors of the sample mean and reflect in-run precision.

Dust Nd isotopic compositions are normalized to the bulk earth (DePaolo and Wasserburg, 1976), in this case $^{143}Nd/^{144}Nd_{CHUR(0)} = 0.512638$, and expressed as $\varepsilon_{Nd}(0)$:

$$\varepsilon_{Nd}(0) = \left(\frac{[^{143}Nd/^{144}Nd]_{Sample(0)}}{[^{143}Nd/^{144}Nd]_{CHUR(0)}} - 1 \right) * 10000$$

Seawater Nd isotopic compositions are given as $\varepsilon_{Nd}(t)$, reflecting values corrected for ingrowth of ^{143}Nd due to ^{147}Sm decay after deposition. The correction uses an average

Table 4-1. Radiogenic Isotope Data for Site 1209 Dust

ODP Site	Core Section/ Interval	Depth (rmcd)	$^{143}Nd/^{144}Nd$	$\varepsilon_{Nd}(0)$	2 S.E.	$^{87}Sr/^{86}Sr$	2 S.E.
1209C	12-4 18-19	229.97	0.512038	-11.7	±0.2		
1209C	12-4 32-33	230.11	0.512048	-11.5	±0.2	0.709743	±.000013
1209C	12-4 38-39	230.17	0.512038	-11.7	±0.2	0.716183	±.000008
1209C	12-4 46-47	230.25	0.512030	-11.9	±0.2	0.718049	±.000018
1209C	12-4 60-61	230.39	0.512038	-11.7	±0.1	0.713641	±.000013
1209C	12-4 64-65	230.43	0.512042	-11.6	±0.2	0.715807	±.000011
1209C	12-4 80-81	230.59	0.512034	-11.8	±0.1	0.719191	±.000008
1209C	12-4 94-95	230.73	0.512042	-11.6	±0.1	-----	
1209C	12-4 118-119	230.97	0.512065	-11.8	±0.1	0.709534	±.000006
1209C	12-4 122-123	231.01	0.512033	-11.5	±0.1	-----	
1209C	12-4 128-129	231.07	0.512049	-11.6	±0.2	0.711658	±.000008
1209C	12-4 132-136	231.11	0.512041	-11.1	±0.2	0.708754	±.000010
1209C	12-5 22-23	231.51	0.512069	-11.5	±0.1	-----	
1209C	12-5 46-47	231.75	0.512047	-11.6	±0.1	0.712162	±.000010
1209C	12-5 50-51	231.79	0.512042	-10.2	±0.1	-----	
1209C	12-5 62-63	231.91	0.512117	-11.6	±0.1	0.709145	±.000009
1209C	12-5 106-107	232.35	0.512045	-12.3	±0.2	-----	
1209C	12-5 122-123	232.51	0.512007	-11.5	±0.1	0.708877	±.000010
1209C	12-5 128-129	232.56	0.512046	-11.4	±0.1	-----	
1209C	12-5 134-135	232.61	0.512055	-11.2	±0.1	0.709269	±.000009
1209C	12-6 2-3	232.77	0.512064	-10.4	±0.3	0.712793	±.000012
1209C	12-6 6-7	232.81	0.512107	-10.5	±0.3	0.709552	±.000011
1209C	12-6 22-23	232.95	0.512101	-11.4	±0.2	0.709495	±.000314
1209C	12-6 30-31	233.03	0.512054	-11.7	±0.1	0.709205	±.000010
1209C	12-6 46-47	233.18	0.512041	-10.7	±1.1	0.709082	±.000012
1209C	12-6 50-51	233.22	0.512091	-11.7	±0.3	0.708346	±.000011
1209C	12-6 64-65	233.35	0.512039	-11.9	±0.1	0.708822	±.000010
1209C	12-6 64-65	233.35	0.512027	-11.9	±0.2	-----	
1209C	12-6 79-81	233.49	0.512026	-11.7	±0.1	0.708697	±.000008
1209C	12-6 80-81	233.5	0.512039	-7.3	±0.1	0.708722	±.000018
1209C	12-6 90-91	233.6	0.512264	-10.2	±0.3	0.708437	±.000010
1209C	12-7 4-5	233.73	0.512114	-11.4	±0.2	0.708275	±.000010
1209C	12-7 6-7	233.75	0.512054	-12.0	±0.1	0.708859	±.000007
1209C	12-7 6-7	233.75	0.512024	-11.7	±0.3	-----	
1209C	12-7 22-23	233.9	0.512040	-10.8	±0.1	0.708905	±.000008
1209C	12-7 22-23	233.9	0.512085	-10.7	±0.5	-----	
1209C	12-7 24-25	233.92	0.512092	-11.6	±0.2	0.708658	±.000016
1209C	12-7 32-33	233.99	0.512045	-11.1	±0.1	0.708601	±.000067
1209C	12-7 38-39	234.05	0.512069	-11.5	±0.1	0.708714	±.000010
1209A	23-3 80-81	234.44	0.512050	-10.1	±0.1	0.708739	±.000005
1209A	23-3 80-81	234.44	0.512123	-9.9	±0.4	-----	
1209A	23-3 96-97B	234.64	0.512130	-10.7	±0.1	0.708633	±.000007

age of 58 million years and a $^{147}Sm/^{144}Nd$ ratio of 0.103, the average value based on previous analyses of Paleogene sediment from Shatsky Rise [*Thomas,* 2004].

Results

The average isotopic compositions of extracted "dust" are -11.2 (±1.8, 2 s.d.) and 0.71047 (±0.00603, 2 s.d.) for $\varepsilon_{Nd}(0)$ and $^{87}Sr/^{86}Sr$, respectively (Table 4-1, Figure 4-1). Dust $\varepsilon_{Nd}(0)$ values exhibit a small range –12.3 to –9.9 except for one anomalous point at 233.50 rmcd with $\varepsilon_{Nd}(0)$ = -7.3. This value is significantly more radiogenic than any other dust $\varepsilon_{Nd}(0)$ measured. Furthermore, analysis of sample 12-6, 79-81cm (233.49 rmcd) which overlaps with the same core interval yielded an $\varepsilon_{Nd}(0)$ value of -11.7. Therefore we believe the anomalously radiogenic value reflects incomplete oxide or fish debris removal during silicate extraction and we do not discuss this analysis further. In general there is very little overall change in dust Nd isotopic composition over the interval. Values are more variable lower in the record with a slight decrease up core.

Dust $^{87}Sr/^{86}Sr$ ratios vary widely, from 0.70828 to 0.71919. Dust Sr isotopes show a slight trend toward more radiogenic values and increasing variability in the younger portion of the record. The $\varepsilon_{Nd}(t)$ of fish debris varied by ~1 epsilon unit, ranging from –4.0 to -2.9 and averaging -3.4 (±0.5, 2 s.d.) (Figure 4-1; Table 4-2). The $^{87}Sr/^{86}Sr$ of the forams averages 0.70779 (±0.00002, 2 s.d.), with a slight decrease up core (Figure 4-1, Table 4-2).

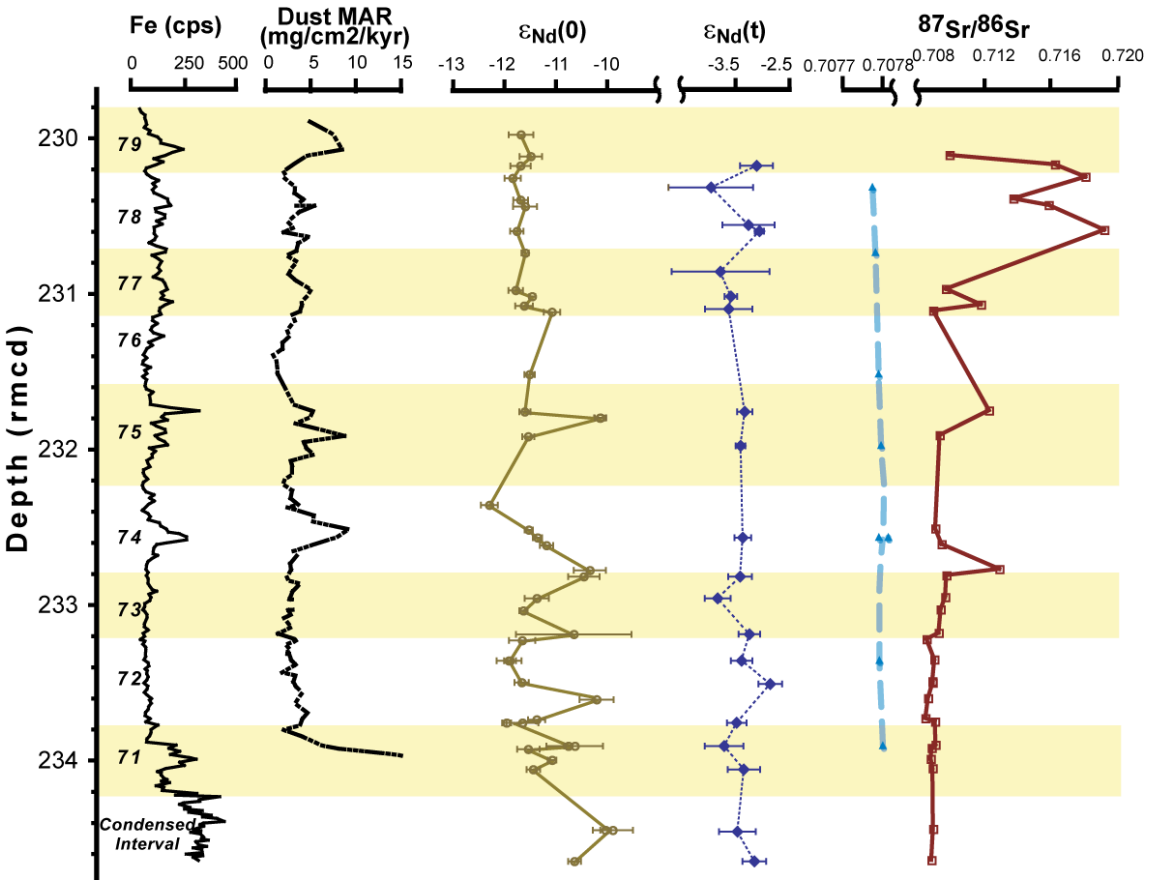

Figure 4-1. Compiled radiogenic isotope data for Shatsky Rise Site 1209. Nd isotopic compositions of extracted dust (brown circles) and fish debris (dk blue diamonds) along with $^{87}Sr/^{86}Sr$ of extracted dust (red squares) and foraminiferal tests (light blue triangles). Dust mass accumulation rates (dotted black line, *Woodard et al.,* 2011) and sedimentary Fe content (solid black line, *Westerhold et al.,* 2008) are plotted for reference. Eccentricty peaks 71-79 from the orbital calibration of Paleocene time [*Westerhold et al.,* 2008] are labeled and highlighted by alternating yellow and white bands.

Discussion

Seawater vs. Dust Signals

In all cases the Sr isotopes of the dust are more radiogenic than coeval seawater while $\varepsilon_{Nd}(t)$ are significantly less radiogenic (Figure 4-1). The Sr isotopic composition of seawater is controlled by changes in continental runoff and weathering (radiogenic) and/or rates of hydrothermalism (unradiogenic). Sr has a long seawater residence time

(~2 Myr), thus open marine waters are isotopically homogenous with respect to Sr. The seawater $^{87}Sr/^{86}Sr$ shows little variation, as expected for an element with a seawater residence time longer than our record (< 1Myr). The average Sr seawater value is similar to $^{87}Sr/^{86}Sr$ ratio for ~58 Ma seawater (0.070778) predicted by the LOWESS model of *McArthur et al.,* 2001, indicating our foraminferal calcite record reflects seawater. The slight trend toward more radiogenic values in younger sediments is consistent with the global (albeit sparse) Sr isotope curve for the late Paleocene [*Denison et al.,* 1993; *McArthur et al.,* 2001].

Table 4-2. Radiogenic Isotope Data for 58 Ma Biogenics from Site 1209

ODP Site	Core Section/ Interval (cm)	Depth (rmcd)	$^{143}Nd/^{144}Nd$ (fish debris)	$\varepsilon_{Nd}(t)$	2 S.E.	$^{87}Sr/^{86}Sr$ (forams)	2 S.E.
1209C	12-4 38-39	230.17	0.5124526	-3.1	±0.15	---------	
1209C	12-4 52-53	230.31	0.5124095	-4.0	±0.39	0.7077718	±.000008
1209C	12-4 76-77	230.55	0.5124449	-3.3	±0.24	---------	
1209C	12-4 80-81	230.59	0.5124554	-3.1	±0.04	---------	
1209C	12-4 94-95	230.73	---------	--------		0.707779	±.000006
1209C	12-4 106-107	230.85	0.5124181	-3.8	±0.46	---------	
1209C	12-4 122-123	231.01	0.5124282	-3.6	±0.06	---------	
1209C	12-4 130-131	231.09	0.5124262	-3.6	±0.22	---------	
1209C	12-5 22-23	231.51	----------	--------		0.707786	±.000006
1209C	12-5 46-47	231.75	0.5124413	-3.4	±0.07	---------	
1209C	12-5 68-69	231.97	0.5124374	-3.4	±0.05	0.7077939	±.000008
1209C	12-5 128-129	232.56	0.5124396	-3.4	±0.08	0.7078121	±.000009
1209C	12-5 128-129	232.56	----------	--------		0.7077883	±.000009
1209C	12-6 6-7	232.81	0.51243697	-3.4	±0.11	---------	
1209C	12-6 22-23	232.95	0.51241558	-3.9	±0.12	---------	
1209C	12-6 46-47	233.18	0.51244570	-3.3	±0.10	---------	
1209C	12-6 64-65	233.35	0.51243836	-3.4	±0.10	0.7077896	±.000007
1209C	12-6 80-81	233.5	0.51246565	-2.9	±0.11	---------	
1209C	12-7 6-7	233.75	0.51243382	-3.5	±0.09	---------	
1209C	12-7 22-23	233.9	0.51242175	-3.7	±0.18	0.707784	±.000009
1209C	12-7 38-39	234.05	0.51244054	-3.4	±0.15	---------	
1209A	23-3 81-82	234.45	0.51243435	-3.5	±0.17	---------	
1209A	23-3 96-97	234.64	0.51245048	-3.2	±0.11	---------	

Neodymium is supplied to the oceans via riverine discharge and acquires the isotopic composition of the rocks being drained [*Piepgras and Wasserburg,* 1980]. Due

to its short seawater residence time (~350-600 yrs) relative to oceanic mixing (~1500 yrs), the Nd isotopic compositions deep and intermediate water masses reflect the surface waters where they formed and subsequent alteration through mixing with other water masses [*Goldstein and Jacobsen*, 1988; *Piepgras and Wasserburg,* 1987; *Jeandel et al.,* 2007; *Arsouze et al.,* 2007; *Tachikawa et al.,* 1999]. The seawater $\varepsilon_{Nd}(t)$ values fluctuate by ~0.5 epsilon units about the average of -3.4. Temporal changes in deep water Nd isotopic composition may result from either restructuring of deep ocean circulation patterns or changes in the Nd composition draining into the area of deep water formation. Previous work suggests a bimodal production of deep water in the Pacific ocean during the early Paleogene (~65-50 Ma) with deep water masses forming in both the Southern Ocean ($\varepsilon_{Nd}(0)$ =-5) and the North Pacific ($\varepsilon_{Nd}(t)$ = -3) [*Thomas*, 2004; *Thomas et al.,* 2008]. Our $\varepsilon_{Nd}(t)$ record indicates deep water at Shatsky Rise was primarily sourced from the North Pacific, 58 Ma, in agreement with *Thomas* [2004]. The fluctuations in $\varepsilon_{Nd}(t)$ may reflect competing influence of the two deep water masses, as periodic increases in Southern deepwater component could account for the less radiogenic $^{143}Nd/^{144}Nd$ signatures we measured. Variations in thermohaline circulation on glacial-interglacial timescales during the Pleistocene caused 1 to 2 epsilon unit shifts in Atlantic deep water $\varepsilon_{Nd}(t)$ [*Rutberg et al.,* 2000]. However, the variations we observe are smaller and do not correlate with changes in either sedimentary carbonate or Fe content (used in astronomical calibration of Paleocene time, *Westerhold et al.* [2008]) implying no connection to orbitally-forced climate change (Figure 4-1). Thus, they may

simply result from periodic increases in radiogenic inputs to North Pacific surface waters.

Nd and Sr associated with eolian inputs at the sea surface have a minimal impact on the radiogenic isotope composition of marine waters [*Jones et al.,* 1994; *Ling et al.,* 2005], yet authigenic minerals precipitated from seawater sometimes contaminate the eolian component extracted from marine sediments [e.g. *Zeigler et al.,* 2007a]. Authigenic minerals acquire the Nd and Sr isotopic signatures of the water from which they formed and, if present in our extracted eolian material, might overprint the true "dust" values. Thus we can use the Nd and Sr isotopic composition of seawater reconstructed from fish teeth and forams to assess the potential for authigenic mineral contamination.

The unradiogenic $\varepsilon_{Nd}(0)$ signature of the extracted "dust" indicates it was derived from older continental sources. The average Nd isotopic value, -11.2, is less radiogenic than the modern dust source to the N. Pacific Ocean, Asian loess ($\varepsilon_{Nd}(0)$= -10) [*Jones et al.,* 1994; *Grousset and Biscaye*, 2005]. This may indicate a different and older source of dust to the subtropical Pacific ~58 Ma. However, the dust composition varies by >2 epsilon units with values reaching as high as -9.9 and low as -12.3. The dust Nd variations are greater in the lower part of the record (Figure 4-1). Above 231.75 rmcd the $\varepsilon_{Nd}(0)$ becomes less variable averaging -11.6 (±0.4, 2 s.d.).

^{232}Th and crustal ^{4}He data for the same sedimentary interval suggest at least two sources of dust to Shatsky Rise ~58 Ma, one from continental material older than that derived from Asia today and another similar to or younger than the Asian source (see

Chapter 3). In general, the "younger" source indicated by ^{232}Th and crustal ^{4}He ratios is more prevalent earlier in the record when we observed higher amplitude variations in our dust $\varepsilon_{Nd}(0)$ composition (Figure 4-1). Periodic inputs of material derived from a younger dust source would contribute more radiogenic Nd to the sediments and is consistent with the higher $^{143}Nd/^{144}Nd$ values recorded by the dust.

The "dust" $^{87}Sr/^{86}Sr$ record shows a pattern opposite to the $\varepsilon_{Nd}(0)$ with relatively stable unradiogenic values in the lower portion of the record followed by high amplitude variations beginning as low as ~232.7 rmcd. There are two explanations for the apparent decoupling of the extracted dust Sr and Nd isotopic compositions. The first involves the potential contribution of another mineral component to the extracted "dust." In particular, barite ($BaSO_4$) (both authigenic and biogenic) is highly refractory in oxic sediments and forms directly from seawater. Barite Sr concentrations are 800-1200 ppm [*Martin et al.,* 1995] more than double that of average continental crust (350 ppm, *Taylor and McLennan,* [1985]). Thus, contaminant barite in the extracted "dust" might overprint the terrestrial Sr isotopic signature with that of coeval seawater. Marine barite contains lower Nd concentrations than continental material, minimizing any potential impact on the "dust" $\varepsilon_{Nd}(0)$ value [*Martin et al.,* 1995].

We argue that it is unlikely that the presence of marine barite impacted the overall values and trends in the extracted dust Sr record. While a contribution from marine barite could explain the apparent convergence of "dust" values and contemporaneous seawater values in the lower portion of the record, such an influence should be seen throughout the short record. The marine barite contribution could not

have merely disappeared suddenly at 233 rmcd. Thus we favor the alternative explanation which involves fractionation of the Sr from Nd during weathering and transport.

The degree of physical versus chemical weathering on land can cause large temporal shifts in the $^{87}Sr/^{86}Sr$ of marine sediments [*Colin et al.,* 2006; *Jung et al.,* 2004]. Mica and K-feldspar minerals are generally enriched in radiogenic Sr and are highly susceptible to chemical weathering. Preferential breakdown of these minerals releases radiogenic Sr which is removed from the source rock (hence dust) due to its high solubility. In contrast, rare earth elements such as Nd are relatively immobile and experience little isotopic fractionation during weathering. The differing susceptibility to mobility during weathering may explain the relatively small changes in Nd isotopic composition in the extracted dust versus the large range in Sr values (~2 epsilon unit range in Nd is small compared to the ~0.011 range in Sr values). In addition, the range in [Rb]/[Sr] ratios in continental rocks is much greater than [Sm]/[Nd] [*Dickin,* 2005], making it likely that that the differences in the Sr isotopic ratios of the source rocks were initially much larger than those of Nd.

Decoupling of detrital sediment Sr and Nd isotope values may indicate periods of more intense chemical weathering. For example, radiogenic isotope analyses of sediments from ODP site 658C off the west coast of North Africa record a shift toward lower Sr isotopic values in the non-dissolvable mineral component but invariant Nd isotope values, which corresponds to the African Humid Period ~12 ka [*Cole et al.,* 2009]. The lower, more nonradiogenic Sr values in our record may be the result of

intense chemical weathering and preferential removal of Sr enriched mineral phases in the dust's source region [e.g. *Jung et al.,* 2004]. Many regions likely experienced enhanced chemical weathering during the early Paleogene greenhouse due to a more humid global climate and overall warmer temperatures [e.g. *Zachos et al.,* 2008; *Wing,* 2003]. However, it is interesting to note that dust accumulation rates spanning the same sedimentary interval vary on orbital timescales, implying a connection between climate and dust production [*Woodard et al.,* 2011]. While the data presented here indicate temporal variations in the Nd and Sr isotopic composition of the dust, there is no correlation between dust accumulation (or overall sediment lithology based on the Fe content) and the radiogenic isotopic composition of that same dust. Thus it is unlikely that orbitally driven changes in climate and weathering controlled the dust's geochemical signature. As an alternative explanation, we consider the potential influence of changes in the dust source regions on the dust isotopic composition recorded at Shatsky Rise.

Dust Provenance

The combined $^{87}Sr/^{86}Sr$ and $\varepsilon_{Nd}(0)$ data indicates a relatively old continental source (Figure 4-2). The dust analyzed from Site 1209 plots in domain 'C' identified in a compilation of Sr-Nd isotopic composition of worldwide aerosols, loess and sand deposits by *Grousset and Biscaye* [2005]. Domain C describes most of the current major dust source regions and is not uniquely diagnostic. The Site 1209 dust data overlap with

the South Africa/Australia, Asia and North Africa domains on the Sr-Nd isotope plot (Figure 4-2).

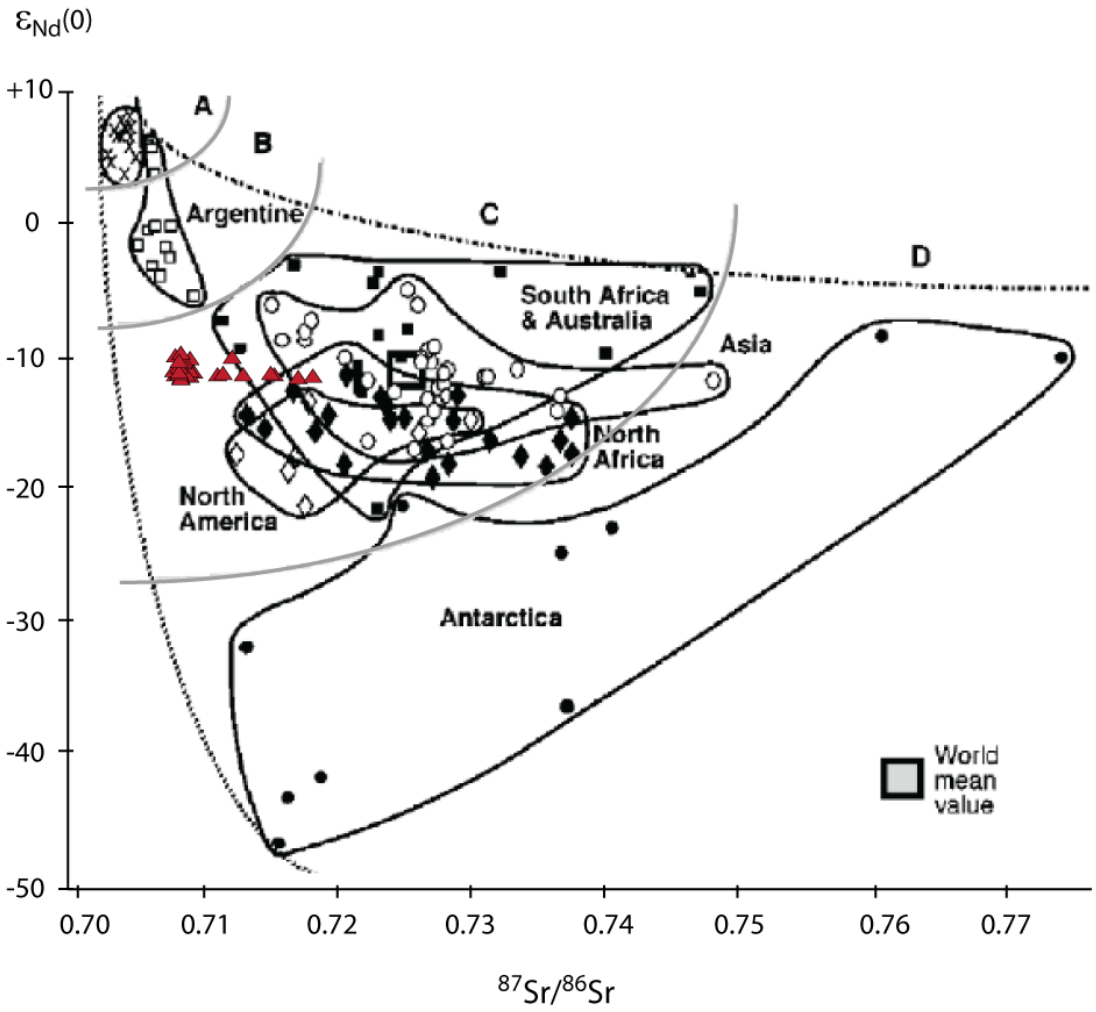

Figure 4-2. Sr-Nd isotope source plot for dust. Site 1209 "dust" (red triangles) plotted with worldwide aerosols, loess and sand deposits from *Grousset and Biscaye,* [2005]. Grey lines separate dust sources into domains A-D [*Grousett and Biscaye*, 2005].

Though hyperarid and deflated of dust today, Australia was potentially a significant source of atmospheric dust during the early Cenozoic. Paleoclimate reconstructions suggest northeastern Australia was dry with occasional wet periods, which may have recharged floodplains with fine-grained material capable of eolian

transport [*Martin,* 2006]. Dust accumulation rates at Shatsky Rise were low at 58 Ma, implying either small source regions or long transport distances [*Woodard et al.,* 2011]. Yet, in order for Australia to be a plausible source region, it must have produced large amounts of dust (similar to Asia today) and Shatsky Rise must have been located south of the ITCZ (thus allowing transport of atmospheric aerosols to the northern hemisphere, Figure 4-3a). This scenario is reasonable given the hypothesized paleoposition of the ITCZ was ~23°N prior to ~40 Ma [*Pettke et al.,* 2002].

The Site 1209 dust Sr-Nd isotope range falls outside the mixing envelope between Asian loess and an average volcanic end-member (Figure 4-4). Therefore, Asia would have been a possible source region only if the extracted "dust" contains a non-eolian component with high unradiogenic in Sr concentrations and negligible Nd (e.g. barite as discussed above) or was generated in a regions with different average Sr-Nd compositions than Asian dust sources today. Asian loess fields are dominant suppliers of dust to the North Pacific today [e.g. *Rea,* 1994 and references therein]. These deposits were generated in large deserts during intensification of the Himalayan uplift and are relatively young, <22 Myrs old [*Guo et al.,* 2002; *Whalley et al.,* 1982]. Thus, modern Asian loess fields could not have been the dust source to Shatsky Rise ~58 Ma. Paleontological and mineralogical evidence, however, suggest a semi-arid belt spanned much of Asia during the Paleocene, providing conditions conducive to dust production [*Guo et al.,* 2008]. An Asian dust source constrains the paleolocation of Shatsky Rise to north of the ITCZ (Figure 4-3b), in conflict with other studies which use dust

geochemistry from nearby site GPC-3 to argue that the ITCZ was pushed northward to ~23°N during the early Paleogene [*Kyte et al.*, 1993; *Pettke et al.*, 2002]. If the dust in

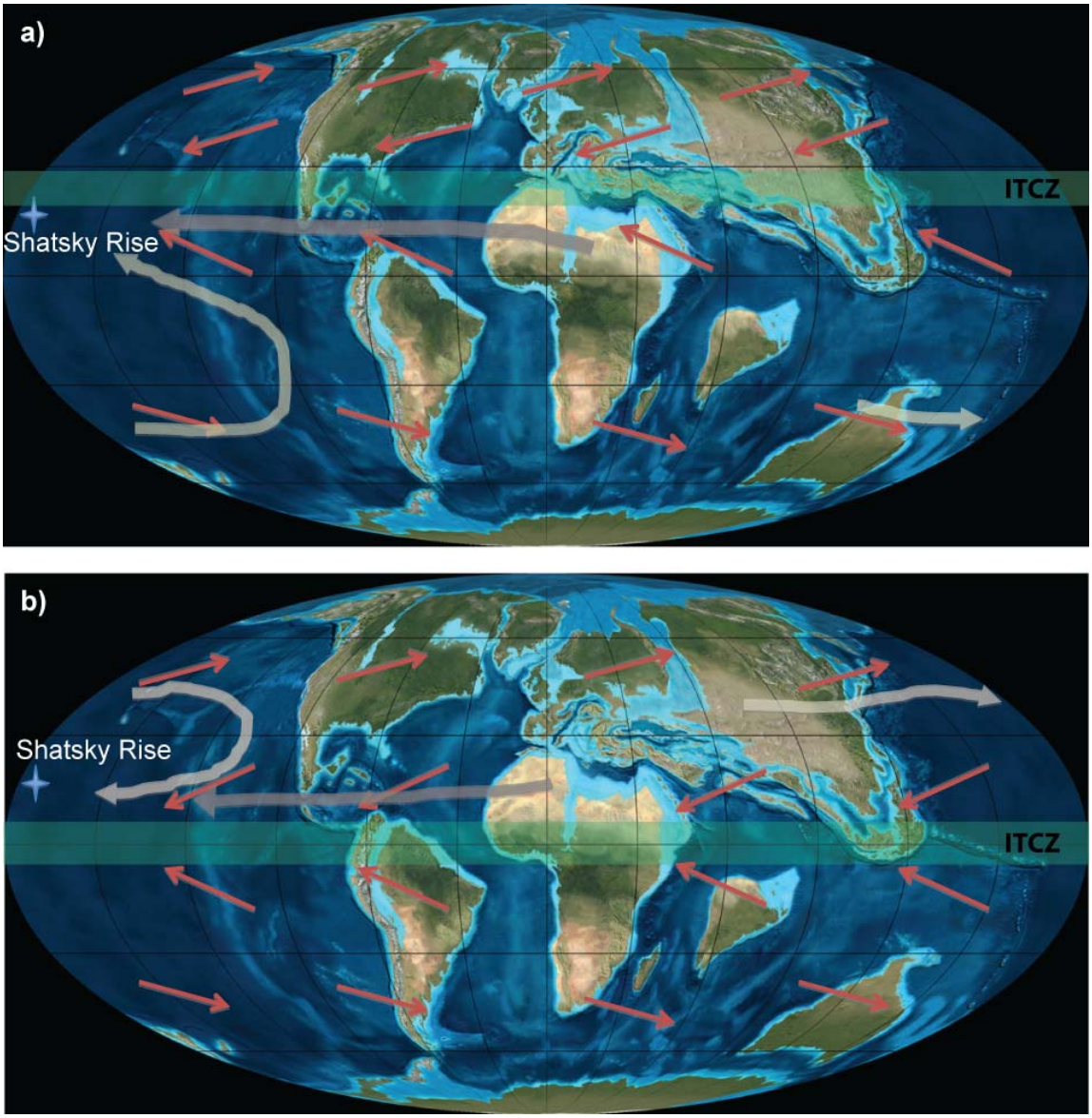

Figure 4-3. Potential dust sources and transport pathways to Site 1209, 58 Ma. If **a)** the ITCZ were pushed northward to ~25°N (Australia (tan) or Africa (grey)), **b)** the ITCZ position was similar to modern (Asia (tan) or Africa (grey)). Paleogeographic reconstruction is from *Blakey* [NAU Geology] with the position of westerlies and trade winds indicated by red arrows. Paleolocation of Shatsky Rise (Site 1209) is indicated by light blue star.

our record was generated in Asia, it implies an atmospheric circulation pattern similar to that today, where dust is transported over the northern Pacifc via the westerlies, sinks through the troposphere where it is entrained in the northeast trade winds and transported back across the Pacific at lower latitudes [*Duce et al.,* 1980]. We consider this a possibility, but do not have enough data to fully evaluate the likelihood of Asia as a dust source region.

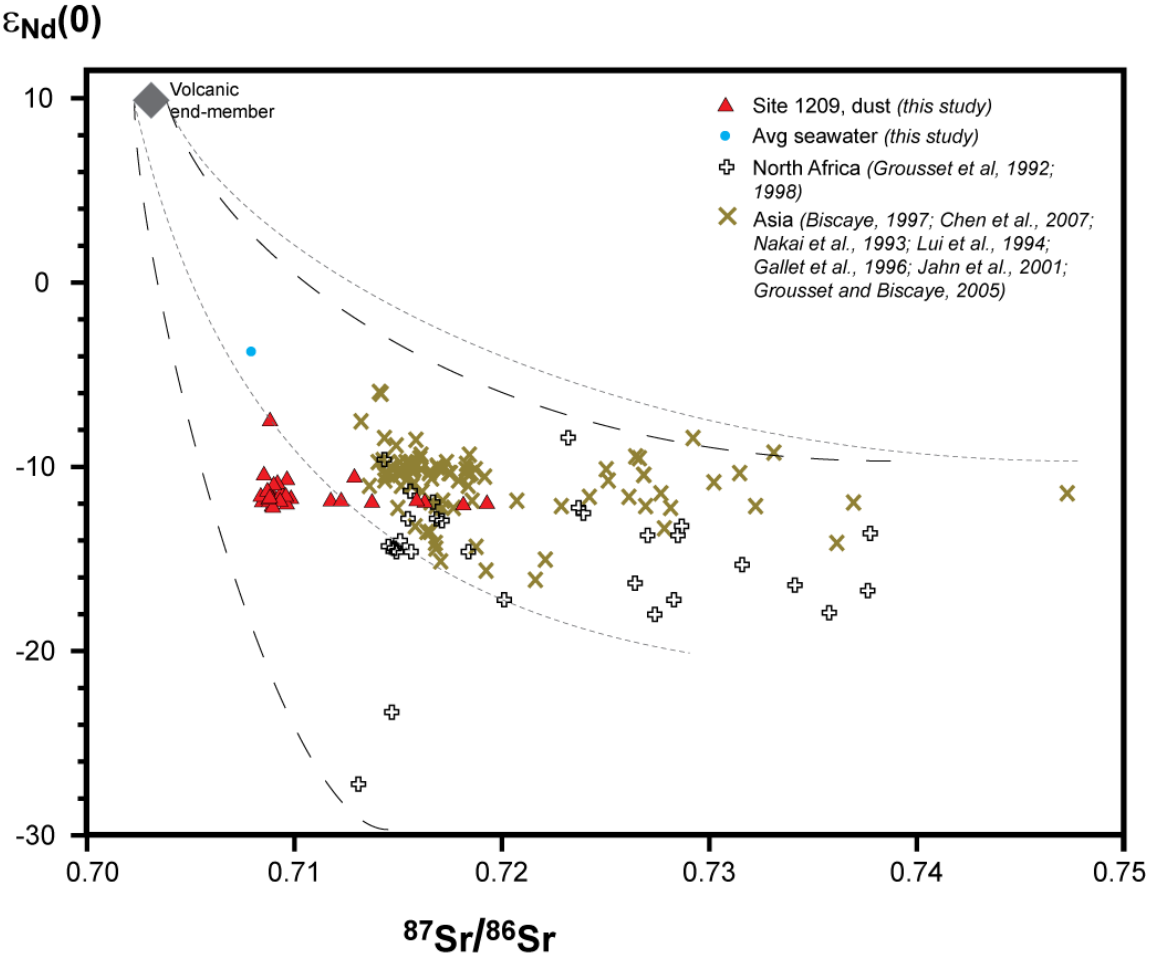

Figure 4-4. Sr-Nd isotope source plot for Shatsky Rise, North Africa and Asia. Dust from Shatsky Rise (red) is plotted with data from potential sources in North Africa (white) [*Grousset et al.,* 1992; 1998] and Asia (gold) [*Biscaye,* 1997; *Chen et al.,* 2007; *Nakai et al.,* 1993; *Lui et al., 1994*; *Gallet et al.,* 1996; *Jahn et al.,* 2001; *Grousset and Biscaye,* 2005]. Mixing envelopes are defined between a generic volcanic end-member (grey diamond) and African (dashed line) and Asian (dotted line) sources. Average Sr-Nd isotopic composition of Pacific deep watermass, 58 Ma, is plotted for reference (blue).

We favor the possibility of Africa as a source region for dust to Shatsky Rise. Paleo-environmental reconstructions of North Africa indicate a semi-arid to arid climate and grassland vegetation during the Paleogene [*Jacobs et al.,* 1999; *Zaier et al.,* 1998], conditions conducive to dust production. Assuming atmospheric circulation patterns similar to modern, dust supplied to the central North Pacific (Shatsky Rise) would be transported via the trade winds. The lack of a land bridge between the North and South American continents would have allowed winds to cross from the Atlantic to the Pacific unimpeded [*Hovan*, 1995]. This scenario of dust transport to Shatsky Rise precludes determination of the ITCZ's paleo-location because the both the northern and southern hemisphere trades provide a westward flow of air capable of bringing dust from a source located east of ODP Site 1209 (Figure 4-3a,b). The presence of a shale-like component, possibly derived from Africa, has been identified in Paleogene age sediments from nearby site GPC-3 using elemental geochemistry and mineral assemblages [*Kyte et al.,* 1993; *Leinen and Heath,* 1981].

Dust derived from the Saharan region of Africa is a primary component of mineral aerosol being deposited in the Caribbean today [*Prospero et al.,* 1970; *Muhs et al.,* 1990]. The central Atlantic Ocean wasn't as wide during the Paleocene, making the transport distance from Africa shorter. The Sr-Nd composition of Site 1209 dust falls within a mixing envelope between North Africa and a volcanic end member (Figure 4-3). Additions of younger volcanic material from South/Central America to African dust during transport via the trade winds would explain shifts toward more radiogenic $\varepsilon_{Nd}(0)$ and less radiogenic $^{87}Sr/^{86}Sr$ at Site 1209. The Central American region experienced

active tectonism and arc volcanism throughout the Mesozoic and early Cenozoic. The erupted magmas were both basaltic and andesitic with diverse geochemical compositions [*Kerr et al.,* 2002]. An andesitic eolian component has been identified in Paleogene age sediments from the Pacific [*Kyte et al.,* 1993]. Material from Central America may provide the "younger" component in dust to Shatsky Rise as suggested by ^{232}Th and He isotopes [*Marcantonio et al.,* 2009; Chapter 3]. A primary supply of dust from North Africa with periodic inputs of Central American arc volcanic material of variable Sr-Nd isotopic composition explains the lack of cyclicity in the timing of changes in dust source since volcanic eruptions are not driven by climate.

Conclusions

The Nd and Sr isotopic composition of extracted "dust" from Shatsky Rise, ODP Site 1209 indicates a relatively old continental dust source. In all cases the seawater $\varepsilon_{Nd}(0)$ was more radiogenic and $^{87}Sr/^{86}Sr$ less radiogenic than the dust. This implies little contamination of the "dust" isotopic signal by authigenic minerals. Unradiogenic dust $^{87}Sr/^{86}Sr$ values may be the result of enhanced chemical weathering in the dust source region due to an overall warmer and more humid global climate. With our limited data we cannot positively identify the source region supplying dust to Shatsky Rise. Potential dust sources include Australia, Asia and North Africa. Transport of dust from North Africa by the trade winds seems plausible. Periodic additions of andesitic material from active arc-volcanism in the Caribbean may account for radiogenic increases in dust

$\varepsilon_{Nd}(0)$ observed in our record. Future analyses of Pb isotopes in the extracted "dust" may help determine source regions.

CHAPTER V

RADIOGENIC ISOTOPE COMPOSITION OF CARBONIFEROUS SEAWATER FROM NORTH AMERICAN EPICONTINENTAL SEAS

Introduction

The Carboniferous Period (359-299 Ma) marks a critical time in Earth's history when a series of tectonic and biological events conspired to cause a shift in the mean climate state from a global "greenhouse" to an "icehouse". The climate transition is characterized by a major reorganization of tectonic plates resulting in the closure of the Rheic, a circum-equatorial ocean connecting the Paleo-Tethys Ocean with Panthalassa, as two large landmasses, Laurussia (of which North America is a part) and Gondwana collided to form the Pangean supercontinent (Figure 5-1). Coincident with this tectonism there is evidence for widespread glaciation in the southern hemisphere, large tropical/sub-tropical coal deposits indicating fundamental changes in carbon cycling, and a likely restructuring of ocean circulation and weathering patterns.

Near field records indicate glaciation in Gondwana began in the late Devonian to early Mississippian [*Isbell et al.,* 2003] and after a brief repose, became more widespread throughout the mid- to late-Carboniferous and into the early Permian [*Frakes et al,* 1992; *Crowley and Baum*, 1991, *Gulbranson et al.,* 2010]. The appearance and disappearance of glaciogenic deposits in South America [*Gulbranson,* 2010; *Caputo et al.,* 2008; *Isbell et al.,* 2003], Australia [*Fielding et al,* 2008a,b] and South Africa [*Stollhofen et al.,* 2008] document multiple episodes of ice sheet development in the

Southern Hemisphere. The impact of glacial advance and retreat appears as cyclothems in far field sedimentary records from the paleotropics (North America, Europe and Asia)

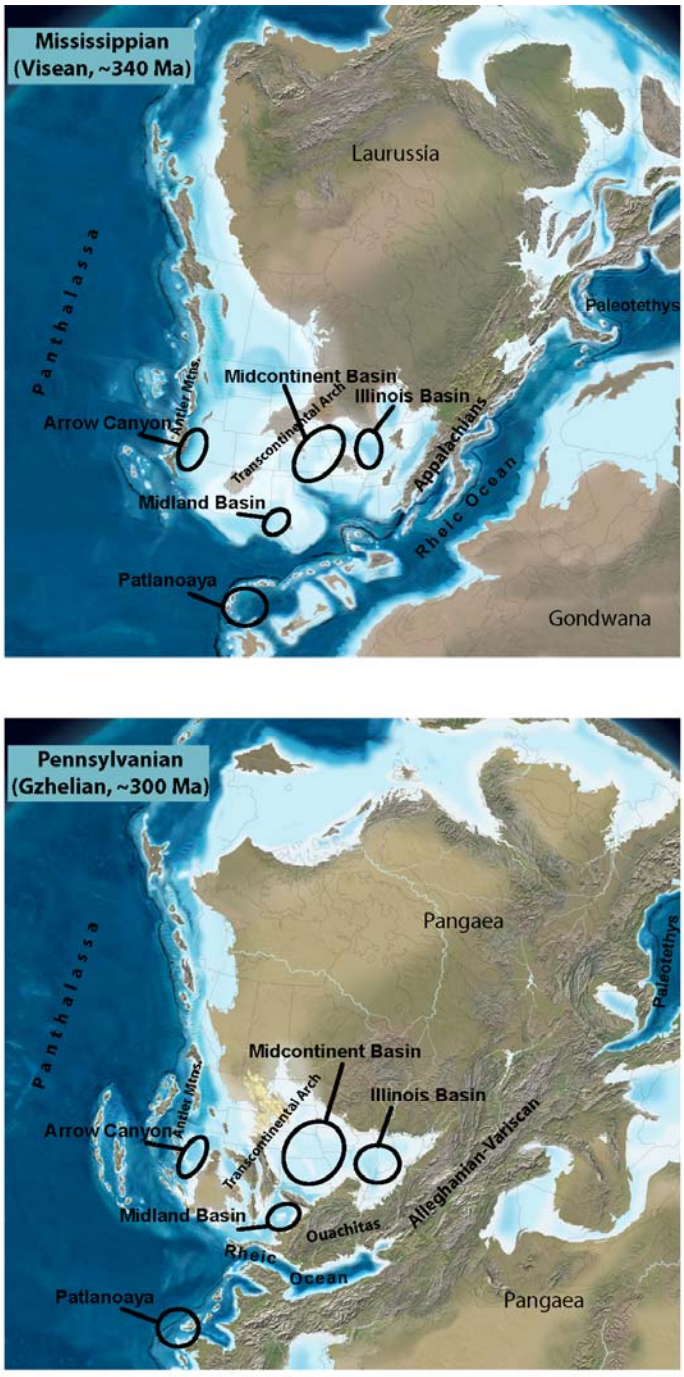

Figure 5-1. Paleogeographic reconstructions of Carboniferous North America. Approximate locations of study sites are highlighted for the Mississippian (~340 Ma) and Pennsylvanian (~300 Ma) [modified from *Blakey,* NAU Gelogy].

indicating low latitudes were subject to rhythmic high order sea level fluctuations [*Heckel,* 2002; *Wright and Vanstone,* 2001].

Geochemical records derived from sediments deposited in tropical/sub-tropical epicontinental seas are commonly used to understand links between tectonics, carbon cycling and climate [*Fielding et al.,* 2008a] Positive excursions in the $\delta^{18}O$ and $\delta^{13}C$ of well-preserved marine carbonates from N. America, Russia and Europe coincide with the onset of the major phase of glaciation during the mid-Carboniferous [e.g. *Popp et al.,* 1986; *Bruckshen et al.,* 1999; *Mii et al.,* 1999; 2001; *Grossman et al.,* 2002]. These records have been used to link global cooling and ice build-up with decreased atmospheric CO_2 levels caused by the burial of organic matter [*Berner and Kothalava,* 2001; *Royer et al.,* 2004]. Enhanced continental weathering rates inferred from a shift toward more radiogenic $^{87}Sr/^{86}Sr$ values during the late Mississippian are thought to reflect initiation of the Alleghanian-Variscan orogeny and the closure of the Rheic Ocean, potentially restructuring atmospheric and oceanic circulation patterns and facilitating Southern Hemisphere ice build-up by driving moisture poleward [*Smith and Read,* 2000; *Saltzman et al.,* 2003]. However, interpreting geochemical records from epicontinental seaways in terms of the global ocean-climate system assumes they reflect the chemistry of well-mixed ocean water and have been little influenced by regional environmental processes.

We investigate the extent to which the Carboniferous North American epicontinental seas recorded global open-ocean conditions using radiogenic isotope tracers with different seawater residence times. In modern oceans, Neodymium (Nd) has

a residence time of ~350-600 yrs [*Tachikawa et al.,* 1999; *Arsouze et al.,* 2007], relatively short compared to whole ocean mixing (>1000 yrs). The Nd isotopic composition ($^{143}Nd/^{144}Nd$) of oceanic surface waters reflects the age and composition of material weathered and drained into a given region, thus seawater $^{143}Nd/^{144}Nd$ is a useful tracer of mixing between basins. In contrast, Strontium (Sr) has a long oceanic residence time of 2-5 Myrs [*Ritcher and Turekian,* 1993; *Taylor and McLennan,* 1985]. Thus, seawater exhibits a globally homogenous $^{87}Sr/^{86}Sr$ signature that varies through geologic time depending on the relative inputs of Sr from continental (radiogenic) and hydrothermal (unradiogenic) sources. Biogenic apatite (e.g. fish teeth, scales and conodonts) acquires high concentrations of Nd at the seafloor postmortem and reliably records $^{143}Nd/^{144}Nd$ ratio of the water bathing the seafloor [*Staudigel et al.,* 1985; *Wright et al.,* 2002]. Sr is incorporated into organisms' bones and teeth by substituting for calcium during growth [*Schmitz et al.,* 1991; *Martin and Scher,* 2004]. To constrain the degree of geochemical coupling between the epicontinental sea and the open ocean, we measured Nd and Sr isotopes in biogenic apatite spanning a transect across the North American paleotropics from the continental interior (US Midcontinent and Midland Basins) west to Arrow Canyon and the Mixteco Terrane (most oceanic) (Figure 5-1).

Geologic Setting and Samples

Patlanoaya

Paleozoic deposits of the Mixteco terrane are exposed in San Salvador Patlanoaya in south-central Mexico. A succession of Carboniferous age marine

sedimentary rocks (Patlanoaya Formation) rests atop a small remnant of Paleozoic age oceanic crust, a Pre-Mississippian ophiolite of the Acatlan complex [*Ortega-Gutierrez et al.,* 1994]. The complex is the only vestige of Rheic Ocean seafloor the remainder of which was subducted ~360-345 Ma during the assembly of the Pangaean supercontinent [*Nance et al.,* 2007]. The sedimentary sequence consists of argillaceous and calcareous sandstones containing abundant brachiopod molds followed by red-green shales with black chert interbeds. Above are several sequences of fossiliferous limestones, some bearing chert nodules or interbedded with shales and mudstones. Paleontological studies suggest the formation is of early Mississippian to Permian in age [*Vachard et al.,* 2000; 2002; *Caridriot et al.,* 2002]. However there are several depositional hiatuses, and the mid-Carboniferous boundary is not well defined [*Vachard et al.,* 2000]. Samples were collected from the upper limestones which are Kasimovian to Lower Permian in age. These rocks contain abundant brachiopods, gastropods, bryzoans and crinoids, many of which have been replaced by silica, as well as the remains of fish and several types of conodonts [*Caridroit et al.,* 2002; *Deryke-Khatir et al.,* 2005]. Sedimentary structures indicate a shallow depositional environment periodically subject to reworking by storms and/or turbidity currents [*El Albani et al.,* 2005; *Deryke-Khatir et al.,* 2005].

Arrow Canyon, Bird Spring Shelf

Arrow Canyon, located in eastern Nevada, was named the Global Stratotype Section and Point (GSSP) for the Mid-Carboniferous Boundary in 1995 due to

its nearly complete exposure of relatively undeformed Carboniferous age strata [*Lane,* 1999; *Richards et al.,* 2002]. During the late Paleozoic, Arrow Canyon was located near the equator and flooded by a shallow sea that extended along the entire western margin of the present day US and Canada [*Poole and Sandburg,* 1991]. A foreland basin, created by successive uplifts during the late Devonian-early Mississippian Antler Orogeny to the west and north [*Saleeby et al.,* 1994], allowed for accumulation of thick muddy carbonate sediments. We collected samples from the Indian Springs (late-Mississippian) and Bird Spring Formations (Mid-Carboniferous boundary to Gzhelian). The sedimentary succession is primarily shallow marine carbonates with abundant invertebrate fossils and chert nodules. Muddy interbeds and paleokarst surfaces are observed near the Mississippian-Pennsylvanian boundary, and indicate the paleo-environment was subjected to multiple episodes of sea level rise and fall [*Bishop et al.,* 2009; *Barnett and Wright*, 2008; *Richards et al.,* 2002].

US Midcontinent

The Midwestern United States contains extensive marine and terrestrial sedimentary deposits of Carboniferous age. Tectonic pressures related to successive orogenic events of the Paleozoic lead to downwarping of the central North America craton and the development of a broad epieric seaway [*Rankin,* 1994]. The structural pressures created several separate deeper basins (e.g. Midcontinent Basin, Illinois Basin and Appalachian Basin), which were connected during sea level highstands and periodically separated during lowstands. Evidence of high order eustatic change during

the Carboniferous manifests as rhythmic variations in sediment accumulation or cyclothems, spanning the entire mid-continental interior [e.g. *Heckel,* 1986]. The cyclothems consist of four basic members representing various stages of marine transgression/regression: 1) a thin transgressive limestone that rests atop a paleosol or nearshore shale, 2) a "core" black/dark grey shale deposited in an offshore environment within a physically stratified water column, 3) a regressive limestone with abundant invertabrate fossils grading into peritidal facies, 4) nearshore shale or mudstone deposited during the final stages of regression that is sometimes topped by a paleosol and/or coal indicating complete subaerial exposure or the development of peat swamps [*Heckel,* 2002; 2008]. The cycles are best developed during the mid- to late-Pennsylvanian, where they also appear in sedimentary records from Europe and China [*Heckel*, 2002; *Davies and Gibling,* 2010], and have been described extensively by *Heckel et al,* [1989], [1990], [2008]; *Wright and Vanstone,* [2001] and *Cecil et al.,* [2003]. Our samples include Mississippian and Pennsylvanian age limestones and shales deposited in the Mid-continent and Illinois basins during fully marine conditions.

Eastern Shelf of the Midland Basin

The Midland Basin located in west Texas developed as structural basin western edge of the Ouachita orogen during the continental collison which marks the closure of the Rheic ocean [*Miall and Blakey,* 2008]. The basin experienced marine sedimentation throughout the Carboniferous. The deepest part of the basin records nearly continuous deposition of offshore shale, however, cyclothem deposits of late-Pennsylvanian age

have been identified along the basin's eastern shelf [*Heckel,* 1994, 2008]. These cyclothems correlate with those of the US midcontinent, indicating the region experienced significant sea level fluctuations [*Adlis et al.,* 1988; *Boardman et al.,* 1989; *Heckel et al.,* 1991]. We analyzed conodonts extracted from upper Pennsylvanian (Gzhelian) shales (Necessity and Wayland cycles) deposited on the eastern shelf of the Midland Basin.

Methods

Rock samples (~2-3 kg) were washed and/or trimmed to remove contamination, then broken into cobble-sized pieces. Carbonates were dissolved in a 2-3% acetic acid or 1% formic acid solution buffered with ~1 g sodium triphosphate, pH >4 [*Feldman et al.,* 1989; *Jeppsson et al.,* 1999]. Black shales were soaked in dilute hydrogen peroxide. The sediment fines (~500-88 μm fraction) were collected every two days, rinsed and dried at 50°C. The sediments were further separated into light and heavy mineral fractions using low viscosity polytungstate (LVPT, ρ = ~2.83 g/cc) [after *Krukowski,* 1988]. Approximately 15 – 20 cc of sediment + 100 g LVPT were mixed in a 50 cc tube, then centrifuged at 2500 rpm for 20 minutes to aid density separation. The heavy mineral fraction was isolated by freezing the tip of the centrifuge tube in liquid nitrogen and pouring off the LVPT + light minerals. The heavy fraction was rinsed repeatedly with distilled water to remove any traces of chemical. Biogenic apatite fragments (conodonts, phosphatic brachiopods, fish teeth debris) were hand-picked picked from the heavy fraction under a binocular microscope.

Picked material was divided into separate samples: conodont elements (c), fish teeth (t), fish debris (d) and phosphatic brachiopods (b), weighing ~70 –150 μg each. Samples were gently sonicated 2x in ultra-pure Milli-Q water, 3x in ethanol and then cleaned following the oxidative-reductive protocol refined by *Boyle and Keigwin* [1985]. Organic material and pyrite were removed by heating samples to 80°C for 10 minutes in an oxidizing solution of 0.1% H_2O_2 buffered with 0.1N NaOH. Samples were rinsed 3x with MQ then subjected to a hydrazine, citric acid, NH_4OH reducing solution for 30 minutes at 80°C. A final dilute acid leach to remove any remaining surface contamination was applied before samples were dissolved in HNO_3.

The dissolved samples were run through two sets of column procedures to isolate the Nd and Sr. RE Spec cation exchange resin was used to obtain bulk REE and Sr splits. The Sr was further purified using Sr Spec cation exchange resin with HNO_3. Nd was separated from the REE split by chromatographic separation using methyllactic acid in quartz glass columns. Isotopes were analyzed via thermal ionization mass spectrometry (TIMS) in the R. Ken Williams Radiogenic Isotope Geosciences Laboratory at Texas A&M. Sr was loaded in ~2 μL 0.0035M H_3PO_4 on single rhenium filaments between 0.5 μL aliquots of TaF. Nd was loaded in ~1 μL 2N HCL on double rhenium filaments and analyzed as a metal. Within run normalization factors were 0.1194 for $^{86}Sr/^{88}Sr$ and 0.7219 for $^{146}Nd/^{142}Nd$. Machine performance was monitored by running Sr standard NBS 987 ($^{87}Sr/^{86}Sr = 0.710245$) and Nd standard JNdi-1 ($^{143}Nd/^{144}Nd = 0.512103459$). External machine reproducibility based on the above standards was 29 ppm (2 s.d.) for

Sr and 17 ppm (2 s.d.) for Nd. All errors given in Table 5-1 are 2 S.E. of the sample mean and reflect in-run precision.

We report initial Nd isotopic values, thought to reflect seawater composition

Table 5-1. Sr and Nd Isotopic Data for CarboniferousBiogenic Apatite

ARROW CANYON

SAMPLE	TYPE/ROCK		AGE (Ma)	$^{143}Nd/^{144}Nd$	$\varepsilon_{Nd}(t)$	2 S.E.	$^{87}Sr/^{86}Sr$	2 S.E.
AC08-55	*c*	*LS*	304	------	------		0.708440	± 0.000011
	c	*LS*	304	------	------		0.708290	± 0.000013
AC08-53	*t*	*LS*	305.5	------	------		0.708711	± 0.000008
AC08-51	*c*	*LS*	308	------	------		0.708300	± 0.000014
AC08-45	*c*	*LS*	309.5	------	------		0.708354	± 0.000007
AC08-36	*c*	*LS*	311	------	------		0.708470	± 0.000010
AC08-33	*c*	*LS*	311	------	------		0.708369	± 0.000008
	t	*LS*	311	------	------		0.708681	± 0.000008
AC08-24	*c*	*LS*	313	------	------		0.708322	± 0.000007
AC08-26	*d*	*LS*	313.5	0.512001	-10.3 ±	0.3	0.708598	± 0.000012
AC08-21	*c*	*LS*	314	0.511946	-11.4 ±	1.0	------	
AC08-20	*t*	*LS*	314.5	0.512130	-7.8 ±	0.7	------	
AC08-19	*c*	*LS*	315	0.512238	-5.7 ±	0.1	------	
AC08-18	*c*	*LS*	316	------	------		0.708310	± 0.000012
	t	*LS*	316	0.512081	-8.7 ±	1.7	------	
AC08-2B	*c*	*LS*	317	0.512012	-7.3 ±	0.5	------	
AC08-2A	*b*	*LS*	317	0.512157	-10.1 ±	0.2	------	
AC08-3	*c*	*LS*	317.5	0.512139	-7.6 ±	0.3	0.709270	± 0.000181
	t	*LS*	317.5	0.512147	-7.5 ±	0.1	0.709060	± 0.000020
	t	*LS*	317.5	0.512137	-7.6 ±	0.3	------	
AC08-4	*c*	*LS*	318	0.512129	-7.8 ±	0.4	0.708490	±
	t	*LS*	318	0.512088	-8.6 ±	0.2	0.708920	± 0.000009
AC08-5	*c*	*LS*	318.5	0.512076	-9.9 ±	0.2	0.708480	± 0.000030
	t	*LS*	318.5	0.512021	-9.4 ±	0.1	0.708950	± 0.000019
	b	*LS*	318.5	0.512049	-8.8 ±	0.2	------	
AC08-7	*c*	*LS*	319.5	0.512048	-9.4 ±	1.2	0.708260	± 0.000011
AC08-8	*c*	*LS*	320	0.512169	-6.4 ±	0.3	------	
	t	*LS*	320	0.512199	-7.0 ±	0.3	------	
AC08-9	*d*	*LS*	321	0.512132	-7.7 ±	0.2	0.709010	±
AC08-11	*d*	*LS*	322	0.512144	-7.5 ±	0.2	0.708690	±
AC08-12	*c*	*LS*	330	0.512234	-5.7 ±	0.2	0.707920	± 0.000013
AC08-15	*c*	*LS*	335	------	------		0.708650	± 0.000013

PATLANOAYA

SAMPLE	TYPE/ROCK		AGE (Ma)	$^{143}Nd/^{144}Nd$	$\varepsilon_{Nd}(t)$	2 S.E.	$^{87}Sr/^{86}Sr$	2 S.E.
PAT08-22	*t*	*LS*	296	0.512225	-6.5 ±	0.1	0.709540	± 0.000013
PAT08-22	*d*	*LS*	296	0.512204	-6.1 ±	0.1	0.709180	± 0.000009
PAT08-21	*c*	*LS*	299	0.512261	-5.3 ±	0.3	------	
PAT08-18	*d*	*LS*	299.5	------	------		0.709260	± 0.000034
PAT08-16	*t*	*LS*	303	0.512214	-6.2 ±	2.2	0.710150	± 0.000014
PAT08-14	*d*	*LS*	305	0.512161	-7.3 ±	0.1	0.709760	± 0.000011
PAT08-12	*d*	*LS*	306.5	0.512171	-7.0 ±	0.1	0.710510	± 0.000016
PAT08-11	*d*	*LS*	308	0.512198	-6.5 ±	0.1	0.709630	± 0.000009

Table 5-1. continued

US MIDCONTINENT

SAMPLE	TYPE/ROCK		AGE (Ma)	$^{143}Nd/^{144}Nd$	$\varepsilon_{Nd}(t)$	2 S.E.	$^{87}Sr/^{86}Sr$	2 S.E.
MC2	*c*	*LS*	299.5	------	------		0.708300	± 0.000016
WP62B	*c*	*sh*	300	------	------		0.708800	± 0.000025
MC3	*c*	*sh*	301	0.512133	-7.8	± 0.2	0.708250	± 0.000025
MC1	*c*	*LS*	302	------	------		0.708310	± 0.000015
CR2	*c*	*LS*	314	0.512283	-4.8	± 0.2	------	
CR3	*c*	*LS*	320	0.512150	-7.4	± 0.2	------	
CR4	*c*	*sh*	335	0.512289	-4.6	± 0.2	------	

MIDLAND BASIN

SAMPLE	TYPE/ROCK		AGE (Ma)	$^{143}Nd/^{144}Nd$	$\varepsilon_{Nd}(t)$	2 S.E.	
TX2	*c*	*sh*	301	0.512188	-6.8	± 0.2	------
TX3	*c*	*sh*	302	0.512190	-6.7	± 0.2	------
TX4	*c*	*sh*	302	0.512247	-5.6	± 0.2	------

during the Carboniferous, in epsilon notation ($\varepsilon_{Nd}(t)$) calculated using the estimated stratigraphic age of the sample (see Table 5-1):

$$\varepsilon_{Nd}(t) = \frac{[^{143}Nd/^{144}Nd]_{Sample(t)}}{[^{143}Nd/^{144}Nd]_{CHUR(t)}} - 1 * 10000$$

where $[^{143}Nd/^{144}Nd]_{sample(t)}$ and $[^{143}Nd/^{144}Nd]_{CHUR(t)}$ are the $^{143}Nd/^{144}Nd$ measured on the sample and that of the chondritic uniform reservoir (CHUR, present value $^{143}Nd/^{144}Nd$ = 0.512638) corrected for the ingrowth of ^{143}Nd due to the decay of ^{147}Sm since the time of deposition (t):

$$[^{147}Sm/^{144}Nd]_{(t)} = [^{147}Sm/^{144}Nd]_{(sample, CHUR)} (e^{\lambda t} - 1)$$

where, λ is the radioactive decay constant for ^{147}Sm to ^{143}Nd (6.54×10^{-12}), the $[^{147}Sm/^{144}Nd]_{(CHUR)} = 0.1967$ and a $[^{147}Sm/^{144}Nd]$ ratio of 0.144 is assumed for our

samples which represents an average literature value for Paleozoic age conodonts from North America [*Keto and Jacobsen,* 1988; *Holmden et al,* 1996, 1998].

Results

Conodont $\varepsilon_{Nd}(t)$ values for all samples analyzed ranged from -11.4 to -4.6 (Table 5-1). Nd isotope values of co-occurring conodonts, fish teeth and debris and phosphatic brachiopods (e.g., those fractions picked from the same sample) agree within 0.5 epsilon units, with one exception (Figure 5-2). The $\varepsilon_{Nd}(t)$ of phosphatic brachiopods and conodonts from sample AC08-5 differ by >1 epsilon unit. Regardless of the magnitude in Nd isotopic composition among the different apatite components, no systematic offset in $\varepsilon_{Nd}(t)$ exists among the different materials analyzed. Thus we apply average $\varepsilon_{Nd}(t)$ values from the different fractions in the interpretation of the data.

The Arrow Canyon samples exhibit the largest Nd isotopic range, from -11.4 to -5.7. The record shows high frequency variations in $\varepsilon_{Nd}(t)$ with an overall trend toward nonradiogenic values from the Upper Mississippian to Middle Pennsylvanian (Figure 5-3; Table 5-1). The $\varepsilon_{Nd}(t)$ values for Patlanoaya, US Midcontinent and Midland Basin were more radiogenic, ranging from -7.8 to -4.6. Tournaisian and upper Moscovian age conodonts from Jacob's Creek Shale and Alum Cave Limestone in the US Midcontinent recorded the most radiogenic $\varepsilon_{Nd}(t)$ values, -4.6 and -4.8 respectively.

Conodont Sr isotopic data from the sections investigated varied significantly. The $^{87}Sr/^{86}Sr$ values of the Patlanoaya samples are the most radiogenic, ranging from 0.70918 to 0.71051 (N=7). The $^{87}Sr/^{86}Sr$ composition of Arrow Canyon samples,

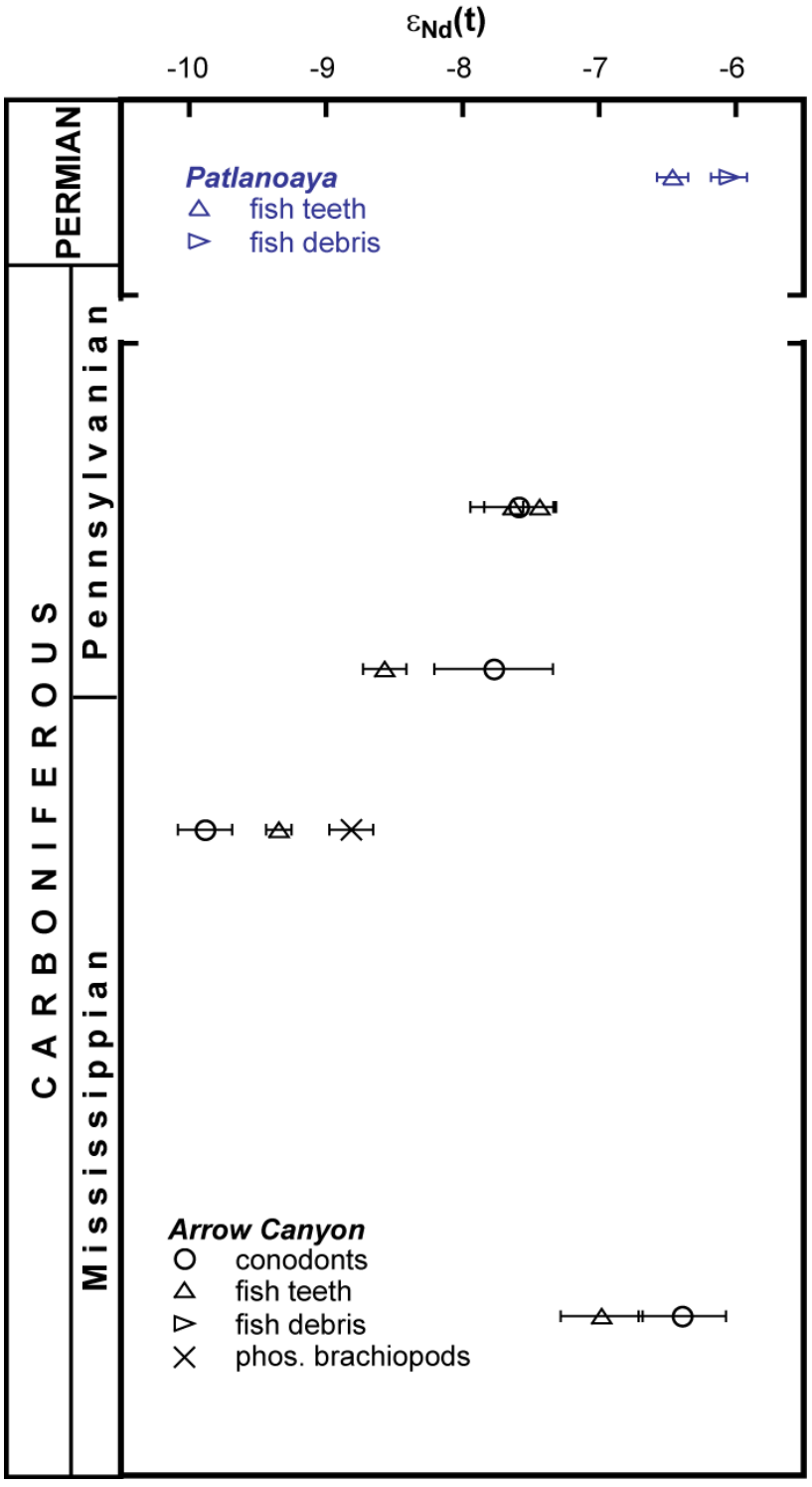

Figure 5-2. Comparison of Nd isotope records from different types of biogenic apatite. Splits were picked from the same disaggregated rock sample. Most samples show good agreement between conodont apatite and fish teeth/debris.

0.70792 to 0.70927 (N=20), overlaps slightly with the least radiogenic (lowest) values from Patlanoaya and includes the entire $^{87}Sr/^{86}Sr$ range measured on conodonts from the US Midcontinent (0.70825 to 0.7088, N=4). Furthermore, the Sr isotopic ratios of the conodont fractions are less radiogenic than fish teeth and debris, averaging 0.708423 ±0.00029, s.d. (conodonts) versus 0.708828 ±0.00018, s.d. (fish). This difference is similar in magnitude to the intersite differences in Sr isotopic composition.

Assessing the Preservation of the Biogenic Apatite Radiogenic Isotope Signals

The most reliable record of seawater $^{87}Sr/^{86}Sr$ for the Carboniferous derives from analyses of well-preserved biogenic calcite – primarily brachiopod shells – deposited in the epicontinental seas of North America, Europe and Russia [e.g. *Bruckshen et al.,* 1999; *McArthur,* 2009]. Recent work by *Brand et al*. [2009] confirms that these values match the $^{87}Sr/^{86}Sr$ of biogenic calcite from "open ocean" sites in Japan and South China. The majority of the biogenic apatite $^{87}Sr/^{86}Sr$ values we report are significantly higher than the accepted contemporaneous seawater value, and in fact, the majority of the new data exceed the maximum seawater $^{87}Sr/^{86}Sr$ value for the entire Carboniferous (0.70845; Figure 5-4). While several samples seem to have preserved the seawater signal, the divergence of the majority of our data from the global trend likely reflects alteration of the original Sr signal.

The original seawater Sr isotope signal in biogenic apatite is susceptible to late diagenetic alteration, particularly fish teeth, scales and phosphatic shells [*Cummins and*

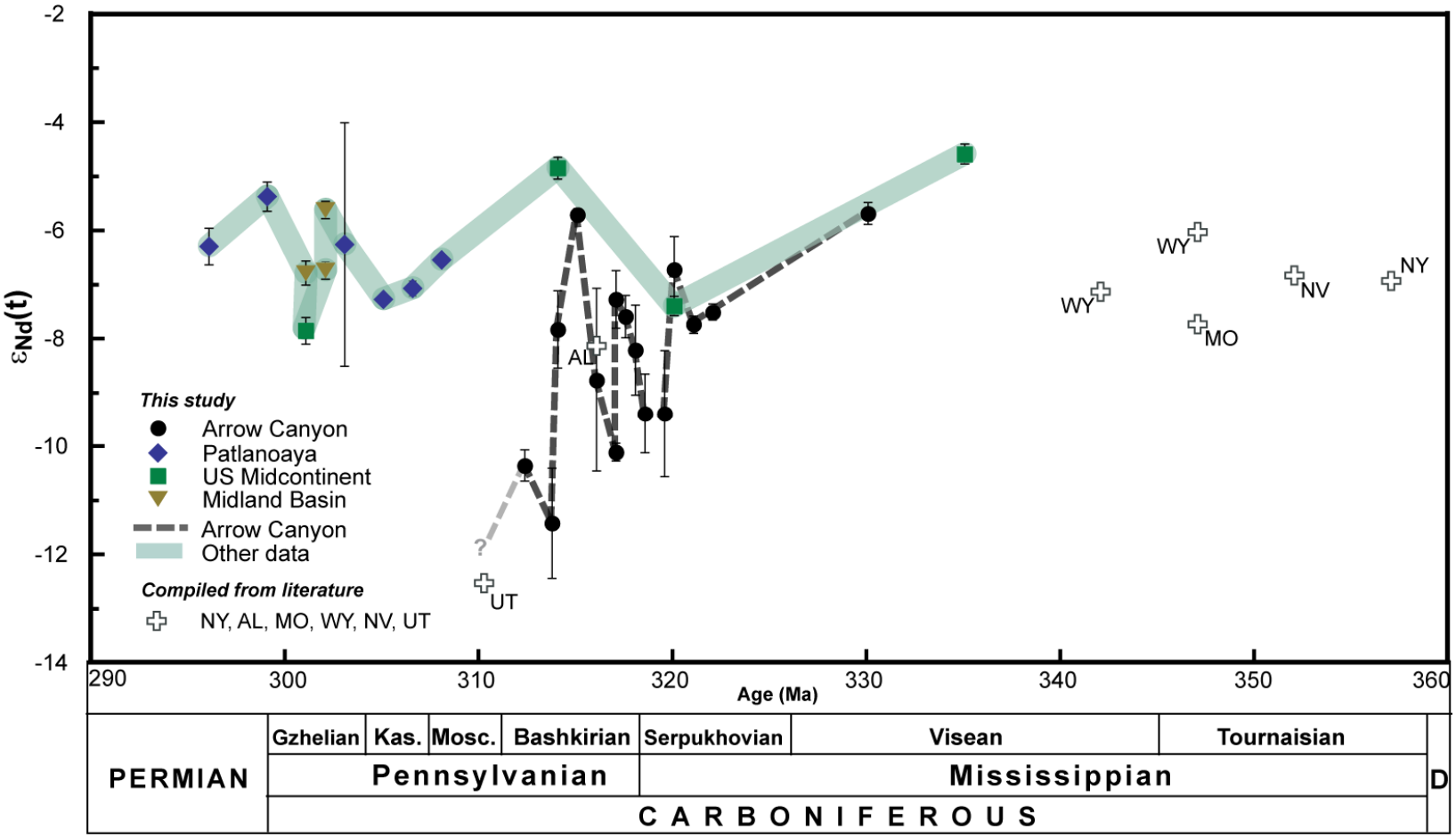

Figure 5-3. Carboniferous $\varepsilon_{Nd}(t)$ of North American epicontinental seas. Dotted grey line traces variations in $\varepsilon_{Nd}(t)$ at Arrow Canyon; pale blue line traces all other $\varepsilon_{Nd}(t)$ values obtained in this study. Where multiple analyses of one sample were performed, the average value is plotted. White crosses are data from Utah, Nevada, Wyoming, Missouri, New York and Alabama [*Keto and Jacobsen,* 1987; *Shaw and Wasserburg,* 1984 and *Wright et al.,* 1984] Ages of literature data have been adjusted to that of *Gradstein et al.* [2004].

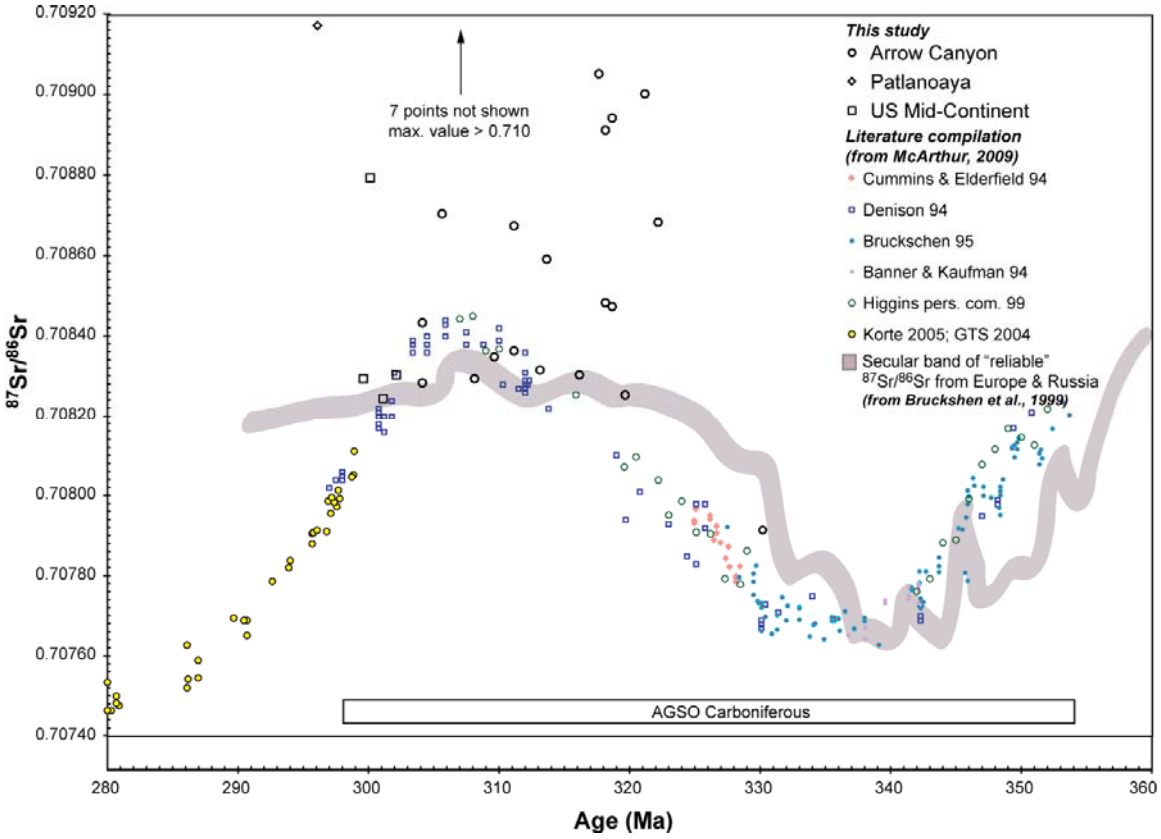

Figure 5-4. Carboniferous global marine Sr isotope curve. New Sr isotopic data (this study) plotted with the secular Sr isotopic curve from *Bruckshen* [1999] and the compiled global marine Sr curve [*McArthur,* 2009]. Sr values used in the global curve were obtained from best-preserved marine calcite from Europe, North America and the Urals (see figure for references).

Elderfield, 1994; *Bertram et al.,* 1992; *Martin and Scher,* 2004]. Indeed, all of fish teeth and debris samples we analyzed yielded $^{87}Sr/^{86}Sr$ values more radiogenic than coeval seawater (Table 5-1). However, some of the conodont $^{87}Sr/^{86}Sr$ from the US midcontinent and Arrow Canyon fall on the Carboniferous Sr seawater curve assembled from the best-preserved epicontinental samples (Figure 5-4). Conodonts may preserve the original $^{87}Sr/^{86}Sr$ signal depending on the thermal history of their host rock. The conodont color alteration index (CAI) reflects the extent to which conodonts have undergone late diagenetic thermal heating [e.g. *Rejebian et al.,* 1987], and only

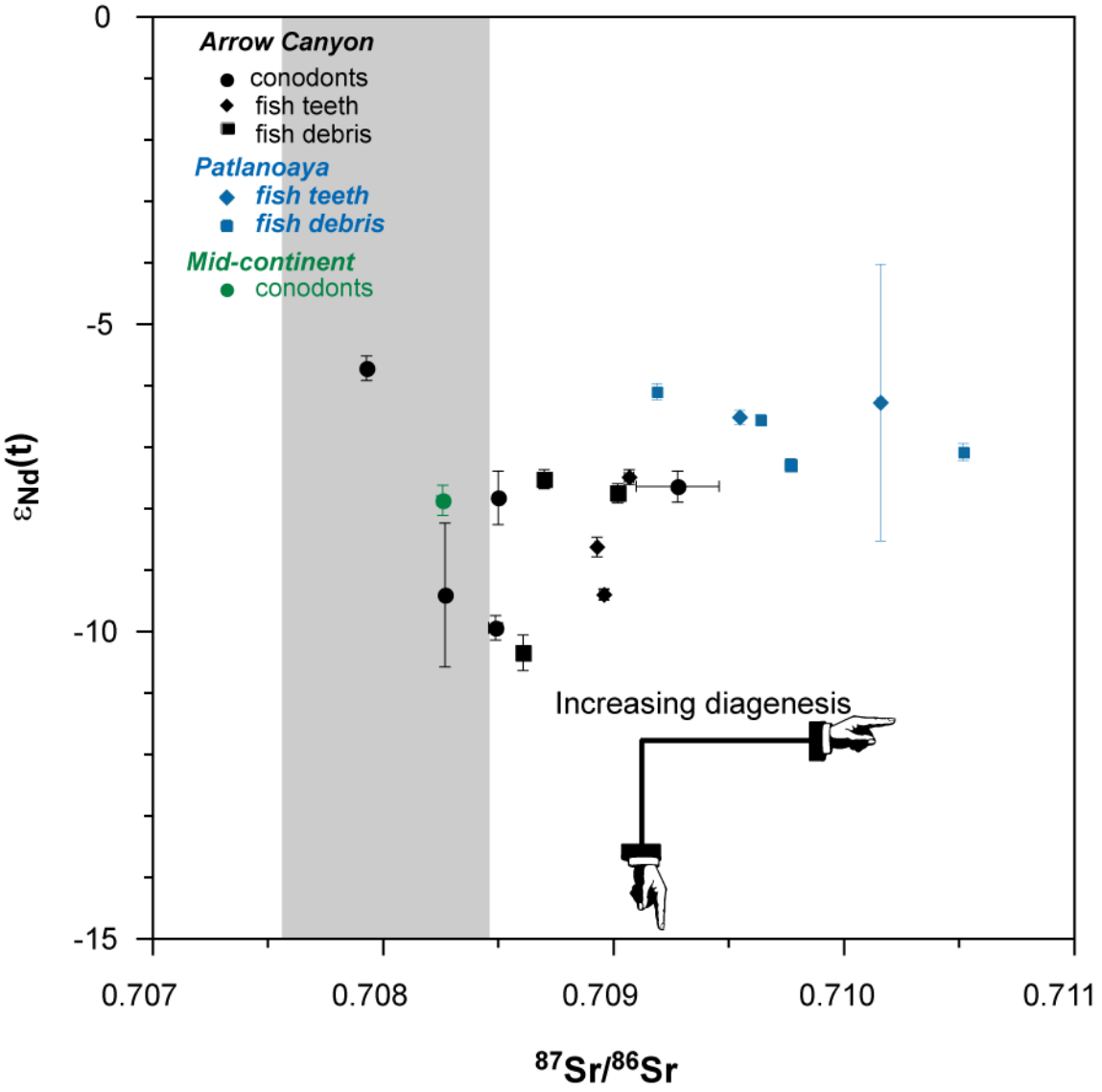

Figure 5-5. Crossplot of $\varepsilon_{Nd}(t)$ and $^{87}Sr/^{86}Sr$. Grey bar indicates range of seawater $^{87}Sr/^{86}Sr$ for the entire Carboniferous. Trend toward more radiogenic Sr likely reflects diagenetic alteration but $\varepsilon_{Nd}(t)$ values appear uninfluenced by diagenesis.

conodonts with low CAI values (<2.5) appear to reliably preserve the seawater Sr isotopic composition [e.g. *Bertram et al.,* 1992]. Our conodont samples from the US Midcontinent have CAI of ~2, indicating good preservation, while conodonts from Arrow Canyon and Patlanoaya are typically 3 or higher and probably reflect alteration

due to the longer and more complex burial and tectonic history of the developing cordillera along western N. America.

The over-printing of the primary seawater $^{87}Sr/^{86}Sr$ by exchange with groundwater or country rock bearing a higher $^{87}Sr/^{86}Sr$ composition due to late diagenetic heating, makes it difficult to use Sr to infer interbasinal changes in marine residence times, continental weathering or hydrothermalism. However, the relationship between the Sr and Nd isotopes suggests the Nd isotopic composition of our samples was not affected by post depositional alteration. Altered samples (CAI $\geq$ 3) show a distinct trend toward more radiogenic Sr values. Typically crustal rocks with radiogenic Sr isotopic ratios contain unradiogenic $^{143}Nd/^{144}Nd$ because Sm and Sr are more incompatible leading to elevated Nd and Rb concentrations in differentiated upper continental crust. Therefore, the diagenetic source of radiogenic Sr should be accompanied by unradiogenic Nd, yet there is no systematic decrease in $\varepsilon_{Nd}(t)$ coincident with the $^{87}Sr/^{86}Sr$ increase (Figure 5-5). The $^{87}Sr/^{86}Sr$ broadly defines two groups within our samples (i.e. Patlanoaya and the rest) except for one data point. One conodont sample from Arrow Canyon contains relatively radiogenic $\varepsilon_{Nd}(t)$ and unradiogenic $^{87}Sr/^{86}Sr$ compared with the other samples (Figure 5-5). We note, however, that this sample is mid-Mississippian in age whereas the other samples date from the Mid-Carboniferous boundary to late Pennsylvanian, and is likely recording significantly different seawater chemistry prior to the initiation of the Alleghenian-Variscan orogeny. Therefore, we assume little alteration of the primary Nd isotopic signal and interpret the

$\varepsilon_{Nd}(t)$ of our samples to reflect that of the overlying seawater during or shortly after deposition.

Carboniferous Record of Nd Isotopes in North American Epicontinental Seas

One advantage of using tracers with relatively short seawater residence times (e.g. Nd) is that basins with seawater recharge rates less than the residence time of the tracer will develop geochemical gradients reflecting the composition of weathered materials input from the surrounding watershed. The $\varepsilon_{Nd}(t)$ of seawater is determined by the combination of inputs of radiogenic Nd derived from young, mantle-derived material and older felsic materials with unradiogenic $^{143}Nd/^{144}Nd$. Therefore, we would expect to see temporal and geographic differences in the reconstructed $\varepsilon_{Nd}(t)$ signatures of the basins comprising the North American epicontinental seaway related to water circulation patterns and communication with the open ocean. Our discussion of the Nd isotopic composition of the epicontinental basins here focuses on the potential interactions between the epicontinental seas and the fully marine open ocean end-members. Thus we use "open ocean" to refer to the deep ocean basins floored by oceanic crust to distinguish these provinces from the more shallow and restricted epicontinental seas.

Prior to its closure, the Rheic Ocean would likely have contributed open ocean waters to the N. American epicontinental basins. We assume the waters of the Rheic would have had a fairly radiogenic $\varepsilon_{Nd}(t)$ due to numerous subduction zones and arc magmatism. Furthermore, the Rheic was genetically related to the Iapetus Ocean [*Murphy et al.,* 2010]. Early Paleozoic reconstructions indicate Iapetus seawater $\varepsilon_{Nd}(t)$

was ~-5 to -7 [*Keto and Jacobsen,* 1987, 1988]. Our combined $\varepsilon_{Nd}(t)$ data (Figure 5-3) indicate early-mid Mississippian $\varepsilon_{Nd}(t)$ averaging ~-5.1 and decreasing to ~-7 through the late Mississippian, followed by high amplitude fluctuations to values as low as -11 across the M-P boundary before returning to more radiogenic values (~-5.5 to -7.5) in the late Pennsylvanian/Permian. Previous studies of conodont $\varepsilon_{Nd}(t)$ from eastern North America to the midcontinent also indicate relatively radiogenic values in the early Mississipppian (Figure 5-3) [*Shaw and Wasserburg,* 1985; *Wright and Shaw,* 1984; *Keto and Jacobsen,* 1988].

The trend toward unradiogenic $\varepsilon_{Nd}(t)$ coincides with a major sea level regression [*Saunders and Ramsbottom,* 1986; *Wright and Vanstone,* 2001] and suggests restricted mixing of seawater in the shallow epicontinental seas with the relatively radiogenic open Rheic ocean coincident with the expansion of Gonwandan ice sheets at the M-P boundary. Weathering of older cratonic material into the North American epicontinental basins during sea level lowstands combined with periodic flushing by waters from the Rheic ocean driven by glacio-eustasy could account for the variations in our $\varepsilon_{Nd}(t)$ record over the second half of the Carboniferous. This implies that variations in mixing occur on Milankovitch timescales. The higher amplitude fluctuations observed for Arrow Canyon may merely be an artifact of data density, since we have few data points for the interior US continent spanning the same interval.

We would expect differences in $\varepsilon_{Nd}(t)$ to develop between the various North American basins as falling sea level restricted circulation and increased basinal residence times. The cyclothems, which dominate the lithology of Late Carboniferous rocks from

the North American epicontinental seas, are evidence of high order sea level changes [e.g. *Heckel,* 2002 and references therein]. However, the limited Nd isotope data from the upper Pennsylvanian/lower Permian US Midcontinent, Midland Basin and Patlanoaya all indicate similar and relatively high $\varepsilon_{Nd}(t)$ values. Due to its location along the edge of the Rheic Ocean, $\varepsilon_{Nd}(t)$ values from Patlanoaya likely record changes in the open ocean endmember. Therefore variations in the Nd isotopic composition of the Rheic Ocean controlled the seawater composition of the epicontinental basins. On the other hand, the similarities might also reflect the proximity of the locations to sources of radiogenic eNd(t). Arc volcanism along the subducting edge of the Rheic Ocean would contribute to higher eNd(t) values recorded at Patlanoaya, while erosion of the uplifting Ouachita mountains shed moderately radiogenic Nd into the restricted Midcontinent basins [*Gleason et al.,* 1994]. The one $\varepsilon_{Nd}(t)$ value for the Midcontinent during this interval is slightly less radiogenic (-7.8), suggesting a possible geochemical gradient extending out from continental interior, but more analyses are needed to confirm or deny this trend. It is important to note that the lack of a strong geochemical gradient from the continental interior to Patlanoaya may simply relate to our sampling strategy. Nearly all of the Midland Basin and Midcontinent samples come from shales deposited during sea level highstand when the continental interior was more likely to be influenced by transgressive open ocean waters.

$\varepsilon_{Nd}(t)$ as an Indicator of Glacio-eustasy, Bird Spring Shelf, Arrow Canyon, NV

The Mid-Carboniferous boundary is marked by major sea level regression, which

appears as a prominent unconformity in many shallow shelf records from around the world [*Saunders and Ramsbottom,* 1986; *Rygel et al.,* 2008]. The Nd isotope record at Arrow Canyon is characterized by relatively stable $\varepsilon_{Nd}(t)$ values of ~-6.9 ±0.8, 1s.d. (N=5) leading up to the M-P boundary. These transition to generally less radiogenic but more variable values (~-8.6 ±1.4, 1 s.d.; N=16) across the boundary and into the early Pennsylvanian (Figures 5-5 and 5-6). Although deposition at Arrow Canyon was nearly continuous (the basis for its selection as the mid-Carboniferous GSSP) [*Lane et al.,* 1999; *Richards et al.,* 2001], a series of sedimentological indicators, including exposure surfaces, root traces and paleosols, imply the region experienced a number of glacio-eustatic sealevel changes [e.g. *Richards et al.,* 2001; *Barnett and Wright,* 2008; *Bishop et al.,* 2009].

The beginning of the shift toward unradiogenic $\varepsilon_{Nd}(t)$ values approximately coincides with, or possibly slightly leads, a negative $\delta^{13}C$ excursion in bulk carbonate from Arrow Canyon (Figure 5-6). The light carbon isotope values reflect diagenetic alteration by groundwater due to prolonged periods of subareal exposure during glacio-eustatic regression [*Saltzman,* 2005]. The lowest $\varepsilon_{Nd}(t)$ values appear to correlate with reported glacio-eustatic cycle boundaries, e.g. ravinement surfaces or marine sequences bounding paleosols (Figure 5-6). The prominent decreases in Nd isotopic composition occur in fossils extracted from: 1) a fossiliferous limestone overlain by grey-orange mudstone with rootlets [*Barnett and Wright,* 2008], 2) a limestone topped by a paleokarst surface ~2.5 m below the mid-Carboniferous (Chesterian-Morrowan) boundary [*Bishop et al.,* 2009], and 3) a limestone bed ~ 3m above which directly

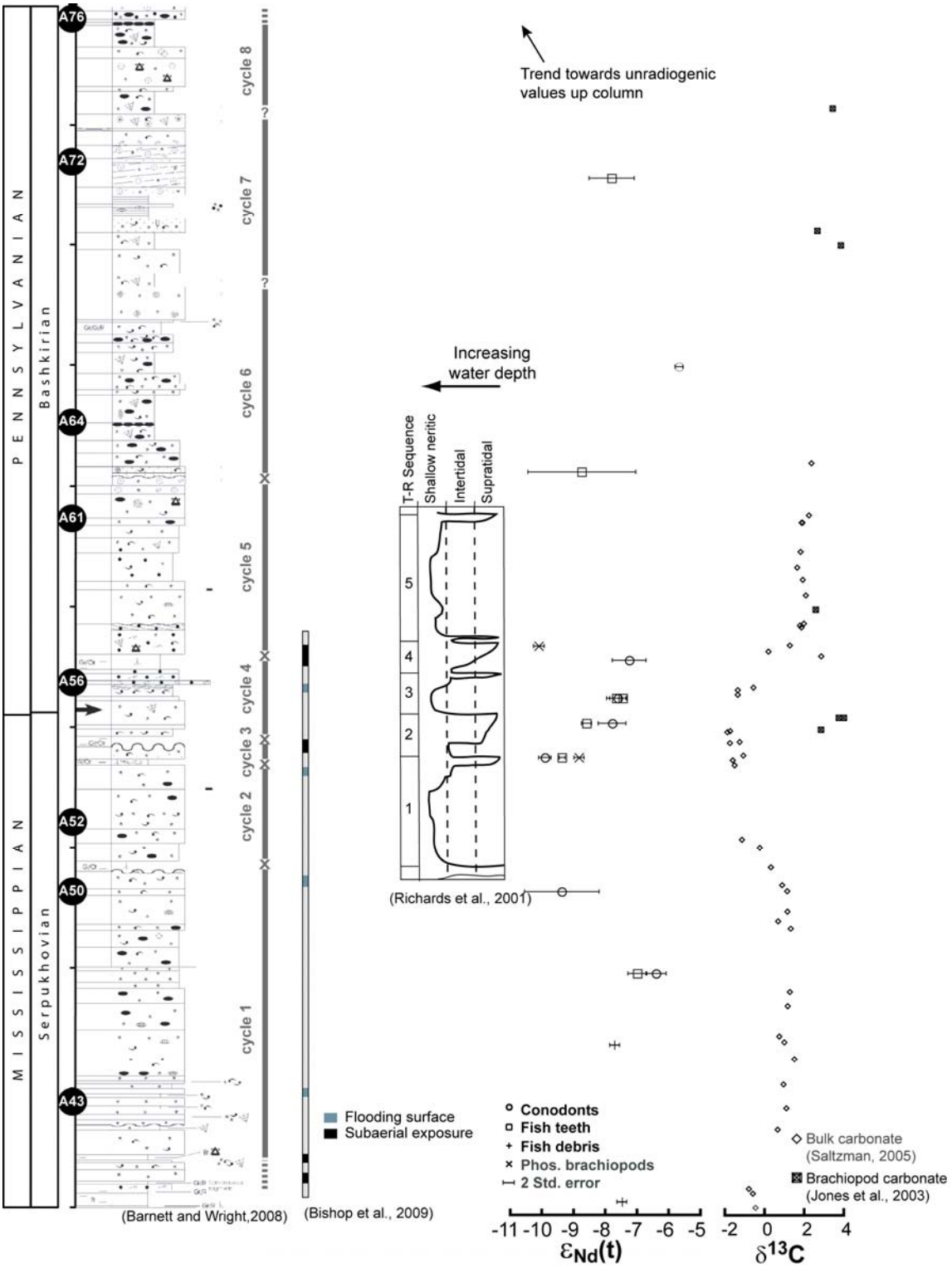

Figure 5-6. Mid-Carboniferous $\varepsilon_{Nd}(t)$ record for Arrow Canyon. High order transgressive-regressive cycles boundaries are interpreted from lithology. Stratigraphic column modified from *Barnett and Wright* [2008]. "A" numbers refer to Amoco tags placed 1.5m apart on the outcrop. Two unradiogenic values from samples taken well above the boundary are not shown.

overlies a green-brown shale containing root traces [*personal observation, SCW* 2008; *Barnett and Wright,* 2008]. The decrease in Nd isotope values near exposure surfaces implies glacio-eustatic sea level fall restricted basin circulation and/or enhanced contributions from an unradiogenic Nd source. The $\varepsilon_{Nd}(t)$ returns to more radiogenic values (~-7) in deposits between these intervals which we interpret to reflect flooding of North American craton with Rheic Ocean water as sea levels rose.

There are a number of sources of unradiogenic Nd to Arrow Canyon (Figure 5-7, Table 5-2). Deposition at Arrow Canyon occurred in a foreland basin at the foot of the emerging Antler highlands to the west during the Carboniferous. Tectonic evidence suggests the Antler orogeny occurred as a siliciclastic wedge that was emplaced along the passive margin of western North America [*Saleeby et al.,* 1994]. Nd isotopic analyses indicate a range of $\varepsilon_{Nd}(t)$ values for the Antler Highlands ~ -5 to -11 [*Smith and Gehrels,* 1992a,b]. Weathering of the least radiogenic material from these ranges could have produced the trend toward decreased $\varepsilon_{Nd}(t)$ we observe. However, it is also likely that enhanced weathering of the transcontinental arch was the source of unradiogenic material. The transcontinental arch is an extension of the Canadian Shield stretching across North America from the present day western Great Lakes region to Arizona. The arch is comprised of unradiogenic Precambrian basement, $\varepsilon_{Nd}(t)$ = -13 to -22 [*Patchett et al.*, 1999*; Fanton et al.,* 2002; *Haidl et al.,* 2003]. Runoff from the arch contributed the unradiogenic Nd composition of North American epicontinenal seas earlier in the Paleozoic [*Holmden et al.,* 1998]. During the Devonian and early Carboniferous this feature was submerged and accumulated carbonates, but there is evidence of shoaling in

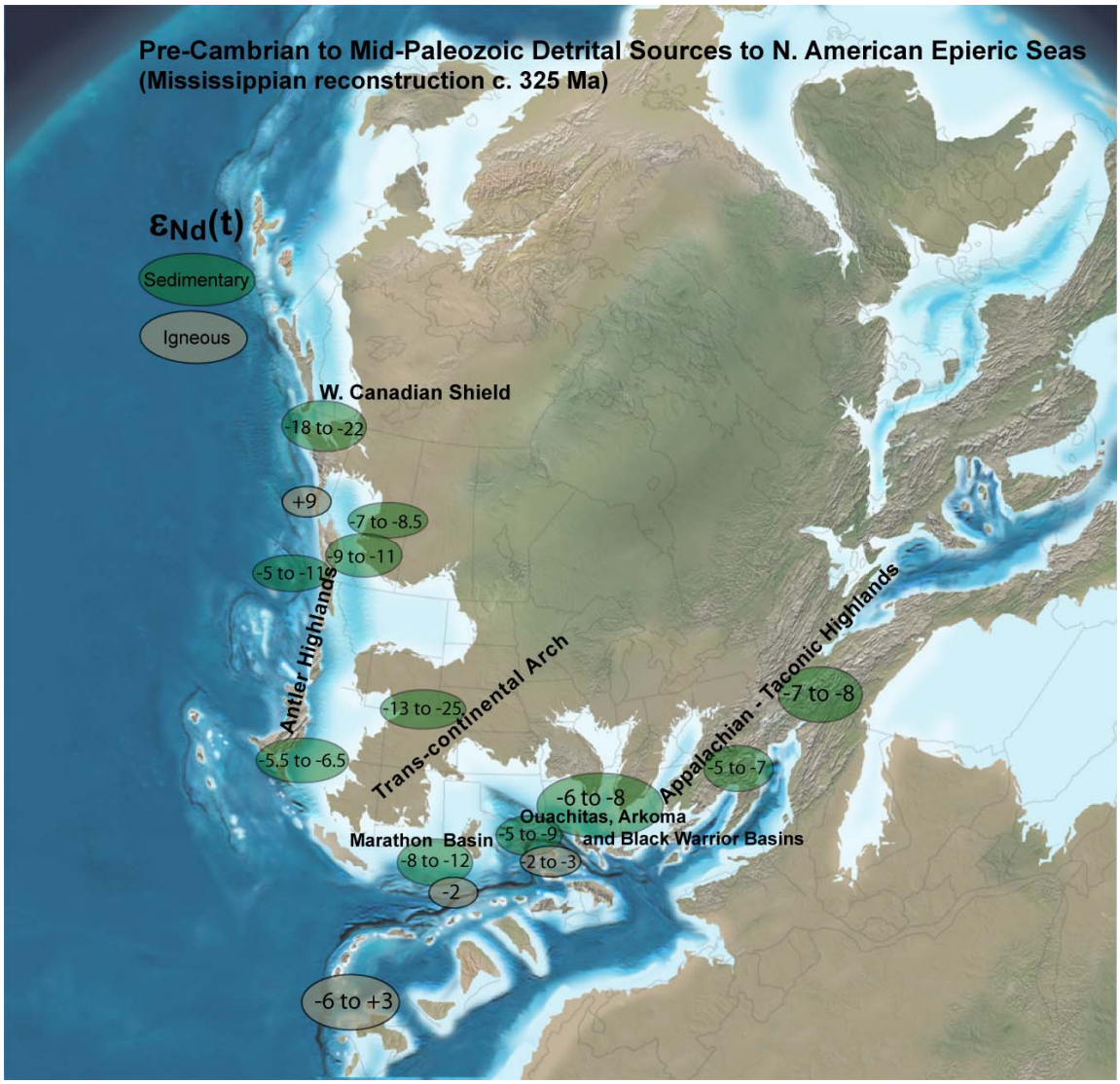

Figure 5-7. Detrital sources to North American epicontinental seas. Locations and $\varepsilon_{Nd}(t)$ of potential detrital sources are highlighted. Refer to Table 5-2 for $\varepsilon_{Nd}(t)$ data and references. Late Mississippian (~325Ma) paleoreconstruction [modified from *Blakey,* NAU Geology].

the late Mississippian and the emergence of continental clastic source areas [*Carlson,* 1999]. The lack of early Pennsylvanian sediments across the central western US indicates uplift, due to tectonic pressures to the east and south, exposed the Transcontinental Arch to extensive erosion [*Carlson,* 1999].

Our data are insufficient to investigate whether variations in $\varepsilon_{Nd}(t)$ of the waters

Table 5-2. Detrital Sources to North American Epicontinental Seas

Era (Age Ma)	Location	$\varepsilon_{Nd}(t)$	References
Northeastern USA			
Late Ordovician (440)	Taconic Highlands	-7 to -8	*Gleason et al.* [1994]; [1995]
Late Ordovician (450)	Appalachian Basin	-5 to -7	*Keto and Jacobsen* [1987]; *Patchett et al.* [1999]
South - Central USA			
Mississippian (340)	Ouachita - Stanley Fm.	-5 to -9	
Mississippian (340)	Ouachita - Stanley Fm. (tuff)	-2 to -3	
Miss. – Pennsylvanian (320)	Arkoma Basin	-6 to -8	
Pennsylvanian (300)	Black Warrior Basin	-7	*Gleason et al.* [1994]; [1995]
Ordovician (480)	Marathon Basin	-15	
Mississippian (340)	Marathon Basin	-9 to -11.5	
Mississippian (340)	Marathon Basin (tuff)	-2	
Miss. – Pennsylvanian (320-300)	Marathon Basin	-8 to -9.5	
PreCambrian - early Paleozoic	Transcontinental Arch and Canadian Shield	-13 to -22	*Patchett et al.* [1999]; *Fanton et al.* [2002]; *Haidl et al.* [2003]
Western USA and Canadian Cordillera			
Mississippian (350)	British Columbia and Yukon – Kootenay and Cassar Terranes	-18 to -22	
Miss. – Pennsylvanian (320)	British Columbia - Slide Mt (Basalt)	+9	*Patchett and Gehrels* [1998]
Late Devonian (380)	Alberta - Mount Hawk Fm.	-7 to -9	
Late Devonian (365)	Alberta - Sassenach Fm.	-10 to -11	*Stevenson et al.* [2000]
Late Devonian (365)	Northern WA - Kootenay	-5 to -11	*Smith and Gehrels* [1992]
Southwestern USA			
Miss. – Pennsylvanian (320)	Arrow Canyon, NV - Bird Spring Fm.	-5.5 to -6.5	*Hensley et al.* [2009]
S. - Central Mexico			
PreCambrian -early Phanerozoic	Oaxaca, Sierra Madre Terranes (ig. basement)	-6 to +3	*Ruiz et al.* [1988]

bathing Arrow Canyon correlated to the glacio-eustatic cycles of the Upper Pennsylvanian. However, the least radiogenic values in our new record ($\varepsilon_{Nd}(t)<-10$)

derive from mid-Bashkirian limestones that form part of a larger regressive sequence [*Briggs et al.,* 2005]. An even more unradiogenic value, -12.5, is reported for one mid-Pennsylvanian sample from the Morgan formation in the Uinta Mountains of Utah [*Keto and Jacobsen,* 1988]. It is reasonable to assume a genetic connection between the waters of the Uintas and Arrow Canyon since a shallow seaway west of the Transcontinental Arch connected the entire region. An influx of unradiogenic waters draining old cratonic basement combined with increased basinal residence times (due to restricted circulation which initiated at the M-P boundary and continued throughout the Pennsylvanian) is a plausible explanation for the decreased $\varepsilon_{Nd}(t)$ in our record.

We must also consider the possibility that wholesale changes in the seawater source to Arrow Canyon produced the changes in the Nd isotopic composition, rather than variations in weathering or basinal residence times. Major restructuring of ocean circulation due to the closure of the tropical oceanic gateway between Panthalassa and the Paleotethys is indicated by a divergence in the magnitude of the mid-Carboniferous marine carbonate $\delta^{13}C$ excursion from North American epicontinental seas and those of Europe and Russia [*Mii et al.,* 1999, 2001; *Grossman et al.,* 2008; *Bruckshen et al.,* 1999; *Popp et al.,* 1986]. The divergence of the $\varepsilon_{Nd}(t)$ values at Arrow Canyon from the other locations indicate a change in circulation in North America at the same time (Figure 5-3). It is possible that the source of open ocean water feeding the basin at Arrow Canyon changed due to the combined influence of tectonic pressures as the Antler Mountains were uplifted, the Rheic Ocean closed and sea level fell.

The Nd isotopic composition of Panthalassa is poorly constrained during the

Carboniferous, but studies of Ordovician age conodonts and phosphatic brachiopods from North America and Baltica indicate an $\varepsilon_{Nd}(t)$ of -10 to -20 for the early Paleozoic [*Keto and Jacobsen*, 1987]. Our Patlanoaya $\varepsilon_{Nd}(t)$ values suggest the waters of the Rheic were radiogenic probably related to active subduction volcanism. Fresh, young material composed of volcanic glasses and Fe-rich minerals are readily weathered, controlling the composition of the Rheic. Panthalassa, however, was a vast global ocean and likely less influenced by inputs of radiogenic Nd due to its large volume. Some lateral transport and mixing of radiogenic waters almost certainly occurred along the Panthalassa-Rheic boundary. Due to the spin of the Earth and east to west progression of Alleghenian-Variscan and Ouachita orogenies, surface waters from the Rheic would likely have flowed westward toward Panthalassa. The boundary between the two oceans was located south of the equator [*Scotese and McKerrow,* 1990], making it likely that the radiogenic signal derived from Rheic seawater would have propagated southward in Panthalassa due to the Coriolis Effect. Thus, incursion of Panthalassic waters with an unradiogenic Nd signature along the western margin of North America could explain the change in $\varepsilon_{Nd}(t)$ observed at Arrow Canyon. Tectonic loading from the obducting Antler Highlands may have created connections between the western US basins and Panthalassa. During sea level regression and low stands, these connections would allow seawater in the region to be sourced from Panthalassa to the west, while restricting communication with the remnant Rheic Ocean and epicontinental basins to the south and east. Transgression would restore connections with the interior basins driving $\varepsilon_{Nd}(t)$ values up. In this scenario, the more radiogenic $\varepsilon_{Nd}(t)$ signal preserved in the interior basins of North

America and at Patlanoaya reflects their proximity to radiogenic sources of Nd. Therefore, restricted circulation between the basins and Rheic during times of regression would have had little effect on the Nd iotopic composition of the interior waters.

Paleoclimatic Implications

Our $\varepsilon_{Nd}(t)$ records implies decoupling of North American epieric seaways from the open ocean (Panthalassa) by the latest Mississippian. The Arrow Canyon $\varepsilon_{Nd}(t)$ record indicates that the epicontinental seas of the western US were periodically separated from the rest of the North American epieric basins and received unradiogenic inputs of Nd (Figure 5-3), a trend that continues at least through the early to middle Pennsylvanian. $\varepsilon_{Nd}(t)$ values for the US Midcontinent, Midland Basin and Patlanoaya all fall within the same broad range (~-5 to -8) during the Carboniferous, implying a similar marine source – probably the closing Rheic Ocean. The upper Pennsylvanian (Gzhelian) $\varepsilon_{Nd}(t)$ values of the Midcontinent are slightly lower than values from Midland Basin and Patlanoaya suggesting the development of a geochemical gradient.

Comparison of our $\varepsilon_{Nd}(t)$ record with marine carbonate $\delta^{18}O$ and $\delta^{13}C$ reveals a correspondence between decreasing $\varepsilon_{Nd}(t)$ at Arrow Canyon across the M-P boundary and positive $\delta^{18}O$ and $\delta^{13}C$ excursions in brachiopod calcite [e.g. *Popp et al.,* 1986; *Mii et al.,* 1999, 2001; *Bruckshen et al.,* 1999; *Grossman et al.,* 1993] which are typically used to link global icehouse conditions to organic carbon burial and atmospheric CO_2 levels [*Berner and Kothavala, 2001; Royer et al.,* 2004]. While these records can be explained in terms of a global shift to an icehouse climate, they are likely recording the

response of regional marine environments to the climate rather than the mechanisms driving global climate change. Future detailed studies are needed to fully understand the extent to which these systems were decoupled from the open ocean and unravel the connection between climate and shallow marine environments.

CHAPTER VI

CONCLUSIONS

The dust accumulation record from Shatsky Rise suggests that source regions supplying dust to the tropical North Pacific, 58 Ma, may have experienced amplified wet-dry cycles corresponding with orbital eccentricity maxima. The dust flux record is corroborated by sedimentary ^{232}Th data, an independent proxy for eolian material. Overall dust fluxes, were substantially less than modern due to a more humid atmosphere and/or fewer/smaller dust source regions during the early Paleogene. However, the relative response of dust supply to orbital forcing during the last major interval of greenhouse climate was comparable to that during the Pleistocene implying changes in solar insolation exert a primary control over global climate regardless of overall climate state.

The recorded dust changes likely contributed to the orbitally-paced lithologic cycles by diluting the accumulating calcium carbonate, but changes in dust flux can account for only a fraction of the total carbonate change. Therefore, some other mechanism controlling carbonate preservation at the seafloor must also have responded to orbital forcing and account for the remaining difference in carbonate content.

The Nd and Sr isotopic composition of extracted “dust” from Shatsky Rise, ODP Site 1209 indicates a relatively old continental dust source. There appear to be at least two source regions. Potential dust sources include Australia, Asia and North Africa. Transport of dust from North Africa by the trade winds seems plausible. Periodic

additions of andesitic material from active arc-volcanism in the Caribbean may account for radiogenic increases in dust $\varepsilon_{Nd}(0)$ observed in our record. Pb isotopes may help to more positively determine dust provenance.

The Carboniferous $\varepsilon_{Nd}(t)$ record derived from biogenic apatite implies decoupling of N. American epieric seaways from the open ocean (Panthalassa) by the latest Mississippian. The record from Arrow Canyon indicates that the epicontinental seas of the western US were periodically separated from the rest of the N. American epieric basins and received unradiogenic inputs of Nd. The onset of glaciation and subsequent eustatic changes influenced circulation in the epicontinental seas, however these environments appear to record the regional response to climate change rather than mechanisms driving climate. Additional studies are needed to fully understand the extent to which these systems were decoupled from the open ocean and unravel the connection between climate and shallow marine environments.

REFERENCES

Adkins, J. F., H. Cheng, E. A. Boyle, E. R. M. Druffel, and R. L. Edwards (1998), Deep-sea coral evidence for rapid change in ventilation of the deep North Atlantic 15,400 years ago, *Science*, *280*(5364), 725-728.

Adlis, D. S., E. L. Grossman, T. E. Yancey, and R. D. McLerran (1988), Isotope stratigraphy and paleodepth changes of Pennsylvanian cyclical sedimentary deposits, *Palaios*, *3*(5), 487-506.

Alfaro, S., and L. Gomes (2001), Modeling mineral aerosol production by wind erosion: Emission intensities and aerosol size distributions in source areas, *Journal of Geophysical Research-Atmospheres, 106*(D16), 18075-18084.

Anderson, R. F., M. Q. Fleisher, and Y. Lao (2006), Glacial-interglacial variability in the delivery of dust to the central equatorial Pacific Ocean, *Earth and Planetary Science Letters*, *242*(3-4), 406-414.

Antal, P. S. (1966), Diagenesis of Thorium isotopes in deep-sea sediments, *Limnology and Oceanography*, *11*(2), 278-292.

Arsouze, T., J. C. Dutay, F. Lacan, and C. Jeandel (2007), Modeling the neodymium isotopic composition with a global ocean circulation model, *Chemical Geology*, *239*(1-2), 165-177.

Arsouze, T., J. C. Dutay, F. Lacan, and C. Jeandel (2009), Reconstructing the Nd oceanic cycle using a coupled dynamical - biogeochemical model, *Biogeosciences*, *6*(12), 2829-2846.

Arthur, M. A., D. J. Bottjer, W. E. Dean, A. G. Fischer, D. E. Hattin, E. G. Kauffman, L. M. Pratt, and P. A. Scholle (1986), Rhythmic bedding in Upper Cretaceous pelagic carbonate sequences: varying sedimentary response to climatic forcing, *Geology, 14*(2), 153-156.

Bacon, M. P., and R. F. Anderson (1982), Distribution of Thorium isotopes between dissolved and particulate forms in the deep-sea, *Journal of Geophysical Research-Oceans and Atmospheres*, *87*(NC3), 2045-2056.

Barnett, A. J., and V. P. Wright (2008), A sedimentological and cyclostratigraphic evaluation of the completeness of the Mississippian–Pennsylvanian (Mid-

Carboniferous) Global Stratotype Section and Point, Arrow Canyon, Nevada, *Journal of the Geological Society*, *165*(4), 859-873.

Barron, E. J. (1995), Tropical climate stability and implications for the distribution of life, in *Effects of Past Global Change on Life*, edited by B. o. E. S. a. Resources, C. o. G. E. a. Resources and N. R. Council, pp. 108-117, National Academy Press, Washington, D.C.

Bergengren, J., S. Thompson, D. Pollard, and R. DeConto (2001), Modeling global climate–vegetation interactions in a doubled CO_2 world, *Climatic Change, 50*(1), 31-75.

Berger, A., and M. F. Loutre (2004), Astronomical theory of climate change, *J. Phys. IV France*, *121*, 1-35.

Bernat, M., and E. D. Goldberg (1969), Thorium isotopes in marine environment, *Earth and Planetary Science Letters*, *5*(5), 308-312.

Berner, R. A., and Z. Kothavala (2001), GEOCARB III: A revised model of atmospheric CO2 over Phanerozoic time, *American Journal of Science*, *301*(2), 182-204.

Bertram, C. J., H. Elderfield, R. J. Aldridge, and S. C. Morris (1992), SR-87 SR-86, $^{143}Nd/^{144}Nd$ and REES in Silurian phosphatic fossils, *Earth and Planetary Science Letters*, *113*(1-2), 239-249.

Biscaye, P. E., F. E. Grousset, M. Revel, S. VanderGaast, G. A. Zielinski, A. Vaars, and G. Kukla (1997), Asian provenance of glacial dust (stage 2) in the Greenland Ice Sheet Project 2 Ice Core, Summit, Greenland, *Journal of Geophysical Research-Oceans*, *102*(C12), 26765-26781.

Bishop, J. W., I. P. Montanez, E. L. Gulbranson, and P. L. Brenckle (2009), The onset of mid-Carboniferous glacio-eustasy: Sedimentologic and diagenetic constraints, Arrow Canyon, Nevada, *Palaeogeography Palaeoclimatology Palaeoecology*, *276*(1-4), 217-243.

Blakey, R. C. (NAU Geology), Reconstructing the ancient EARTH, Colorado Plateau Geosystems (CPG), available at: http://cpgeosystems.com/index.html. Accessed February, 2011.

Boardman, D. R., and P. H. Heckel (1989), Glacial-eustatic sea-level curve for early Late Pennsylvanian sequence in north-central Texas and biostratigraphic correlation with curve for midcontinent North America, *Geology*, *17*(9), 802-805.

Bottjer, D. J., M. A. Arthur, W. E. Dean, D. E. Hattin, and C. E. Savrda (1986), Rhythmic bedding produced in Cretaceous pelagic carbonate environments: Sensitive recorders of climatic cycles, *Paleoceanography*, *1*(4), 467-481.

Boyd, P. W., C.S. Law, D.A. Hutchins, E.R. Abraham, P.L. Croot, et al. (2005), Fe Cycle: Attempting an iron biogeochemical budget from a mesoscale SF_6 tracer experiment in unperturbed low iron waters, *Global Biogeochemical Cycles, 19*(4), GB4S20.

Boyle, E. A., and L. D. Keigwin (1985), Comparison of Atlantic and Pacific paleochemical records for the last 215,000 years – changes in deep ocean circulation and chemical inventories, *Earth and Planetary Science Letters*, *76*(1-2), 135-150.

Boyle, E. A., and L. D. Keigwin (1987), North Atlantic thermohaline circulation during the past 20,000 years linked to high-latitude surface temperature, *Nature, 330*(6143), 35-40.

Bralower, T. J., and S. Party (2006), New evidence for abrupt climate change in the Cretaceous and Paleogene: An Ocean Drilling Program expedition to Shatsky Rise, northwest Pacific, in *Proceedings of the Ocean Drilling Program, Scientific Results 198*, edited by T. J. Bralower, pp. 1-47, IODP, College Station, TX.

Bralower, T. J., I. P. Silva, and M. J. Malone (2002), New evidence for abrupt climate change in the Cretaceous and Paleogene: An Ocean Drilling Program expedition to Shatsky Rise, northwest Pacific, *GSA Today, 12*(11), 4-10.

Brand, U., J. Tazawa, H. Sano, K. Azmy, and X. Q. Lee (2009), Is mid-late Paleozoic ocean-water chemistry coupled with epeiric seawater isotope records?, *Geology*, *37*(9), 823-826.

Briggs, K. P. (2005), Establishing a high-frequency standard reference sequence stratigraphy, sea-level curve, and biostratigraphy for Morrowan strata of the Lower Absaroka I time slice based upon the Bird Spring Formation, Arrow Canyon, Nevada, M.S. thesis, Bringham Young Univeristy, Provo, UT.

Broecker, W.S. and E. Clark (1999), $CaCO_3$ size distribution: A paleocarbonate ion proxy? *Paleoceanography, 14*(5) 596-604.

Bruckschen, P., S. Oesmann, and J. Veizer (1999), Isotope stratigraphy of the European Carboniferous: Proxy signals for ocean chemistry, climate, and tectonics, *Chemical Geology*, *161*(1-3), 127-163.

Cande, S. C., and D. V. Kent (1995), Revised calibration of the geomagnetic polartity timescale for the Late Cretaceous and Cenozoic, *Journal of Geophysical Research-Solid Earth*, *100*(B4), 6093-6095.

Caputo, M. V., J. H. G. de Melo, M. Streel, and J. L. Isbell (2008), Late Devonian and Early Carboniferous glacial records of South America, in *Resolving the Late Paleozoic Ice Age in Time and Space*, edited by C. R. Fielding, T. D. Frank and J. L. Isbell, pp. 161-173. GSA, Boulder, CO.

Caridroit, M., A. Lamerandt, J. M. Degardin, A. F. de Dios, and D. Vachard (2002), Discovery of radiolaria and conodonts in the Carboniferous-Permian of San Salvador Patlanoaya (Puebla, Mexico); biostratigraphic implications, *Comptes Rendus Palevol*, *1*(4), 205-211.

Carlson, M. P. (1999), Transcontinental Arch - a pattern formed by rejuvenation of local features across central North America, *Tectonophysics*, *305*(1-3), 225-233.

Carroll, D. (1958), Role of clay minerals in the transportation of iron, *Geochimica et Cosmochimica Acta, 14*(1-2), 1-27.

Cecil, C. B., F. T. Dulong, R. R. West, R. Stamm, B. Wardlaw, and N. T. Edgar (2003), Climate controls on the stratigraphy of a Middle Pennsylvanian cyclothem in North America, in *Climate Controls on Stratigraphy*, edited by C. B. Cecil and T. N. Edgar, pp. 151-182, SEPM Special Publication, Tulsa, OK.

Chen, J. H., R. L. Edwards, and G. J. Wasserburg (1986), U-238,U-234 and Th-232 in seawater, *Earth and Planetary Science Letters*, *80*(3-4), 241-251.

Chuey, J. M., D.K. Rea, and N.G. Pisias (1987), Late Pleistocene paleoclimatology of the central equatorial Pacific: A quantitative record of eolian and carbonate deposition, *Quaternary Res*, *28*(3), 323-339.

Clegg, S. L., and M. Whitfield (1991), A generalized model for the scavenging of trace-metals in the open ocean, 2, Thorium scavenging, *Deep-Sea Research Part a-Oceanographic Research Papers*, *38*(1), 91-120.

Clemens, S. C. (1998), Dust response to seasonal atmospheric forcing: Proxy evaluation and calibration, *Paleoceanography*, *13*(5), 471-490.

Clemens, S. C., and W. L. Prell (1990), Late Pleistocene variability of Arabian Sea summer monsoon winds and continental aridity: Eolian records from the lithogenic component of deep-sea sediments, *Paleoceanography, 5*(2), 109-145.

Cole, J. M., S. L. Goldstein, P. B. Demenocal, S. R. Hemming, and F. E. Grousset (2009), Contrasting compositions of Saharan dust in the eastern Atlantic Ocean during the last deglaciation and African Humid Period, *Earth and Planetary Science Letters*, *278*(3-4), 257-266.

Colin, C., L. Turpin, D. Blamart, N. Frank, C. Kissel, and S. Duchamp (2006), Evolution of weathering patterns in the Indo-Burman Ranges over the last 280 kyr: Effects of sediment provenance on Sr-87/Sr-86 ratios tracer, *Geochemistry Geophysics Geosystems, 7*(3), Q03007.

Crowley, T. J., and S. K. Baum (1991), Estimating Carboniferous Sea-level fluctuations from Gondwanan ice extent, *Geology*, *19*(10), 975-977.

Cummins, D. I., and H. Elderfield (1994), The Strontium isotopic composition of Brigantian (Late Dinantian) Seawater, *Chemical Geology*, *118*(1-4), 255-270.

Davies, N. S., and M. R. Gibling (2010), Cambrian to Devonian evolution of alluvial systems: The sedimentological impact of the earliest land plants, *Earth-Science Reviews*, *98*(3-4), 171-200.

DeConto, R. M., and D. Pollard (2003), A coupled climate - ice sheet modeling approach to the Early Cenozoic history of the Antarctic ice sheet, *Palaeogeography, Palaeoclimatology, Palaeoecology*, *198*(1-2), 39-52.

Delaney, M. L., and E. A. Boyle (1983), Uranium and Thorium isotope concentrations in foraminiferal calcite, *Earth and Planetary Science Letters*, *62*(2), 258-262.

Denison, R. E., R. B. Koepnick, A. Fletcher, D. A. Dahl, and M. C. Baker (1993), Re-evaluation of the Early Oligocene, Eocene, and Paleocene seawater Strontium isotope ratios using outcrop samples from the United States Gulf coast, *Paleoceanography*, *8*(1), 101-126.

DePaolo, D.J. and G.J. Wasserburg (1976), Nd isotopic variations and petrogenetic models, *Geophys. Research Letters. 3*(5), 249–252.

DePaolo, D. J., F. T. Kyte, B. D. Marshall, J. R. Oneil, and J. Smit (1983), Rb-Sr, Sm-Nd, K-Ca, O, and H isotopic study of Cretaceous-Tertiary boundary sediments, Caravaca, Spain – Evidence for an Oceanic impact site, *Earth and Planetary Science Letters*, *64*(3), 356-373.

Derycke-Khatir, C., D. Vachard, J. M. Degardin, A. F. de Dios, B. Buitron, and M. Hansen (2005), Late Pennsylvanian and Early Permian chondrichthyan microremains from San Salvador Patlanoaya (Puebla, Mexico), *Geobios*, *38*(1), 43-55.

Dickin, A. (2004), *Radiogenic Isotope Geology*, 2nd ed., 512 pp., Cambridge University Press, New York, NY.

Dinares-Turell, J., J. I. Baceta, G. Bemaola, X. Orue-Etxebarria, and V. Pujalte (2007), Closing the Mid-Palaeocene gap: Toward a complete astronomically tuned Palaeocene Epoch and Selandian and Thanetian GSSPs at Zumaia (Basque Basin, W Pyrenees), *Earth and Planetary Science Letters, 262*(3-4), 450-467.

Duce, R. A., and N. W. Tindale (1991), Atmospheric transport of iron and its deposition in the ocean, *Limnology and Oceanography*, *36*(8), 1715-1726.

Duce, R. A., C. K. Unni, B. J. Ray, J. M. Prospero, and J. T. Merrill (1980), Long-range atmostpheric transport of soil dust from Asia to the tropical North Pacific – Temporal variability, *Science, 209*(4464), 1522-1524.

El Albani, A., D. Vachard, F. Fursich, B. Buitron, and A. F. de Dios (2005), Depositional environment and biofacies characterization of the Upper Pennsylvanian-Lower Permian deposits of the San Salvador Patlanoaya section (Puebla, mexico), *Facies*, *50*(3-4), 629-645.

EPICA (2004), Eight glacial cycles from an Antarctic ice core, *Nature, 429*(6993), 623-628

Fanton, K. C., C. Holmden, G. S. Nowlan, and F. M. Haidl (2002), Nd-143/Nd-144 and Sm/Nd stratigraphy of Upper Ordovician epeiric sea carbonates, *Geochimica et Cosmochimica Acta*, *66*(2), 241-255.

Farley, K. A. (1995), Cenozoic variations in the flux of interplanetary dust recorded by the He-3 in deep-sea sediment, *Nature, 376*(6536), 153-156.

Farley, K. A., and S. F. Eltgroth (2003), An alternative age model for the Paleocene-Eocene thermal maximum using extraterrestrial He-3, *Earth and Planetary Science Letters, 208*(3-4), 135-148.

Farley, K. A., R. A. Wolf, and L. T. Silver (1996), The effects of long alpha-stopping distances on (U-Th)/He ages, *Geochimica et Cosmochimica Acta, 60*(21), 4223-4229.

Farrell, J. W., and W. L. Prell (1989), Climatic Change and CaCO3 Preservation: An 800,000 Year Bathymetric Reconstruction from The Central Equatorial Pacific Ocean, *Paleoceanography, 4*(4), 447-466.

Faure, G., and T. M. Mensing (2005), *Isotopes: principles and applications*, 3rd ed., Wiley and Sons, Hoboken, NJ.

Feldman, R. M., R. E. Chapman, and J. T. Hannibal (1989), *Paleotechniques*, 358 pp., The Paleontological Society Special Publication, Knoxville, TN.

Fielding, C. R., T. D. Frank, and J. L. Isbell (2008a), The late Paleozoic ice age-A review of current understanding and synthesis of global climate patterns, in *Resolving the Late Paleozoic Ice Age in Time and Space*, edited by C. R. Fielding, T. D. Frank and J. L. Isbell, pp. 343-354. GSA, Boulder, CO.

Fielding, C. R., T. D. Frank, L. P. Birgenheier, M. C. Rygel, A. T. Jones, and J. Roberts (2008b), Stratigraphic record and facies associations of the late Paleozoic ice age in eastern Australia (New South Wales and Queensland), in *Resolving the Late Paleozoic Ice Age in Time and Space*, edited by C. R. Fielding, T. D. Frank and J. L. Isbell, pp. 41-57. GSA, Boulder, CO.

Frakes, L.A., J.E. Francis, and J.I. Skytus (1992), *Climate Modes of the Phanerozoic,* 274 pp., Cambridge University Press, New York, NY.

Gehrels, G. E., W. C. McClelland, S. D. Samson, P. J. Patchett, and M. J. Orchard (1992), Geology of the western flank of the coast mountains between Cape Fanshaw and Taku Inlet, Southeastern Alaska, *Tectonics*, *11*(3), 567-585.

Ghil, M., M.R. Allen, M.D. Dettinger, K. Ide, D. Kondrashov, et al. (2002), Advanced spectral methods for climatic time series, *Reviews of Geophysics, 40*(1) 1003.

Gillette, D. A. (1977), Fine particulate emissions due to wind erosion, *Transactions of the ASABE, 20*(5), 890-897.

Gillette, D. A., I. H. J. R. Blifford, and D. W. Fryrear (1974), The influence of wind velocity on the size distributions of aerosols Generated by the wind erosion of soils, *J. Geophys. Res., 79*(27), 4068-4075.

Gleason, J. D., P. J. Patchett, W. R. Dickinson, and J. Ruiz (1994), Nd isotopes link Ouachita turbidites to Appalachian sources, *Geology*, *22*(4), 347-350.

Gleason, J. D., P. J. Patchett, W. R. Dickinson, and J. Ruiz (1995), Nd isotopic constraints on sediment source of the Ouachita-Marathon fold belt, *Geological Society of America Bulletin*, *107*(10), 1192-1210.

Goldstein, S. J., and S. B. Jacobsen (1988), Nd and Sr isotopic systematics of river water suspended material – implications for crustal evolution, *Earth and Planetary Science Letters*, *87*(3), 249-265.

Gradstein, F., J. Ogg, A. Smith, W. Bleeker, and L. Lourens (2004), A new Geologic Time Scale, with special reference to Precambrian and Neogene, *Episodes 27*(2), 83-100.

Green, O. R. (2001), *A Manual of Practical Laboratory and Field Techniques in Palaeobiology*, p. 538, Kluwer Academic, Boston, MA.

Greenwood, D. R., and S. L. Wing (1995), Eocene continental climates and latitudinal temperature gradients, *Geology, 23*(11), 1044-1048.

Greenwood, D. R., S. B. Archibald, R. W. Mathewes, and P. T. Moss (2005), Fossil biotas from the Okanagan Highlands, southern British Columbia and northeastern Washington State: climates and ecosystems across an Eocene landscape, *Canadian Journal of Earth Sciences, 42*(2), 167-185.

Grossman, E. L., H. S. Mii, and T. E. Yancey (1993), Stable isotopes in Late Pennsylavnian brachiopods from the US – Implications for Carboniferous paleoceanography, *Geological Society of America Bulletin*, *105*(10), 1284-1296.

Grossman, E. L., P. Bruckschen, H.-S. Mii, B. I. Chuvashov, T. E. Yancey, and J. Veizer (2002), Carboniferous paleoclimate and global change: Isotopic evidence from the Russian Platform, in *Carboniferous stratigraphy and Paleogeography in Eurasia.*, edited by I. o. G. a. Geochemistry, pp. 61-71, Russian Academy of Sciences, Ekaterinburg.

Grossman, E. L., T. E. Yancey, T. E. Jones, P. Bruckschen, B. Chuvashov, S. J. Mazzullo, and H. S. Mii (2008), Glaciation, aridification, and carbon sequestration in the Permo-Carboniferous: The isotopic record from low latitudes, *Palaeogeography Palaeoclimatology Palaeoecology*, *268*(3-4), 222-233.

Grousset, F. E., and P. E. Biscaye (2005), Tracing dust sources and transport patterns using Sr, Nd and Pb isotopes, *Chemical Geology*, *222*(3-4), 149-167.

Gulbranson, E., I. Montanez, M. Schmitz, C. Limarino, J. Isbell, S. Marenssi, and J. Crowley (2010), High-precision U-Pb calibration of Carboniferous glaciation and climate history, Paganzo Group, NW Argentina, *Geological Society of America Bulletin 122*(9-10), 1480-1498.

Guo, L. D., P. H. Santschi, M. Baskaran, and A. Zindler (1995), Distribution of dissolved and particulate Th-230 and Th-232 in seawater from the Gulf of Mexico and off Cape Hatteras as measured by SIMS, *Earth and Planetary Science Letters, 133*(1-2), 117-128.

Guo, Z. T., W. F. Ruddiman, Q. Z. Hao, H. B. Wu, Y. S. Qiao, R. X. Zhu, S. Z. Peng, J. J. Wei, B. Y. Yuan, and T. S. Liu (2002), Onset of Asian desertification by 22 Myr ago inferred from loess deposits in China, *Nature, 416*(6877), 159-163.

Guo, Z. T., B. Sun, Z.S. Zhang, S.Z. Peng, G.Q. Xiao, et al. (2008), A major reorganization of Asian climate by the early Miocene, *Climate of the Past, 4*(3), 153-174.

Gutjahr, M., M. Frank, C. H. Stirling, V. Klemm, T. van de Flierdt, and A. N. Halliday (2007), Reliable extraction of a deepwater trace metal isotope signal from Fe-Mn oxyhydroxide coatings of marine sediments, *Chemical Geology*, *242*(3-4), 351-370.

Haidl, F.M., C. Holmden, G.S. Nowlan, and K.C. Fanton (2003): Preliminary report on conodont and Sm-Nd isotope data from Upper Ordovician Red River strata (Herald and Yeoman formations) in the Williston Basin, Berkley et al Midale 12-2-7-11W2, southeastern Saskatchewan, in *Summary of Investigations 2003*, edited by Saskatchewan Geological Survey, pp. 1-13, Sask. Industry Resources, Regina.

Haley, B. A., G. P. Klinkhammer, and J. McManus (2004), Rare earth elements in pore waters of marine sediments, *Geochimica et Cosmochimica Acta*, *68*(6), 1265-1279.

Harrison, S. P., K. E. Kohfeld, C. Roelandt, and T. Claquin (2001), The role of dust in climate changes today, at the last glacial maximum and in the future, *Earth Science Reviews, 54*(1-3), 43-80.

Hay, W. W., R. DeConto, C.N. Wold, K.M. Wilson, S. Voigt, et al. (1999), Alternative global Cretaceous paleogeography, *Geological Society of America Special Paper, 332*, 1-47.

Heckel, P. H. (1986), Sea-level curve for Pennsylvanian eustatic marine transgressive-regressive depositional cycles along Midcontinent outcrop belt, North America, *Geology*, *14*(4), 330-334.

Heckel, P. H. (1990), Evidence for global (glacial-eustatic) control over upper Carboniferous (Pennsylvanian) cyclothems in Midcontinent North America, in *Tectonic Events Responsible for Britains Oil and Gas Reserves*, edited by R. F. P. Hardman and J. Brooks, pp. 35-47, Geological Society, London.

Heckel, P. H. (1994), Evaluation of evidence for glacio-eustatic control over marine Pennsylvanian cyclothems in North America and consideration of possible tectonic effects, *SEPM-Concepts in Sedimentology and Paleontology, 4*, 65-87.

Heckel, P. H. (2002), Overview of Pennsylvanian cyclothems in Midcontinent North America and brief summary of those elsewhere in the world, in *Carboniferous and*

Permian of the World, edited by L. V. Hills, C. M. Henderson and E. W. Bamber, pp. 79-98, Canadian Society of Petroleum Geologists, Calgary.

Heckel, P. H. (2008), Pennsylvanian cyclothems in Midcontinent North America as far-field effects of waxing and waning of Gondwana ice sheets, in *Resolving the Late Paleozoic Ice Age in Time and Space*, edited by C. R. Fielding, T. D. Frank and J. L. Isbell, pp. 275-289, GSA, Boulder, CO.

Heckel, P. H., M. R. Gibling, and N. R. King (1998), Stratigraphic model for glacial-eustatic Pennsylvanian cyclothems in highstand nearshore detrital regimes, *Journal of Geology*, *106*(4), 373-383.

Heckel, P. H., J. E. Barrick, D. R. Boardman, L. L. Lambert, W. L. Watney, and C. P. Weibel (1991), Biostratigraphic correlation of eustatic cyclothems (basic Pennsylvanian sequence units) from Midcontinent to Texas and Illonois, *AAPG Bulletin-American Association of Petroleum Geologists*, *75*(3), 592-593.

Hensley, M., D. J. Thomas, and S. C. Woodard (2009), Radiogenic isotope geochemistry of Carboniferous detrital sediments, Arrow Canyon, Nevada, *GSA Annual Meeting, Paper No. 257-6*.

Herbert, T. D., and S. L. Dhondt (1990), Precessional climate cyclicity in Late Cretaceous – Early Tertiary marine sediments – A high-resolution chronometer of Cretaceous-Tertiary boundary events, *Earth and Planetary Science Letters, 99*(3), 263-275.

Herbert, T. D., I. Premoli-Silva, E. Erba, and A. G. Fischer (1995), Orbital chronology of Cretaceous-Paleocene marine sediments, *Special Publication - SEPM (Society for Sedimentary Geology), 54*, 81-93.

Hirose, K., and Y. Sugimura (1987), Thorium isotopes in the surface air of the western North Pacific Ocean, *Journal of Environmental Radioactivity*, *5*(6), 459-475.

Hiyagon, H. (1994), Retention of solar helium and neon in IDPs in deep-sea sediment, *Science, 263*(5151), 1257-1259.

Holmden, C., R. A. Creaser, K. Muehlenbachs, S. M. Bergstrom, and S. A. Leslie (1996), Isotopic and elemental systematics of Sr and Nd in 454 Ma biogenic apatites: Implications for paleoseawater studies, *Earth and Planetary Science Letters*, *142*(3-4), 425-437.

Holmden, C., R. A. Creaser, K. Muehlenbachs, S. A. Leslie, and S. M. Bergstrom (1998), Isotopic evidence for geochemical decoupling between ancient epeiric seas and bordering oceans: Implications for secular curves, *Geology*, *26*(6), 567-570.

Holmes, M. A., D. K. Watkins, and R. D. Norris (2004), Paleocene cyclic sedimentation in the western North Atlantic, ODP Site 1051, Blake Nose, *Marine Geology, 209*(1-4), 31-43.

Honeyman, B.D., and P.H. Santschi (1989), A Brownian-pumping model for oceanic trace metal scavenging: Evidence from Th isotopes, *Journal of Marine Research 47*(4), 951-992.

Hoose, C., J. E. Kristjansson, J. P. Chen, and A. Hazra (2010), A Classical-Theory-Based Parameterization of Heterogeneous Ice Nucleation by Mineral Dust, Soot, and Biological Particles in a Global Climate Model, *Journal of the Atmospheric Sciences*, *67*(8), 2483-2503.

Hovan, S. A. (1995), Late Cenozoic atmospheric circulation intensity and climatic history recorded by eolian deposition in the eastern Equatorial Pacific Ocean, Leg 138, *Proceedings of the Ocean Drilling Program, Scientific Results, 138*, 615-625.

Hovan, S. A., and D. K. Rea (1992), Paleocene Eocene boundary changes in atmospheric and oceanic circulation - A southern hemisphere record, *Geology, 20*(1), 15-18.

Hovan, S. A., D. K. Rea, and N. G. Pisias (1991), Late Pleistocene continental climate and oceanic variability recorded in Northwest Pacific sediments, *Paleoceanography, 6*(3), 349-370.

Hovan, S. A., D. K. Rea, N. G. Pisias, and N. J. Shackleton (1989), A direct link between the China loess and marine delta 18O records aeolian flux to the North Pacific, *Nature, 340*(6231), 296-298.

Huber, B. T. (2000), *Warm climates in Earth history*, 462 pp., University of Cambridge, Cambridge.

Hunt, R. J., and I. Poole (2003), Paleogene West Antarctic climate and vegetation history in light of new data from King George Island, *Special Paper - Geological Society of America, 369*, 395-412.

Hyeong, K., S. H. Park, C. M. Yoo, and K. H. Kim (2005), Mineralogical and geochemical compositions of the eolian dust from the northeast equatorial Pacific and their implications on paleolocation of the Intertropical Convergence Zone, *Paleoceanography*, *20*(1), PA1010.

Hyeong, K., C. M. Yoo, J. Kim, S. B. Chi, and K. H. Kim (2006), Flux and grain size variation of eolian dust as a proxy tool for the paleo-position of the Intertropical

Convergence Zone in the northeast Pacific, *Palaeogeography Palaeoclimatology Palaeoecology, 241*(2), 214-223.

Imbrie, J., A. Berger, E.A. Boyle, S.C. Clemens, A. Duffy, et al. (1993), On the structure and origin of major glaciation cylcles 2: The 100,000-year cycle, *Paleoceanography, 8*(6), 699-735.

Isbell, J. L., P. A. Lenaker, R. A. Askin, M. F. Miller, and L. E. Babcock (2003), Reevaluation of the timing and extent of late Paleozoic glaciation in Gondwana: Role of the Transantarctic Mountains, *Geology*, *31*(11), 977-980.

Jacobs, B. F., J. D. Kingstonj, and L. L. Jacobs (1999), The origin of grass-dominated ecosystems, *Annals of the Missouri Botanical Garden*, *86*, 590–643.

Janecek, T. R. (1985), Eolian sedimentation in the northwest Pacific Ocean - A preliminary examination of the data from DSDP Site 576 and Site 578, *Initial Reports of the Deep Sea Drilling Project*, *86*, 589-603.

Janecek, T. R., and D. K. Rea (1983), Eolian deposition in the northeast Pacific ocean – Cenozoic history of atmospheric circulation, *Geological Society of America Bulletin*, *94*(6), 730-738.

Janecek, T. R., and D. K. Rea (1985), Quaternary fluctuations in the Northern Hemisphere trade winds and westerlies, *Quaternary Research, 24*(2), 150-163.

Jeandel, C., T. Arsouze, F. Lacan, P. Techine, and J. C. Dutay (2007), Isotopic Nd compositions and concentrations of the lithogenic inputs into the ocean: A compilation, with an emphasis on the margins, *Chemical Geology*, *239*(1-2), 156-164.

Jeppsson, L., R. Anehus, and D. Fredholm (1999), The optimal acetate buffered acetic acid technique for extracting phosphatic fossils, *Journal of Paleontology*, *73*(5), 964-972.

Jickells, T. D., Z.S. An, K.K. Andersen, A.R. Baker, G. Bergametti, et al. (2005), Global iron connections between desert dust, ocean biogeochemistry, and climate, *Science*, *308*(5718), 67-71.

Johnson, L. R. (1979), Mineralogical dispersal patterns of North Atlantic deep-sea sediments with particular reference to eolian dusts, *Marine Geology*, *29*(1-4), 335-345.

Jones, C. E., A. N. Halliday, D. K. Rea, and R. M. Owen (1994), Neodymium isotopic variations in North Pacific modern silicate sediment and the insignificance of detrital REE contributions to seawater, *Earth and Planetary Science Letters*, *127*(1-4), 55-66.

Jung, S. J. A., G. R. Davies, G. M. Ganssen, and D. Kroon (2004), Stepwise Holocene aridification in NE Africa deduced from dust-borne radiogenic isotope records, *Earth and Planetary Science Letters*, *221*(1-4), 27-37.

Kaufman, Y. J., D. Tanre, and O. Boucher (2002), A satellite view of aerosols in the climate system, *Nature*, *419*(6903), 215-223.

Kerr, A.C., J.A. Aspden, J. Tarney, and L.F. Pilatasig (2002), The nature and provenance of accreted oceanic terranes in western Ecuador: Geochemical and tectonic constraints, *Journal of the Geological Society of London, 159*(5), 577-594.

Keto, L. S., and S. B. Jacobsen (1987), Nd and Sr isotopic variations of early Paleozoic oceans, *Earth and Planetary Science Letters*, *84*(1), 27-41.

Keto, L. S., and S. B. Jacobsen (1988), Ns isotopic variations of Phanerozoic paleoceans, *Earth and Planetary Science Letters*, *90*(4), 395-410.

Koczy, F. F. (1961), Ratio of Thorium-230 to Thorium-232 in Deep-Sea Sediments, *Science*, *134*(349), 1978-1979.

Kohfeld, K. E., and S. P. Harrison (2001), DIRTMAP: the geological record of dust, *Earth Science Reviews, 54*(1-3), 81-114.

Kroon, D., R. D. Norris, and A. Klaus (Eds.) (2001), *Proceedings of ODP, Scientific Results, 171B*, Ocean Drilling Program, College Station, TX.

Krissek, L.A. and T.R. Janecek (1993), Eolian deposition on the Ontong Java Plateau since the Oligocene: unmixing a record of multiple dust sources, *Proc. ODP, Sci. Res. 130*, 471–490.

Krukowski, S. T. (1988), Sodium metatungstate – a new heavy mineral separation medium for the extraction of conodonts from insoluble residues, *Journal of Paleontology*, *62*(2), 314-316.

Kutzbach, J. E. (1989), Possible effects of orbital variations on past source and transports of eolian material – estimates from general circulation model experiments, in *Paleoclimatology and Paleometeorology : Modern and Past Patterns of Global Atmospheric Transport*, edited by M. Leinen and M. Sarnthein, pp. 513-521, Kluwer Academic, Dordrecht.

Kyte, F. T., M. Leinen, G. R. Heath, and L. Zhou (1993), Cenozoic sedimentation history of the central North Pacific – inferences from the elemental geochemistry of Core LL44-GPC3, *Geochimica et Cosmochimica Acta*, *57*(8), 1719-1740.

Labeyrie, L., J. Cole, K. Alverson, T. Stocker, and Contributors (2002), The History of Climate Dynamics in the Late Quaternary in *Paleoclimates, Global Change and the Future*, edited by R. B. K. Alverson and T. Pedersen, pp. 33-62, Springer, Berlin.

Lane, H. R., P. L. Brenckle, J. F. Baesemann, and B. Richards (1999), The IUGS boundary in the middle of the Carboniferous: Arrow Canyon, Nevada, USA, *Episodes*, *22*(4), 272-283.

Laskar, J., P. Robutel, F. Joutel, M. Gastineau, A. C. M. Correia, and B. Levrard (2004), A long-term numerical solution for the insolation quantities of the Earth, *Astronomy & Astrophysics, 428*(1), 261-285.

Lawrence, K.T., L.C. Sloan, and J.O. Sewall (2003), Terrestrial climatic response to precessional orbital forcing in the Eocene, *in Causes and Consequences of Globally Warm Climates in the Early Paleogene*, edited by S. L. Wing, pp. 263-274, GSA Special Papers, Boulder, CO.

Leinen, M. and G.R. Heath (1981), Sedimentary indicators of atmospheric activity in the Northern Hemisphere during the Cenozoic, *Palaeogeogr., Palaeoclimatol., Palaeoecol., 36*(1-2), 1–21.

Leinen, M., D. Cwienk, G.R. Heath, P.E. Biscaye, V. Kolla, et al. (1986), Distribution of silica and quartz in recent deep-sea sediments, *Geology*, *14*(3), 199-203.

Ling, H. F., S. Y. Jiang, M. Frank, H. Y. Zhou, F. Zhou, Z. L. Lu, X. M. Chen, Y. H. Jiang, and C. D. Ge (2005), Differing controls over the Cenozoic Pb and Nd isotope evolution of deepwater in the central North Pacific Ocean, *Earth and Planetary Science Letters*, *232*(3-4), 345-361.

Liu, Z. H., L. C. Cleaveland, and T. D. Herbert (2008), Early onset and origin of 100-kyr cycles in Pleistocene tropical SST records, *Earth and Planetary Science Letters, 265*(3-4), 703-715.

Lyle, M. (2003), Neogene carbonate burial in the Pacific Ocean, *Paleoceanography, 18*(3), 1059.

Mackenzie, F. T., and L. R. Kump (1995), Reverse weathering, clay mineral formation, and oceanic element cycles, *Science*, *270*(5236), 586-587.

Mackin, J. E., and R. C. Aller (1984), Dissolved Al in sediments and waters of the East China Sea – Implications for authigenic mineral formation, *Geochimica et Cosmochimica Acta*, *48*(2), 281-297.

MacLeod, K. G., B. T. Huber, T. Pletsch, U. Röhl, and M. Kucera (2001), Maastrichtian foraminiferal and paleoceanographic changes on Milankovitch timescales, *Paleoceanography, 16*(2), 133-154.

Maher, B. A., J. M. Prospero, D. Mackie, D. Gaiero, P. P. Hesse, and Y. Balkanski (2010), Global connections between aeolian dust, climate and ocean biogeochemistry at the present day and at the last glacial maximum, *Earth-Science Reviews*, *99*(1-2), 61-97.

Mahowald, N. M., A. R. Baker, G. Bergametti, N. Brooks, R. A. Duce, T. D. Jickells, N. Kubilay, J. M. Prospero, and I. Tegen (2005), Atmospheric global dust cycle and iron inputs to the ocean, *Global Biogeochemical Cycles, 19*(4), GB4025.

Mann, M. E., and J. M. Lees (1996), Robust estimation of background noise and signal detection in climatic time series, *Climatic Change, 33*(3), 409-445.

Marcantonio, F., D. J. Thomas, S. Woodard, D. McGee, and G. Winckler (2009), Extraterrestrial He-3 in Paleocene sediments from Shatsky Rise: Constraints on sedimentation rate variability, *Earth and Planetary Science Letters*, *287*(1-2), 24-30.

Marcantonio, F., R. F. Anderson, M. Stute, N. Kumar, P. Schlosser, and A. Mix (1996), Extraterrestrial He-3 as a tracer of marine sediment transport and accumulation, *Nature*, *383*(6602), 705-707.

Marcantonio, F., S. Higgins, R. F. Anderson, M. Stute, P. Schlosser, and E. T. Rasbury (1998), Terrigenous helium in deep-sea sediments, *Geochimica et Cosmochimica Acta*, *62*(9), 1535-1543.

Marcantonio, F., R. F. Anderson, S. Higgins, M. Q. Fleisher, M. Stute, and P. Schlosser (2001), Abrupt intensification of the SW Indian Ocean monsoon during the last deglaciation: constraints from Th, Pa, and He isotopes, *Earth and Planetary Science Letters*, *184*(2), 505-514.

Marcantonio, F., N. Kumar, M. Stute, R. F. Andersen, M. A. Seidl, P. Schlosser, and A. Mix (1995), Comparative study of accumulation rates derived by He and Th isotope analysis of marine sediments, *Earth and Planetary Science Letters*, *133*(3-4), 549-555.

Martel, D. J., R. K. Onions, D. R. Hilton, and E. R. Oxburgh (1990), The role of element distribution in productions nad release of radiogenic Helium: The Carnmenellis granite, southwest England, *Chemical Geology, 88*(3-4), 207-221.

Martin, H.A. (2006) Cenozoic climatic change and the development of arid vegetation in Australia, *Journal of Arid Environment, 66*(2006), 533-563.

Martin, E. E., and H. D. Scher (2004), Preservation of seawater Sr and Nd isotopes in fossil fish teeth: bad news and good news, *Earth and Planetary Science Letters*, *220*(1-2), 25-39.

Martin, E. E., J. D. Macdougall, T. D. Herbert, A. Paytan, and M. Kastner (1995), Strontium and Neodymium isotopic analyses of marine barite separates, *Geochimica et Cosmochimica Acta*, *59*(7), 1353-1361.

Maslin, M. A., and A. J. Ridgwell (2005), Mid-Pleistocene revolution and the 'eccentricity myth', in *Early-Middle Pleistocene Transitions: the Land-Ocean Evidence*, edited by M. J. Head and P. L. Gibbard, pp. 19-34. Geological Society, London.

McArthur, J. M. (2009), Global seawater Sr isotope curve for the Carboniferous, compiled from literature, unpublished, University College, London.

McArthur, J. M., R. J. Howarth, and T. R. Bailey (2001), Strontium isotope stratigraphy: LOWESS version 3: Best fit to the marine Sr-isotope curve for 0-509 Ma and accompanying look-up table for deriving numerical age, *Journal of Geology*, *109*(2), 155-170.

McGee, D., F. Marcantonio, and J. Lynch-Stieglitz (2007), Deglacial changes in dust flux in the eastern equatorial Pacific, *Earth and Planetary Science Letters*, *257*(1-2), 215-230.

McGee, D., W. S. Broecker, and G. Winckler (2010), Gustiness: The driver of glacial dustiness?, *Quaternary Science Reviews*, *29*(17-18), 2340-2350.

Merrill, J., E. Arnold, M. Leinen, and C. Weaver (1994), Mineralogy of Aeolian dust reaching the North Pacific Ocean, 2, relationship of mineral assemblages to atmospheric transport patterns, *Journal of Geophysical Research-Atmospheres*, *99*(D10), 21025-21032.

Meschede, M., and W. Frisch (1998), A plate-tectonic model for the Mesozoic and Early Cenozoic history of the Caribbean plate, *Tectonophysics*, *296*(3-4), 269-291.

Miall, A. D., and R. C. Blakey (2008), The Phanerozoic tectionic and sedimentary evolution of North America, *Sedimentary Basins of the World*, *5*, 1-29.

Michalopoulos, P., and R. C. Aller (2004), Early diagenesis of biogenic silica in the Amazon delta: Alteration, authigenic clay formation, and storage, *Geochimica et Cosmochimica Acta*, *68*(5), 1061-1085.

Mii, H. S., E. L. Grossman, and T. E. Yancey (1999), Carboniferous isotope stratigraphies of North America: Implications for Carboniferous paleoceanography and Mississippian glaciation, *Geological Society of America Bulletin*, *111*(7), 960-973.

Mii, H. S., E. L. Grossman, T. E. Yancey, B. Chuvashov, and A. Egorov (2001), Isotopic records of brachiopod shells from the Russian Platform - evidence for the onset of mid-Carboniferous glaciation, *Chemical Geology*, *175*(1-2), 133-147.

Mitchell, S. F., and D. Blissett (1999), The Cretaceous-Paleocene Summerfield Formation, Jamaica: One or two ignimbrites? *Caribbean Journal of Science*, *35*(3-4), 304-309.

Moran, K., J. Backman, H. Brinkhuis, S.C. Clemens, T. Cronin, et al. (2006), The Cenozoic palaeoenvironment of the Arctic Ocean, *Nature, 441*(7093), 601-605.

Muhs, D. R., and A. E. Bettis (2003), Quaternary loess-Paleosol sequences as examples of climate-driven sedimentary extremes, *Geological Society of America Special Papers, 370*, 53-74.

Muhs, D. R., C. A. Bush, K. C. Stewart, T. R. Rowland, and R. C. Crittenden (1990), Geochemical evidence of Saharan dust parent materials for soils developed on Quaternary limestones of Caribbean and western Atlantic islands, *Quaternary Research*, *33*(2), 157-177.

Murphy, J.B., J.D. Keppie, R.D. Nance, and J. Dostal (2010), Comparative evolution of the Iapetus and Rheic Oceans: A North America perspective, *Gondwana Research 17*(2010), 482-499.

Nakai, S., A. N. Halliday, and D. K. Rea (1993), Provenance of dust in the Pacific Ocean, *Earth and Planetary Science Letters*, *119*(1-2), 143-157.

Nance, R.D., Miller, B.V., Keppie, J.D., Murphy, J.B., and Dostal, J. (2007), Vestige of the Rheic Ocean in North America: the Acatlán Complex of southern Mexico, in *The evolution of the Rheic Ocean: from Avalonian–Cadomian active margin to Alleghenian–Variscan collision*, edited by U. Linnemann, R.D. Nance, G. Zulaf, and P. Kraft, pp. 4437–4452, GSA, Boulder, CO.

Nier, A. O., and D. J. Schlutter (1992), Extraction of Helium from individual interplanetary dust particles by step-heating, *Meteoritics*, *27*(2), 166-173.

Norris, R. D., and U. Röhl (1999), Carbon cycling and chronology of climate warming during the Palaeocene/Eocene transition, *Nature, 401*(6755), 775-778.

Nozaki, Y., Y. Horibe, and H. Tsubota (1981), The water column distributions of Thorium isotopes in the western Nother Pacific, *Earth and Planetary Science Letters*, 54(2), 203-216.

Nozaki, Y., H. Yang, and M. Yamada (1987), Scavenging of thorium in the ocean, *Journal of Geophysical Research-Oceans, 92*(C1), 772-778.

Olivarez, A. M., R. M. Owen, and D. K. Rea (1991), Geochemistry of eolian dust in Pacific pelagic sediments – Implications for paleoclimatic interpretations, *Geochimica et Cosmochimica Acta*, *55*(8), 2147-2158.

Ortega-Gutierrez, F., R.L. Sedlock, and R.C. Speed (1994) Phanerozoic tectonic evolution of Mexico, in *Phanerozoic Evolution of North American Continent-Ocean Transitions*, edited by R. C. Speed, pp. 265-306, GSA, Boulder, CO.

Pagani, M., N. Pedentchouk, M. Huber, A. Sluijs, S. Schouten, H. Brinkhuis, J. Damste, G. Dickens, and E. Scientists (2006), Arctic hydrology during global warming at the Palaeocene/Eocene thermal maximum, *Nature, 442*(7103), 671-675.

Pälike, H. (2005), Orbital Variation (including Milankovitch Cycles), in *Encyclopedia of geology*, edited by R. C. Selley, et al., pp. 410-421, Elsevier Academic, Amsterdam.

Pälike, H., N. Shackleton and U. Röhl (2001), Astronomical forcing in Late Eocene marine sediments, *Earth Planet Sc Lett.*, *193*(3-4), 589-602.

Patchett, P. J., G. M. Ross, and J. D. Gleason (1999), Continental drainage in North America during the Phanerozoic from Nd isotopes, *Science*, *283*(5402), 671-673.

Patterson, D. B., K. A. Farley, and M. D. Norman (1999), He-4 as a tracer of continental dust: A 1.9 million year record of aeolian flux to the west equatorial Pacific Ocean, *Geochimica et Cosmochimica Acta*, *63*(5), 615-625.

Pease, P. P., V. P. Tchakerian, and N. W. Tindale (1998), Aerosols over the Arabian Sea: geochemistry and source areas for aeolian desert dust, *Journal of Arid Environments*, *39*(3), 477-496.

Petit, J. R., J. Jouzel, D. Raynaud, N.I. Barkov, J.M. Barnola, et al. (1999), Climate and atmospheric history of the past 420,000 years from the Vostok ice core, Antarctica, *Nature*, *399*(6735), 429-436.

Pettke, T., A. N. Halliday, C. M. Hall, and D. K. Rea (2000), Dust production and deposition in Asia and the north Pacific Ocean over the past 12 Myr, *Earth and Planetary Science Letters, 178*(3-4), 397-413

Pettke, T., A. N. Halliday, and D. K. Rea (2002), Cenozoic evolution of Asian climate and sources of Pacific seawater Pb and Nd derived from eolian dust of sediment core LL44-GPC3, *Paleoceanography*, *17*(3), 1031.

Piepgras, D. J., and G. J. Wasserburg (1987), Rare-earth element transport in the western North Atlantiv inferred from Nd isotopic observations, *Geochimica et Cosmochimica Acta*, *51*(5), 1257-1271.

Pokras, E. M., and A. C. Mix (1985), Eolian evidence for spatial variability of late Quaternary climates in tropical Africa, *Quaternary Res*, *24*(2), 137-149.

Poole, F. G., and C. A. Sandberg (1991), *Mississippian paleogeography and conodont biostratigraphy of the western United States*, SEPM Pacific Section, Los Angeles, CA.

Popp, B. N., F. A. Podosek, J. C. Brannon, T. F. Anderson, and J. Pier (1986), $^{87}Sr/^{86}Sr$ ratios in Permo-Carboniferous seawater from the analyses of well-preserved brachiopod shells, *Geochimica et Cosmochimica Acta*, *50*(7), 1321-1328.

Pourmand, A., F. Marcantonio, and H. Schulz (2004), Variations in productivity and eolian fluxes in the northeastern Arabian Sea during the past 110 ka, *Earth and Planetary Science Letters*, *221*(1-4), 39-54.

Prospero, J. M. (1996), Saharan dust transport over the North Atlantic Ocean and Mediterranean: An overview, in *Impact of Desert Dust across the Mediterranean*, edited by S. Guerzoni and R. Chester, pp. 133-151, Kluwer Academic, Dordrecht.

Prospero, J. M. (2002), The chemical and physical properties of marine aerosols: An introduction, in *Chemistry of Marine Water and Sediments*, edited by A. Gianguzza, E. Pelizzetti and S. Sammartano, pp. 35-82. Springer-Verlag, Berlin.

Prospero, J. M., R. A. Glaccum, and R. T. Nees (1981), Atmospheric transport of soil dust from Africa to South America, *Nature, 289*(5798), 570-572.

Prospero, J. M., E. Bonatti, C. Schubert, and T. N. Carlson (1970), Dust in Caribbean atmosphere traced to an African dust storm, *Earth and Planetary Science Letters*, *9*(3), 287-293.

Pye, K. (1987), *Aeolian dust and dust deposits*, 334 pp., Academic Press, London.

Pye, K. (1989), Processes of fine particle formation, dust source regions and climatic changes, in *Paleoclimatology and Paleometeorology : Modern and Past Patterns of Global Atmospheric Transport*, edited by M. Leinen and M. Sarnthein, pp. 3-30. Kluwer Academic, Boston.

Ramanathan, V., P. J. Crutzen, J. T. Kiehl, and D. Rosenfeld (2001), Atmosphere - aerosols, climate, and the hydrological cycle, *Science*, *294*(5549), 2119-2124.

Ramsbottom, W. H. C., and W. B. Saunders (1984), Carboniferous ammonoid zonation., in *Biostratigraphy, Compte Rendu ème Congrès International de Stratigraphie et de Géologie du Carbonifère*, edited by P. K. Sutherland and W. L. Manger, pp. 52-64, Champaign–Urbana, IL.

Rankin, D. W. (1994), Continental margins of the eastern United States: past and present, in *Phanerozoic Evolution of North American Continent-Ocean Transitions*, edited by R. C. Speed, pp. 129-218, GSA, Boulder, CO.

Raymo, M., and K. Nisancioglu (2003), The 41 kyr world: Milankovitch's other unsolved mystery, *Paleoceanography, 18*(1011) PA000791.

Rea, D. K. (1994), The paleoclimatic record provided by eolian deposition in the deep-sea – The geologic history of wind, *Reviews of Geophysics, 32*(2), 159-195.

Rea, D. K., and T. R. Janecek (1981), Mass-accumulation of the nonauthigenic inorganic crystalline (eolian) component of deep-sea sediments from the western mid-Pacific Mountains, Deep Sea Drilling Project Site 463, in *Initial Reports DSDP, 62*, edited by J. Theide and T. L. Vallier, pp. 653-659, U.S. Govt Printing Office, Washington, D.C.

Rea, D. K., and J. M. Dixon (1983), Late Cretaceous and Paleogene tectonic evolution of the North Pacific Ocean, *Earth and Planetary Science Letters*, *65*(1), 145-166.

Rea, D. K., and S. A. Hovan (1995), Grain-size distribution and depositional processes of the mineral component of abyssal sediments – Lessons from the North Pacific, *Paleoceanography, 10*(2), 251-258.

Rea, D. K., and M. W. Lyle (2005), Paleogene calcite compensation depth in the eastern subtropical Pacific: Answers and questions, *Paleoceanography, 20*(1), PA1012.

Rea, D. K., M. Leinen, and T. R. Janecek (1985), Geologic approach to the long-term history of atmospheric circulation, *Science, 227*(4688), 721-725.

Rejebian, V. A., A. G. Harris, and J. S. Huebner (1987), Conodont color and textural alteration – an index to regional metamorphism, contact-metamorphism and hydrothermal alterattion, *Geological Society of America Bulletin*, *99*(4), 471-479.

Retallack, G. J., J. J. Veevers, and R. Morante (1996), Global coal gap between Permian-Triassic extinction and Middle Triassic recovery of peat-forming plants, *Geological Society of America Bulletin*, *108*(2), 195-207.

Revel-Rolland, M., P. De Deckker, B. Delmonte, P. P. Hesse, J. W. Magee, I. Basile-Doelsch, F. Grousset, and D. Bosch (2006), Eastern Australia: A possible source of dust in East Antarctica interglacial ice, *Earth and Planetary Science Letters*, *249*(1-2), 1-13.

Richards, B. C., H. R. Lane, and P. L. Brenckle (2002), The IUGS boundary (Mississippian-Pennsylvanian) in the middle of the Carboniferous: Arrow Canyon, Nevada, in *Permian and Carboniferous of the World*, edited by L. V. Hills, C. M. Henderson and E. W. Bamber, pp. 802-831, Canadian Society of Petroleum Geologists, Calgary.

Richter, F. M., and K. K. Turekian (1993), Simple models for the geochemical response of the ocean to climatic and tectonic forcing, *Earth and Planetary Science Letters, 119*(1-2), 121-131.

Robinson, L. F., N. S. Belshaw, and G. M. Henderson (2004), U and Th concentrations and isotope ratios in modern carbonates and waters from the Bahamas, *Geochimica et Cosmochimica Acta*, *68*(8), 1777-1789.

Robinson, L. F., T. L. Noble, and J. F. McManus (2008), Measurement of adsorbed and total Th-232/Th-230 ratios from marine sediments, *Chemical Geology*, *252*(3-4), 169-179.

Röhl, U., T. J. Bralower, R. D. Norris, and G. Wefer (2000), New chronology for the late Paleocene thermal maximum and its environmental implications, *Geology, 28*(10), 927-930.

Röhl, U., R. D. Norris, and J. G. Ogg (2003), Cyclostratigraphy of upper Paleocene and lower Eocene sediments at Blake Nose Site 1051 (western North Atlantic), *Geological Society of America Special Papers, 369*, 567-588.

Röhl, U., J. G. Ogg, T. L. Geib, and G. Wefer (2001), Astronomical calibration of the Danian time scale, *Geological Society Special Publications, 183*(1), 163-183.

Röhl, U., T. Westerhold, T. J. Bralower, M.-R. Petrizzo, and J. C. Zachos (2004), An Early Late Paleocene global dissolution event and new constraints for an astronomically-tuned Early Paleogene time scale, in *8th International Conference on Paleoceanography*, ICP VIII, Biarritz.

Röhl, U., T. Westerhold, T. J. Bralower, and J. C. Zachos (2007), On the duration of the Paleocene-Eocene thermal maximum (PETM), *Geochemistry Geophysics Geosystems, 8*(12), Q12002.

Ross, C.A. and J.R.P. Ross (Eds.) (1984), *Geology of Coal*, 349 pp., Hutchinson Ross, Stroudsburg, PA.

Roy-Barman, M. (2009), Modelling the effect of boundary scavenging on Thorium and Protactinium profiles in the ocean, *Biogeosciences*, *6*(12), 3091-3107.

Roy-Barman, M., J. H. Chen, and G. J. Wasserburg (1996), ^{230}Th-^{232}Th systematics in the central Pacific Ocean: The sources and the fates of thorium, *Earth and Planetary Science Letters, 139*(3-4), 351-363.

Royer, D. L., R. A. Berner, I. P. Montanez, N. J. Tabor, and D. J. Beerling (2004), $CO_{2\ as}$ a primary driver of Phanerozoic climate *GSA Today*, *14*(3), 4-10.

Ruhlin, D., and R. Owen (1986), The rare earth element geochemistry of hydrothermal sediments from the East Pacific Rise: Examination of a seawater scavenging mechanism, *Geochimica et Cosmochimica Acta, 50*(3), 393-400.

Rutberg, R., S. Hemming, and S. Goldstein (2000), Reduced North Atlantic Deep Water flux to the glacial Southern Ocean inferred from neodymium isotope ratios, *Nature, 405*(6790), 935-938.

Rygel, M. C., C. R. Fielding, T. D. Frank, and L. P. Birgenheier (2008), The magnitude of late Paleozoic glacioeustatic fluctuations: a synthesis, *Journal of Sedimentary Research*, *78*(7-8), 500-511.

Saleeby, J. B., R. C. Speed, and M. C. Blake (1994), Tectonic evolution of the central U.S. cordillera: A synthesis of the C and C2 Continent-Ocean transects, in *Phanerozoic Evolution of North American Continent-Ocean Transitions*, edited by R. C. Speed, GSA, Boulder, CO.

Saltzman, M. R. (2003), Late Paleozoic ice age: Oceanic gateway or pCO(2)?, *Geology*, *31*(2), 151-154.

Saltzman, M. R. (2005), Phosphorus, nitrogen, and the redox evolution of the Paleozoic oceans, *Geology*, *33*(7), 573-576.

Saunders, W. B., and W. H. C. Ramsbottom (1986), The mid-Carboniferous eustatic event, *Geology*, *14*(3), 208-212.

Schmitz, B. (2003), A paleoenvironmental reconstruction of the early late Paleocene North Sea from intrashell delta 18O and delta 13C profiles of molluscks, in *Causes and Consequences of Globally Warm Climates in the Early Paleogene*, edited by S. L. Wing, pp. 263-274, GSA, Boulder, CO.

Schmitz, B., G. Aberg, L. Werdelin, P. Forey, and S. E. Bendixalmgreen (1991), $^{87}Sr/^{86}Sr$, Na, F, Sr and La in skeletal fish debris as a measure of the paleosalinity of fossil fish habitats, *Geological Society of America Bulletin*, *103*(6), 786-794.

Schulte, P., L. Alegret, I. Arenillas, J.A. Arz, P. Barton, P.R. Bown et al. (2010), The Chicxulub Asteroid Impact and Mass Extinction at the Cretaceous-Paleogene Boundary, *Science, 327*(5970), 1214-1218.

Schütz, L., R Jeanicke, and H. Petrick, (1981), Saharan dust transport over the North Atlantic Ocean—model calculations and measurements, in *Desert dust: Origin, characteristics and effects on man*, edited by T. L. Pewe, pp. 87-100, GSA, Boulder, CO.

Scotese, C. R., and W. S. McKerrow (1990), Revised World maps and introduction, *Geological Society Memiors*, *12*, 1-21.

Sewall, J. O., L. C. Sloan, M. Huber, and S. Wing (2000), Climate sensitivity to changes in land surface characteristics, *Global and Planetary Change*, *26*(4), 445-465.

Sevier, R. (1962), Silica solubility, 0°-200°C, and the diagenesis of siliceous sediments, *Jouranl of Geology, 70*(2), 127-150.

Shah, A. V., W. W. Predebon, and B. J. Pletka (1993), Deformation and fracture in directionally solidified co-coal eutectic, *Journal of Materials Science*, *28*(21), 5843-5851.

Shaw, H. F., and G. J. Wasserburg (1985), Sm-Nd in marine carbonates and phosphates – Implications for Nd isotopes in seawater and crustal ages, *Geochimica et Cosmochimica Acta*, *49*(2), 503-518.

Shellito, C.J., L.C. Sloan, and M. Huber (2003), Climate model sensitivity to atmospheric CO2 levels in the Early–Middle Paleogene, *Palaeogeography, Palaeoclimatology, Palaeoecology, 193*(1), 113-123.

Short, D. A., J. G. Mengel, T. J. Crowley, W. T. Hyde, and G. R. North (1991), Filtering of Milankovitch Cycles by Earth's geography, *Quaternary Research, 35*(2), 157-173.

Sluijs, A., S. Schouten, T. H. Donders, P. L. Schoon, U. Rohl, G. J. Reichart, F. Sangiorgi, J. H. Kim, J. S. S. Damste, and H. Brinkhuis (2009), Warm and wet conditions in the Arctic region during Eocene Thermal Maximum 2, *Nature Geoscience, 2*(11), 777-780.

Sluijs, A., S. Shouten, M. Pagani, M. Wolering, H. Brunkhuis, et al. (2006), Subtropical arctic ocean temperatures during the Palaeocene/Eocene thermal maximum, *Nature, 441*(7093), 610-613.

Smith, L. B., and J. F. Read (2000), Rapid onset of late Paleozoic glaciation on Gondwana: Evidence from Upper Mississippian strata of the Midcontinent, United States, *Geology*, *28*(3), 279-282.

Smith, M. T., and G. E. Gehrels (1992a), Stratigraphy and tectonic significance of lower Paleozoic continental margin strata in northeastern Washington, *Tectonics*, *11*(3), 607-620.

Smith, M. T., and G. E. Gehrels (1992b), Structural geology of the Lardeau Group near Trout Lake, British Columnia – Implications for the structural evolution of the Kootenay Arc, *Canadian Journal of Earth Sciences*, *29*(6), 1305-1319.

Somayaju, B., and T. M. Church (1973), Radium, Thorium, and Uranium isotopes in interstitial water from Pacific Ocean sediment, *Journal of Geophysical Research*, *78*(21), 4529-4531.

Speed, R. C. (1994), North American continent-ocean transitions over Phanerozoic time, in *Phanerozoic Evolution of North American Continent-Ocean Transitions*, edited by R. C. Speed, pp. 1-86, GSA, Boulder, CO.

Stancin, A. M., et al. (2008), Miocene to recent eolian dust record from the Southwest Pacific Ocean at 40 degrees S latitude, *Palaeogeography Palaeoclimatology Palaeoecology*, *261*(3-4), 218-233.

Staudigel, H., P. Doyle and A. Zindler (1985), Sr and Nd isotope systematics in fish teeth, *Earth Planetary Science Letters, 76*(1-2), 45-56.

Stollhofen, H., M. Werner, I. G. Stanistreet, and R. A. Armstrong (2008), Single-zircon U-Pb dating of Carboniferous-Permian tuffs, Namibia, and the intercontinental deglaciation cycle framework, in *Resolving the Late Paleozoic Ice Age in Time and Space*, edited by C. R. Fielding, T. D. Frank and J. L. Isbell, pp. 83-96, GSA, Boulder, CO.

Sun, Y. B., R. J. Tada, J. C. Chen, Q. S. Liu, S. Toyoda, A. Tani, J. F. Ji, and Y. Isozaki (2008), Tracing the provenance of fine-grained dust deposited on the central Chinese Loess Plateau, *Geophysical Research Letters*, *35*(1), L01804.

Svensson, A., P. E. Biscaye, and F. E. Grousset (2000), Characterization of late glacial continental dust in the Greenland Ice Core Project ice core, *Journal of Geophysical Research-Atmospheres*, *105*(D4), 4637-4656.

Tachikawa, K., C. Jeandel, and M. Roy-Barman (1999), A new approach to the Nd residence time in the ocean: the role of atmospheric inputs, *Earth and Planetary Science Letters*, *170*(4), 433-446.

Taylor, S. R., and S. M. McLennan (1985), *The Continental Crust: Its Composition and Evolution*, 312 pp., Blackwell, Oxford.

Taylor, S. R., and S. M. McLennan (1995), The Geochemical Evolution of the Continental Crust, *Reviews of Geophysics*, *33*(2), 241-265.

Thomas, D. J. (2004), Evidence for deep-water production in the North Pacific Ocean during the early Cenozoic warm interval, *Nature*, *430*(6995), 65-68.

Thomas, D. J. (2005), Reconstructing ancient deep-sea circulation patterns using the Nd isotopic composition of fossil fish debris, in *Isotopic and Elemental Tracers of Cenozoic Climate Change*, edited by G. Mora and D. Surge, pp. 1-11. GSA, Boulder, CO.

Thomas, D. J., M. Lyle, T. C. Moore, and D. K. Rea (2008), Paleogene deepwater mass composition of the tropical Pacific and implications for thermohaline circulation in a greenhouse world, *Geochemistry Geophysics Geosystems*, *9*(2), GC001748.

Tiedemann, R., M. Sarnthein, and N. Shackleton (1994), Astronomic timescale for the Pliocene Atlantic $\delta^{18}O$ and dust flux records of Ocean Drilling Program Site-659, *Paleoceanography, 9*(4), 619-638.

Tsunogai, S., M. Kawasaki, and K. Harada (1994), Different partitioning among Thorium isotopes in seawater of the North Pacific, *Journal of Oceanography, 50,* 197-207.

Uematsu, M., R. A. Duce, and J. M. Prospero (1985), Deposition of atmospheric mineral particles in the North Pacific Ocean, *Journal of Atmospheric Chemistry, 3*(1), 123-138.

Vachard, D., and A. F. de Dios (2002), Discovery of Latest Devonian/Earliest Mississippian microfossils in San Salvador Patlanoaya (Puebla, Mexico); biogeographic and geodynamic consequences, *Comptes Rendus Geoscience*, *334*(15), 1095-1101.

Vachard, D., A. F. De Dios, B. E. Buitron, and M. Grajales (2000), Biostratigraphy with fusulinids of the Carboniferous and Permian limestones from San Salvador Patlanoaya, *Geobios*, *33*(1), 5-33.

van Andel, T. H. (1975), Cenozoic history and paleoceanography of the central equatorial Pacific Ocean : a regional synthesis of Deep Sea Drilling Project data, *Geological Society of America Memoir*, GSA, Boulder, CO.

Vanden Berg, M. D., and R. D. Jarrard (2004), Cenozoic mass accumulation rates in the equatorial Pacific based on high-resolution mineralogy of Ocean Drilling Program Leg 199, *Paleoceanography, 19*(2), PA2021.

Weber, E. T., R. M. Owen, G. R. Dickens, A. N. Halliday, C. E. Jones, and D. K. Rea (1996), Quantitative resolution of eolian continental crustal material and volcanic detritus in North Pacific surface sediment, *Paleoceanography*, *11*(1), 115-127.

Westerhold, T. (submitted), A complete high-resolution Paleocene benthic stable isotope record for the central Pacific (ODP Site 1209), *Paleoceanography*.

Westerhold, T., and U. Röhl (2006), Data report: Revised composite depth records for Shatsky Rise Sites 1209, 1210, and 1211. , in *Proceedings of ODP, Scientific Results, 198,* edited by T. J. Bralower, I. Premoli Silva and M. J. Malone, Ocean Drilling Program, College Station. TX.

Westerhold, T., U. Rohl, J. Laskar, I. Raffi, J. Bowles, L. J. Lourens, and J. C. Zachos (2007), On the duration of magnetochrons C24r and C25n and the timing of early Eocene global warming events: Implications from the Ocean Drilling Program Leg 208 Walvis Ridge depth transect, *Paleoceanography, 22*(1), PA2201.

Westerhold, T., U. Rohl, I. Raffi, E. Fornaciari, S. Monechi, V. Reale, J. Bowles, and H. F. Evans (2008), Astronomical calibration of the Paleocene time, *Palaeogeography Palaeoclimatology Palaeoecology, 257*(4), 377-403.

Whalley, W. B., J. R. Marshall, and B. J. Smith (1982), Origin of desert loess from some experimental observations, *Nature*, *300*(5891), 433-435.

Williams, M., A. M. Haywood, J. F. Gregory, and D. N. Schmidt (Eds.) (2007), *Deep time perspectives on climate change - marrying the signal from computer models and biological proxies*, 589 pp., Geological Society of London, London.

Winckler, G., R. F. Anderson, M. Q. Fleisher, D. McGee, and N. Mahowald (2008), Covariant glacial-interglacial dust fluxes in the equatorial Pacific and Antarctica, *Science*, *320*(5872), 93-96.

Windom, H. L. (1975), Eolian contributions to marine sediments, *Journal of Sedimentary Petrology, 45*(2), 520-529.

Wing, S. L., P. D. Gingerich, B. Schmitz, and E. Thomas (Eds.) (2003), *Causes and Consequences of Globally Warm Climates during the Early Paleogene*, 614 pp., GSA Special Paper, Boulder, CO.

Woodard, S. C., D. J. Thomas, S. Hovan, U. Röhl, and T. Westerhold (2011), Evidence for orbital forcing of dust accumulation during the early Paleogene greenhouse, *Geochem. Geophys. Geosyst., 12*(2), Q02007.

Woodard, S. C., and D. J. Thomas (2009), Is it eolian dust? Contributions to the fine silicate fraction of deep sea sediments on Shatsky Rise, 58Ma, *Geochimica et Cosmochimica Acta, 73*(13), A1452.

Woodard, S. C., J. D. Herridge, D. J. Thomas, and F. Marcantonio (2009), The impact of orbitally-driven changes in solar insolation on "greenhouse" climates, *Fall Mtg Suppl., EOS Trans. AGU, 90*(52), PP41A-1488.

Woodard, S. C., D. J. Thomas, E. Grossman, T. Olszewski, T. Yancey, A. Raymond, and B. V. Miller (2010), Nd isotopes as indicator of glacio-eustasy, mid-Carboniferous boundary Arrow Canyon, NV, *Geochimica et Cosmochimica Acta, 74*(12), A1140.

Wright, C. A., C. R. Barnes, and S. B. Jacobsen (2002), Neodymium isotopic composition of Ordovician conodonts as a seawater proxy: Testing paleogeography, *Geochemistry Geophysics Geosystems*, *3*(1016), GC000195.

Wright, J., R. S. Seymour, and H. F. Shaw (1984), REE and Nd isotopes in conodont apatite: variations with geological age and depositional environment, in *Conodont Biofacies and Provincialism*, edited by D.L. Clark, pp. 325-340, GSA, Boulder, CO.

Wright, V. P., and S. D. Vanstone (2001), Onset of Late Palaeozoic glacio-eustasy and the evolving climates of low latitude areas: a synthesis of current understanding, *Journal of the Geological Society*, *158*(4), 579-582.

Zachos, J., M. Pagani, L. Sloan, E. Thomas, and K. Billups (2001), Trends, rhythms, and aberrations in global climate 65 Ma to present, *Science, 292*(5517), 686-693.

Zachos, J. C., G. R. Dickens, and R. E. Zeebe (2008), An early Cenozoic perspective on greenhouse warming and carbon-cycle dynamics, *Nature*, *451*(7176), 279-283.

Zaier, A., A. Beji-Sassi, S. Sassi, and R. T. J. Moody (1998), Basin evolution and deposition during the Early Paleogene in Tunisia, in *Petroleum Geology of North Africa.*, edited by D. S. MacGregor, R. T. J. Moody and D. D. Clark-Lowes, pp. 375-393, Geological Society Special Publication, London.

Ziegler, C. L., R. W. Murray, S. A. Hovan, and D. K. Rea (2007a), Resolving eolian, volcanogenic, and authigenic components in pelagic sediment from the Pacific Ocean, *Earth and Planetary Science Letters*, *254*(3-4), 416-432.

Ziegler, C. L., and R. W. Murray (2007b), Geochemical evolution of the central Pacific Ocean over the past 56 Myr, *Paleoceanography*, *22*(2), PA2203.

APPENDIX A

Comparison of 232Th-derived dust fluxes using two sedimentation models.

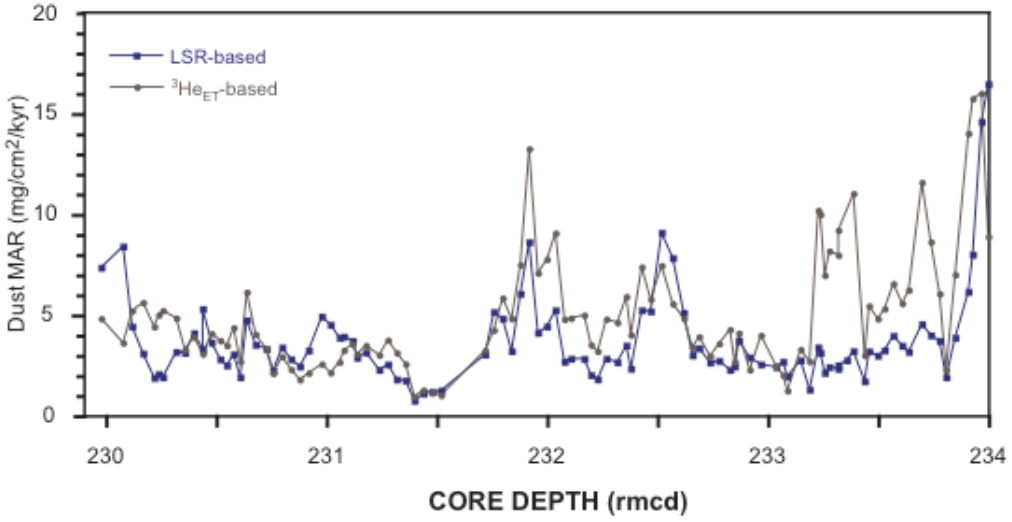

APPENDIX B

Average grain size distribution for extracted "dust" from Shatsky Rise, ODP Site 1209

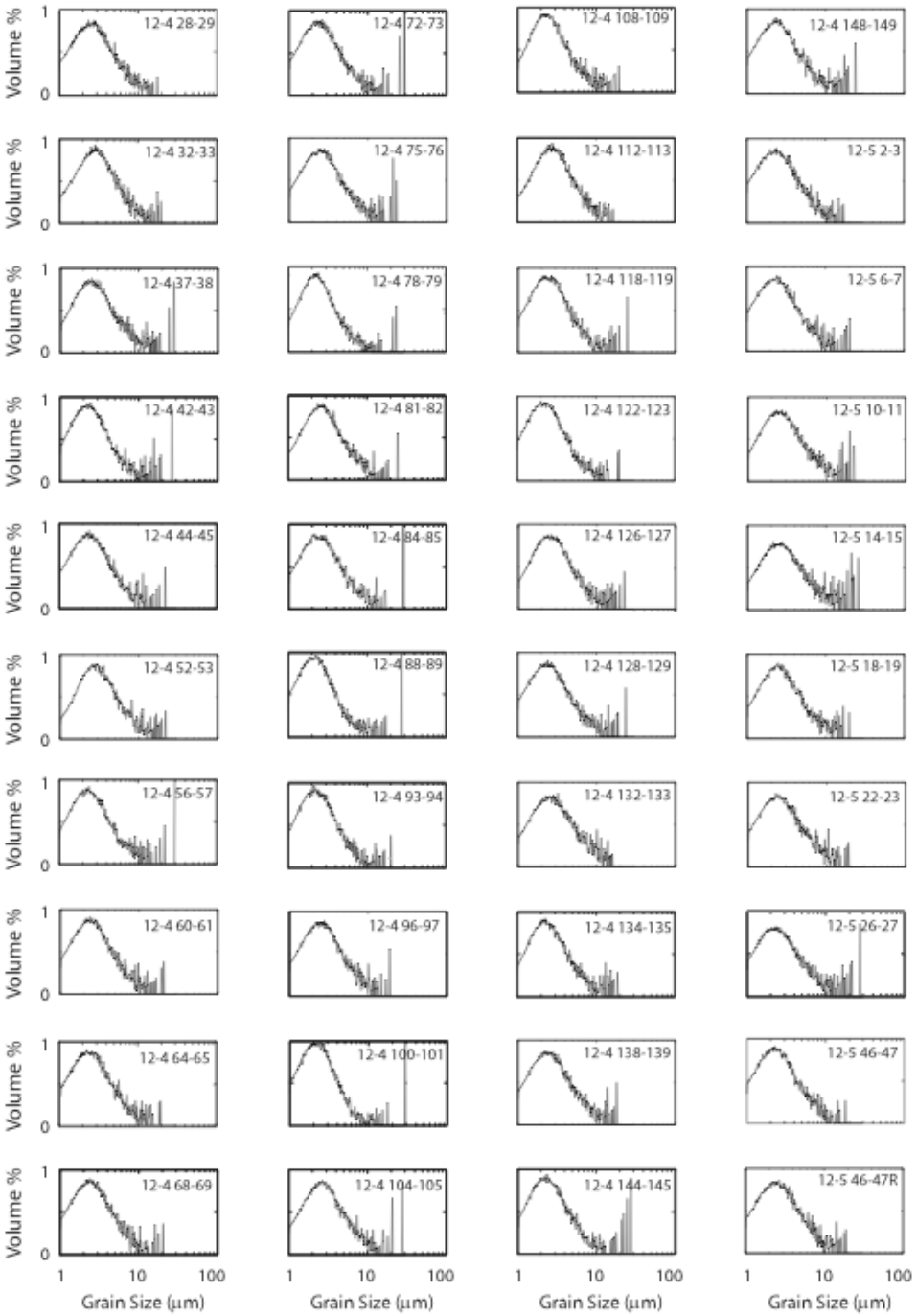

APPENDIX C

Alternate sedimentation rates and age model based on $^{3}He_{ET}$ from *Marcantonio et al.* [2009]

Depth (rmcd)	$^{3}He_{ET}$-based LSR*	Age (kyr)**
229.93	0.28	57924.1
230.01	0.58	57952.6
230.07	0.27	57962.9
230.07	0.27	----
230.16	0.75	57995.9
230.25	1.05	58007.9
230.34	0.44	58016.4
230.43	0.37	58036.9
230.43	0.417	----
230.57	0.60	58075.0
230.72	0.41	58100.2
230.87	0.31	58136.3
231.01	0.20	58181.3
231.07	0.38	58210.8
231.07	0.32	----
231.14	0.46	58232.6
231.21	0.51	58247.8
231.27	0.551	58259.6
231.27	0.621	----
231.31	0.681	58266.8
231.51	0.35	58296.1
231.63	0.66	58330.4
231.75	0.35	58348.6
231.95	1.05	58406.2
232.16	1.08	58426.2
232.38	1.04	58446.6
232.56	0.32	58463.8
232.56	0.42	----
232.65	0.58	58491.7
232.73	0.61	58505.4
232.81	0.77	58518.6
232.82	0.95	58519.9
232.84	0.57	58522.0
232.91	0.41	58534.3
232.95	0.97	58544.0
232.95	0.79	----
233.1	0.24	58563.0
233.24	1.68	58621.3
233.39	1.76	58630.2
233.42	1.09	58631.9
233.42	0.68	----
233.6	0.82	58658.4
233.69	1.38	58669.3
233.8	0.61	58677.3
233.89	1.27	58692.1
233.99	0.25	58700.0
233.99	0.31	----

VITA

Stella C. Woodard received her Bachelor of Arts degree in English and Writing from SUNY Oswego in 2001 where she received the 2001 Academy of American Poet's Prize. She entered the Oceanography program at Texas A&M University in Fall 2006. She was awarded a Merit Fellowship from Texas A&M in 2006 and was a Schlanger Ocean Drilling Fellow in 2009-2010. Her research interests include: the development and use of geochemical proxies to reconstruct past oceanic and climatic change; factors affecting ocean chemistry and climate over varying geologic timescales; geochemical processes in the modern marine environment, and anthropogenic environmental impacts. Stella sailed on four oceanographic research cruises during her time at Texas A&M including the Integrated Ocean Drilling Program Expedition 324 to Shatsky Rise (Fall 2009) and an NSF funded cruise to study Th cycling in the eastern equatorial Pacific Ocean (Fall 2010). She completed her Ph.D. in the spring of 2011.

Stella may be reached at the Department of Oceanography, Texas A&M University, 306F O&M Eller Building, TAMU 3146, College Station, TX 77840. Her email is swoodard@ocean.tamu.edu.